1986

Cyclic strain amplitude and heat treatment effects on the high damping behavior of incramute alloy under random vibration loading in the 50-1000 HZ frequency range.

Reskusich, John.

NAVAL POSTGRADUATE SCHOOL

Monterey, California

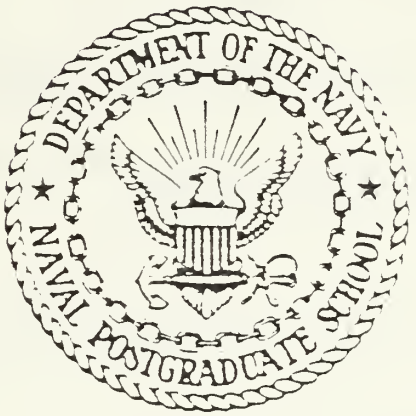

THESIS

CYCLIC STRAIN AMPLITUDE AND HEAT TREATMENT EFFECTS ON THE HIGH DAMPING BEHAVIOR OF INCRAMUTE ALLOY UNDER RANDOM VIBRATION LOADING IN THE 50-1000 HZ FREQUENCY RANGE

by

JOHN RESKUSICH

SEPTEMBER 1986

Thesis Advisor: A. J. Perkins

Approved for public release; distrubution is unlimited.

REPORT DOCUMENTATION PAGE

1a REPORT SECURITY CLASSIFICATION UNCLASSIFIED	1b RESTRICTIVE MARKINGS
2a SECURITY CLASSIFICATION AUTHORITY	3 DISTRIBUTION / AVAILABILITY OF REPORT Approved for public release; Distribution is unlimited.
2b DECLASSIFICATION / DOWNGRADING SCHEDULE	
4 PERFORMING ORGANIZATION REPORT NUMBER(S)	5 MONITORING ORGANIZATION REPORT NUMBER(S)
6a. NAME OF PERFORMING ORGANIZATION Naval Postgraduate School 6b OFFICE SYMBOL (*If applicable*) 69	7a. NAME OF MONITORING ORGANIZATION Naval Postgraduate School
6c. ADDRESS (*City, State, and ZIP Code*) Monterey, CA 93943-5000	7b ADDRESS (*City, State, and ZIP Code*) Monterey, CA 93943-5000
8a NAME OF FUNDING / SPONSORING ORGANIZATION 8b. OFFICE SYMBOL (*If applicable*)	9 PROCUREMENT INSTRUMENT IDENTIFICATION NUMBER
8c. ADDRESS (*City, State, and ZIP Code*)	10 SOURCE OF FUNDING NUMBERS PROGRAM ELEMENT NO / PROJECT NO / TASK NO / WORK UNIT ACCESSION NO

11 TITLE (*Include Security Classification*)
CYCLIC STRAIN AMPLITUDE AND HEAT TREATMENT EFFECTS ON THE HIGH DAMPING BEHAVIOR OF INCRAMUTE ALLOY UNDER RANDOM VIBRATION LOADING IN THE 50-1000 HZ FREQUENCY RANGE

12 PERSONAL AUTHOR(S)
JOHN RESKUSICH

13a TYPE OF REPORT	13b TIME COVERED	14 DATE OF REPORT (*Year, Month, Day*)	15 PAGE COUNT
Engineer's Thesis	FROM _____ TO _____	1986 September	114

16 SUPPLEMENTARY NOTATION

17 COSATI CODES			18 SUBJECT TERMS (*Continue on reverse if necessary and identify by block number*)
FIELD	GROUP	SUB-GROUP	Random Vibration, Strain-Dependent damping, INCRAMUTE, Transmission Electron Microcopy (TEM), X-Ray Diffraction (XRD), Optical Microscopy, Microstructure

19 ABSTRACT (*Continue on reverse if necessary and identify by block number*)

The strain dependence of damping in the alloy INCRAMUTE (58 Cu, 40 Mn, 2 Al) aged at 400°C for various times, was determined using a modified version of the resonant dwell technique. Cantilever beam specimens were vibrated at their first three resonant modes (50-1000 Hz) at room temperature. The highest specific damping capacity (SDC), 68%, was achieved with an average peak strain of 2.27×10^{-3} in mode 1 at a resonant frequency of 49.2 Hz for the 16-hour aging condition.

The INCRAMUTE alloy exhibited variations of Young's modulus, lattice parameter, hardness, tensile hysteresis, and SDC with aging, which is typical of Cu-Mn binary alloys with greater than 50% Mn. However, no FCT transformation or microtwin banding was observed in the aged specimens under zero stress conditions, as verified by transmission electron microscopy (TEM0, X-ray diffraction (XRD) and optical microscopy.

20 DISTRIBUTION / AVAILABILITY OF ABSTRACT	21 ABSTRACT SECURITY CLASSIFICATION
☒ UNCLASSIFIED/UNLIMITED ☐ SAME AS RPT ☐ DTIC USERS	UNCLASSIFIED
22a NAME OF RESPONSIBLE INDIVIDUAL A. J. Perkins	22b TELEPHONE (*Include Area Code*) (408) 646-2216 22c OFFICE SYMBOL 69Ps

The characteristic microstructure observed at the TEM level was a "mottled" or a "tweed" pattern in both the as-quenched and the aged specimens. Neither (200) nor (220) peak splitting corresponding to tetragonality was detected from XRD traces of aged samples. Based on the results, an interpretation of the microstructural damping characteristics of INCRAMUTE is presented.

Approved for public release; distribution is unlimited.

Cyclic Strain Amplitude and Heat Treatment Effects on the High Damping Behavior of INCRAMUTE Alloy under Random Vibration Loading in the 50-1000 Hz Frequency Range

by

John Reskusich
Lieutenant Commander, United States Navy
B.S., United States Naval Academy, 1975

Submitted in partial fulfillment of the
requirements for the degrees of

MASTER OF SCIENCE IN MECHANICAL ENGINEERING
and
MECHANICAL ENGINEER

from the

NAVAL POSTGRADUATE SCHOOL
September 1986

ABSTRACT

The strain dependence of damping in the alloy INCRAMUTE (58 Cu, 40 Mn, 2 Al), aged at 400°C for various times, was determined using a modified version of the resonant dwell technique. Cantilever beam specimens were vibrated at their first three resonant modes (50-1000 Hz) at room temperature. The highest specific damping capacity (SDC), 68%, was achieved with an average peak strain of 2.27×10^{-3} in mode 1 at a resonant frequency of 49.2 Hz for the 16-hour aging condition.

The INCRAMUTE alloy exhibited variations of Young's modulus, lattice parameter, hardness, tensile hysteresis, and SDC with aging, which is typical of Cu-Mn binary alloys with greater than 50% Mn. However, no FCT transformation or microtwin banding was observed in the aged specimens under zero stress conditions, as verified by transmission electron microscopy (TEM), X-ray diffraction (XRD), and optical microscopy. The characteristic microstructure observed at the TEM level was a "mottled" or a "tweed" pattern in both the as-quenched and the aged specimens. Neither (200) nor (220) peak splitting corresponding to tetragonality was detected from XRD traces of aged samples. Based on the results, an interpretation of the microstructural damping characteristics of INCRAMUTE is presented.

TABLE OF CONTENTS

LIST OF TABLES

LIST OF FIGURES

ACKNOWLEDGEMENTS

Sufficient gratitude cannot be given to those who helped me in this effort. I would like to specifically thank Drs. Jeff Perkins, Ming-Hsiung Wu, and Stephen J. Hales, and the rest of the Material Science staff here at the Naval Postgraduate School. Special thanks must also be extended to those in Rock Shop 101 who developed the best definition of INCRAMUTE to date:

"INCRAMUTE is an extinct race of speechless South American indians."

The Appeal

If I have given you delight
By aught that I have done,
Let me lie quiet in that night
Which shall be yours anon:

And for the little, little, span
The dead are borne in mind,
Seek not to question other than
The books I leave behind.

Kipling

I. INTRODUCTION

A. GENERAL

All materials exhibit some form of vibrational damping characteristics through intrinsic, microstructural energy-absorbing, or energy-dissipative, phenomena. These mechanisms can be improved by:

- varying the composition of the constituents within an alloy system,
- optimizing the thermomechanical history,
- operating below a specific threshold temperature, or
- operating above a particular stress level.

Development of alloys with high damping characteristics will improve the service life of machinery and equipment by increasing fatigue life and will reduce the ambient noise generated in machinery and structural components, thereby reducing the potential hearing loss hazards to personnel. Additionally, Naval applications abound in which it is critical to reduce low frequency underwater acoustic emissions of submarines and surface vessels.

B. MACROSTRUCTURAL DAMPING

1. Damping Models and Parameters

Coulomb, in 1784, proposed that damping was stress-dependent [Ref. 1:p. 129]. Since then, several mathematical, viscoelastic models have surfaced to describe damping in materials and structures. These are:

a. two-parameter models of a spring and a dashpot in series (Maxwell, 1868) [Ref. 2:p. 51], or in parallel (Kelvin-Voigt),
b. three-parameter models of two springs and a dashpot with the dashpot and one spring in either parallel or series combination [Ref. 1:p. 133],
c. four parameter models of two springs and two dashpots.[1]

[1]Sogabe, et al [Ref. 3:p. 324], treat this combination as a series dashpot-spring in series with a parallel-arranged dashpot-spring.

d. multi-parallel chains of parallel or series combinations of a dashpot and spring [Ref. 1],

For the most general and simplest case of forced vibration with complex damping, the Kelvin-Voigt model is the best approximation. It accounts for internal stress and afterworking. However, it has the deficiencies of no elastic response during loading or unloading and of no permanent set. The general differential equation of motion for this and any model is of the form:

$$my + c\dot{y} + k\ddot{y} = F \qquad \text{(eqn 1.1)}$$

where

m	mass
c	viscous damping coefficient
k	spring rate, or spring constant
$\dot{F}$	time-dependent, complex forcing function
y	displacement
$\dot{y}$ and $\ddot{y}$	first and second time derivatives of displacement

The viscous damping coefficient, c, can be represented by $2m\zeta\omega_n$, where ω_n is the angular natural frequency of oscillation and ζ is the damping factor, which may vary from 0.0 to 1.0 (e.g., for no damping, $\zeta = 0.0$). The forcing function may be expressed as $Fe^{i\omega t}$, where ω is the excitation frequency.

The steady state solution to Equation 1.1 is of the form:

$$y = Y e^{i(\omega t - \varphi)} = F e^{i\omega t} / [(k - m\omega^2) + i\omega c] \qquad \text{(eqn 1.2)}$$

where φ is the phase angle between the displacement response, y, and the excitation, and Y is the amplitude of the displacement [Ref. 1:p. 130]. For a single degree-of-freedom system, this solution results in the occurrence of one eigenvalue for the frequency, ω_n, at which the vibrating structure resonates. The eigenvalue, or eigenfrequency, is more specifically known as the resonant frequency.

The ability of a material to dampen vibrations can be characterized by several parameters, each of which can be related to the others. Their definitions follow:

a. logarithmic decrement (δ) for exponential, cyclic free decay [Ref. 1:p. 138]

$$\delta = \ln (a_i/a_{i+1}) = (1/n) \ln (a_0/a_n) \qquad \text{(eqn 1.3)}$$

b. damping factor (ζ)

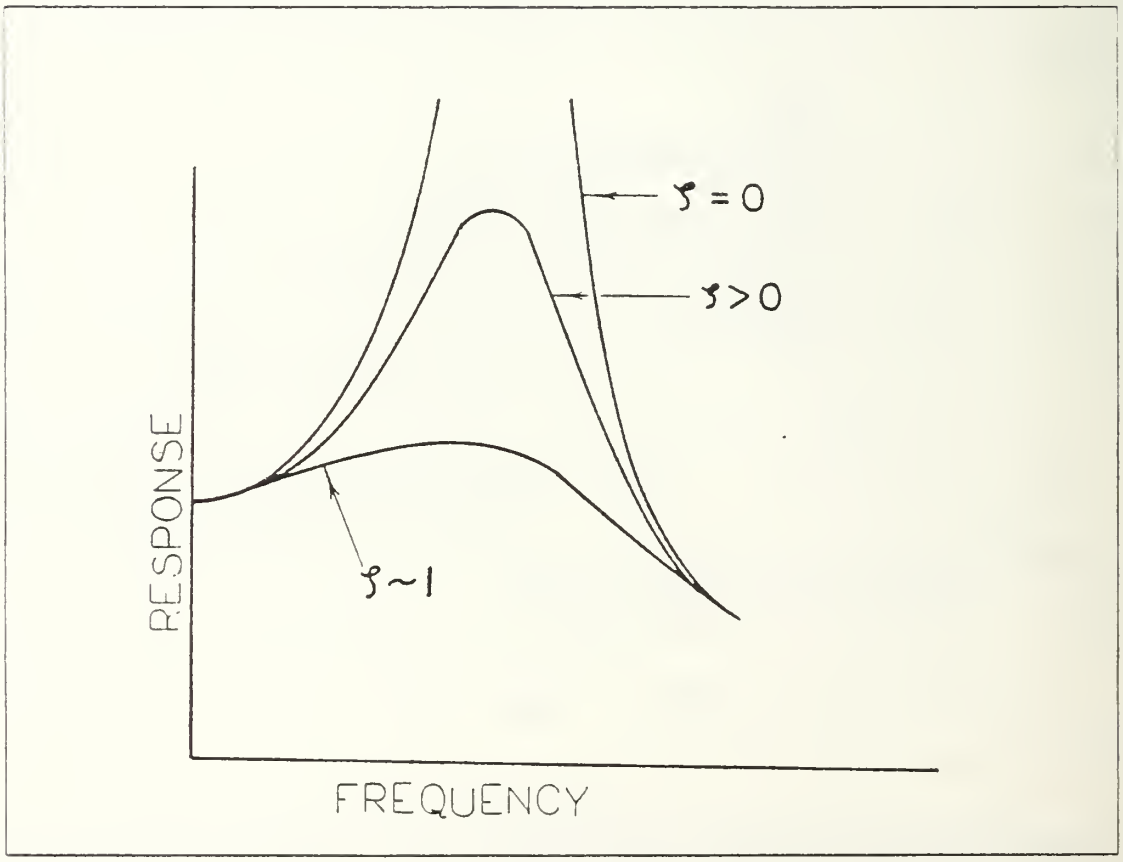

Figure 1.1 Damping Factor.

c. normalized bandwidth - the difference between the two frequencies, ω_1 and ω_2, for which the stored energy is half its maximum value at the resonant frequency, ω_n . [Ref. 2:p. 40] and normalized by the associated resonant frequency [Ref. 1:p. 137].

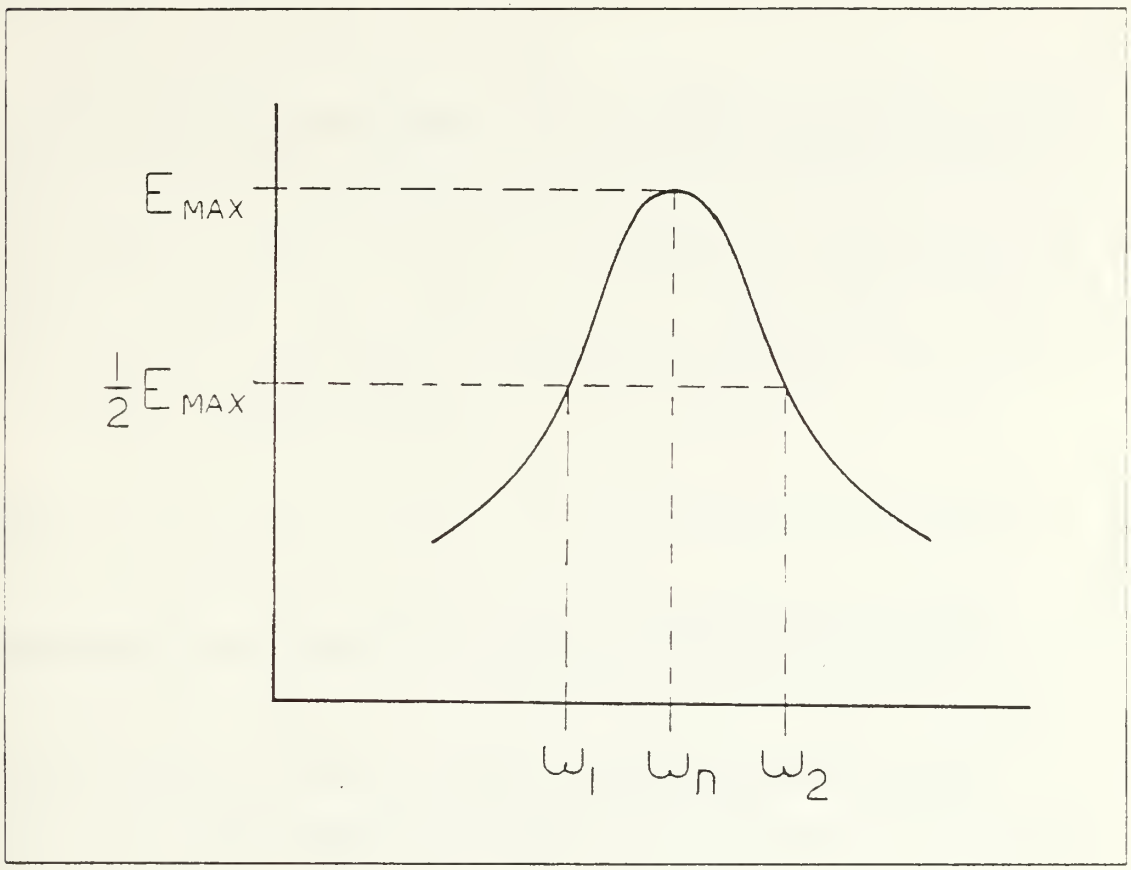

Figure 1.2 Normalized Bandwidth.

d. quality factor (Q) - the inverse of the normalized bandwidth [Ref. 1:p. 137]

$$Q = \omega_n/(\omega_2 - \omega_1) \qquad \text{(eqn 1.4)}$$

e. internal friction (Q^{-1}) - the inverse of the quality factor [Ref. 2:p. 41]

$$Q^{-1} = (\omega_2 - \omega_1)/\omega_n \qquad \text{(eqn 1.5)}$$

f. phase angle (α)[2] - the angle by which the strain lags behind the stress while under cyclic loading [Ref. 4:p. 445]

$$\tan \alpha = (1/\pi) \ln(a_i/a_{i+1}) = \delta \pi \qquad \text{(eqn 1.7)}$$

g. specific damping capacity (SDC) - for an oscillating system under free decay [Ref. 4:p. 444]

$$SDC = (a_{i+1}^2 - a_i^2) / a_i^2 \qquad \text{(eqn 1.8)}$$

If $(a_{i+1} - a_i)$ is small, SDC may be approximated by [Ref. 4:p. 444]

$$SDC = 2(a_{i+1} - a_i) / a_i \qquad \text{(eqn 1.9)}$$

Another definition of SDC is the ratio of the energy loss per cycle (W_d) to the peak potential energy (U) [Ref. 5:p. 70].

Several interrelationships exist among the above parameters as long as the damping is small (i.e., $\zeta << 0.5$). For this case, the following hold:

$$\tan \alpha = \delta / \pi = Q^{-1} = 2\zeta \qquad \text{(eqn 1.10)}$$

---

[2]Bert [Ref. 1:p. 137] refers to the phase angle (α) as the loss angle (γ) such that

$$g = \tan \gamma = E^I / E^R \qquad \text{(eqn 1.6)}$$

where E^I is the loss, or dissipation, modulus and E^R is the storage, or elastic or real, modulus. Tan γ is the loss tangent.

$$SDC(\%) = 200\,\pi\,Q^{-1} \qquad \text{(eqn 1.11)}$$

[Ref. 6:p. 320]

2. Macrostructural Vibration Techniques

Probably the most common technique utilized to measure a specimen's damping during free decay has been the Ke torsion pendulum device. The authors of References 7, 8, 9, and 10 have used this technique for the Cu-Mn alloy system for Mn contents greater than 60%, while Hills [Ref. 11] examined INCRAMUTE. Reference 4 describes its operation. Other techniques which have been used to determine the material damping of Cu-Mn alloys are flexural free decay [Refs. 6,12,13] and stress wave propagation in a long rod [Ref. 3].

An increasingly popular technique has been the use of the resonant dwell method. It utilizes an electromagnetic shaker which drives the clamped end of a cantilever beam specimen. An optical microscope with a reticle is mounted near the beam tip to measure the tip's vertical displacement, which can then be used to determine the specimen's loss factor. Reference 14 describes the operation of the resonant dwell apparatus. This type of apparatus does not measure damping under free decay, but under conditions of continuous vibration. It has the advantages of simulating operational stresses and of determining the stress- or strain-dependence of damping under forced vibrations. Heine [Ref. 15] used this method to determine the damping characteristics of 1018 steel, 2024-T4 aluminum alloy, and 416 stainless steel, while Kaufman, et al [Ref. 16], studied NiTi and CuAlNi damping.

Recently, Professor Y.S. Shin of the Naval Postgraduate School modified the resonant dwell apparatus by replacing the optical microscope with an accelerometer mounted at the beam tip. The signals of the input accelerometer (at the root) and of the output accelerometer (at the tip) are processed by a spectrum analyzer to produce the frequency response of the vibrating cantilever beam at a resonant mode. Specifically, Dew [Ref. 17] compared this method to a forced torsion pendulum device in characterizing the strain-dependent damping of SONOSTON, with a nominal composition of 37 Cu, 54.25 Mn, 4.75 Al, 3 Fe, 1 Ni, developed by Stone Manganese Marine, Ltd.

C. MICROSTRUCTURAL DAMPING MECHANISMS

Damping in any material owes its origin to microstructural effects and interactions. Microstructural responses leading to damping cause irreversibilities when a material is subjected to an alternating stress. Energy losses characterize these irreversibilities, which are evident in hysteresis curves representing magnetic, mechanical, and/or thermal losses. The degree of the loss is a function of composition, structure, thermomechanical history, and environment.

When a crystalline material is cyclically stressed, several microstructural mechanisms may be activated to cause high damping to occur. They are:

a. dislocation damping [Refs. 18,19],
b. boundary migration effects [Ref. 18],
c. phase change effects [Ref. 18].

All crystalline materials exhibit effects due to dislocation damping such that when a force is applied to it, dislocations move and energy is lost. Of course, if the applied load is high enough, the material will react plastically, which is characterized by an irreversible shape change. In this condition, the dislocations will not return to their pre-stressed positions. However, dislocation damping occurs at stress levels well below the plastic limit of materials. In this region below the plastic limit, Hooke's law on the linear elastic behavior of stressed material is not followed and nonlinearities exist. In this region, strain lags stress and exhibits anelastic behavior [Ref. 20:p. 606]. Birchon points out that at very low strains (i.e., $< 10^{-6}$) a material's damping is independent of strain amplitude but frequency-dependent. Higher strains of less than 10^{-4} are of more engineering interest. When stressed to these levels, the damping capacity becomes strain-dependent without regard to frequency, thus signifying non-viscous damping. At high strains, background damping manifests itself primarily as a result of diffusional processes [Ref. 20:pp. 606-607]. Materials with high damping properties exhibit a "false" plasticity in their elastic regions, or a pseudoelasticity. The magnitude of damping imparted by dislocation mechanisms is relatively low when compared with some of the unique mechanisms which arise in so-called high damping alloys.

Krishnan, et al [Ref. 21:pp. 1536-1537], give a very good phenomenological explanation of the pseudoelasticity exhibited by martensitic materials. In the case of stress-induced transformation to martensite, the initial rise upon loading is due to the

elastic response of the matrix (1——>2, in Figure 1.3). The leveling off at point 2 results from the nucleation of martensites. When point 3 is reached the martensitic transformation is complete for that material and the transformation's extent will vary with composition and temperature. The slope of the curve in this region represents the ease of martensitic nucleation and growth. Once the martensite is formed, continued stressing causes the martensite to react elastically, until a martensitic yield point (4) is reached. Releasing the stress somewhere between points 3 and 4 (e.g., 3') causes a stress recovery to occur in stages, following an atomistically reverse transformation path from the loading one. The martensites shrink and disappear until only the parent phase is present. Some residual strain may remain in the fully unloaded condition. The area enclosed within the loading and unloading curves comprises a hysteresis loop and represents the energy dissipated in transforming the material to the martensitic phase and then reverting to the parent phase.

The above description is for a test temperature above the austenite finish temperature, A_f. The stresses necessary to transform the parent to martensite, or vice versa, are linearly dependent on temperature. On the other hand, the plastic yield stress of the austenitic parent phase varies inversely with temperature [Ref. 21:p. 1537].

The preceding applies for a starting condition in which only parent austenite is present. If the microstructure contains pre-existing martensite when initially loaded, the amount of strain experienced to transform the remaining austenite to martensite ($\varepsilon_{2\text{-}3}$) will decrease, such that point 3 moves to the left. There may also be an increase in the slope from 2 to 3, increasing the stress required to complete the martensitic transformation, or making the transformation more difficult to proceed.

High damping alloys typically develop martensitic plates in the form of microtwins upon cooling from a single-phase region to below the martensite start temperature, M_s. When stressed below M_s, the plates grow preferentially in the longitudinal direction. Transverse, or sideways, growth occurs once longitudinal growth ceases, or is impeded, when obstructions are met. These obstacles come in the form of grain boundaries, second-phase particles, dislocation pile-ups, or other microtwins. However, second-phase particles and dislocation pile-ups act as nucleation sites for the microtwins, and this occurs prior to sideways growth. This process is reversed when the loading is reduced or removed and the microtwins disappear in the no-load condition [Refs. 7,22,23]. This sequence is particularly applicable to the Cu-Mn binary alloy system [Refs. 8,24,25,26,27,28].

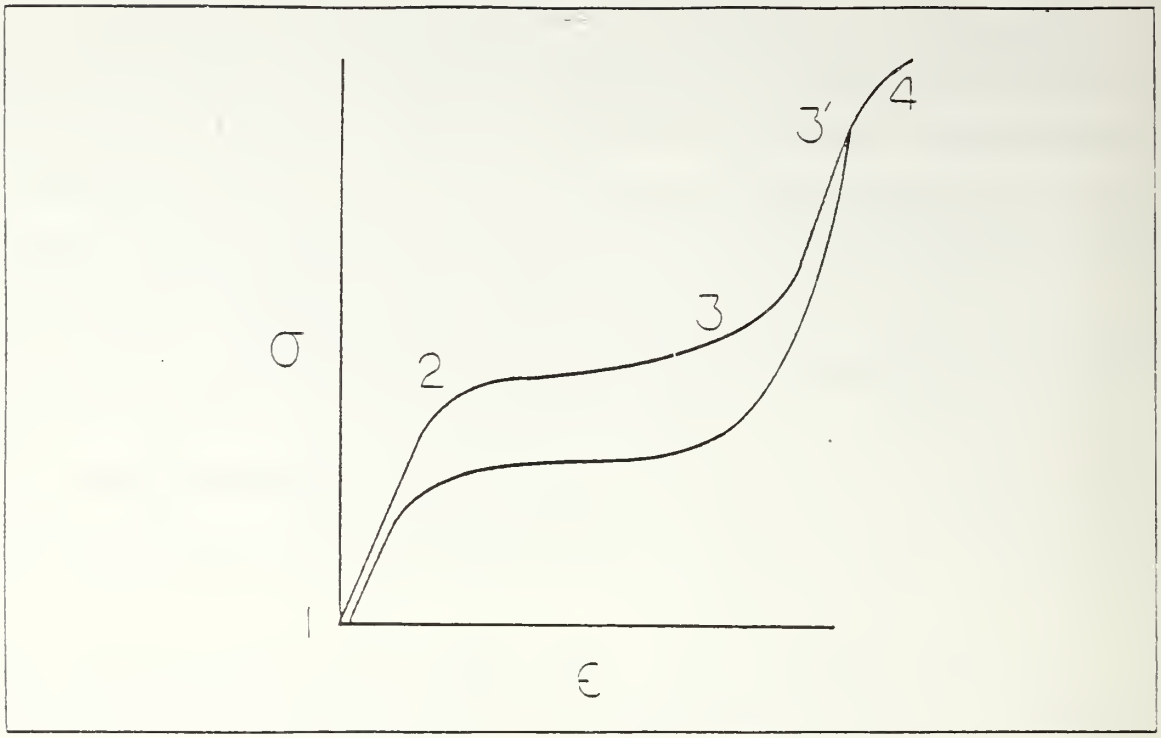

Figure 1.3 Stress-Strain Hysteresis Loop.

D. METALLURGY OF THE COPPER-MANGANESE ALLOY SYSTEM

1. Physical Properties of Cu-Mn Alloys

The Cu-Mn binary alloys are characterized by an extensive single-phase solid miscibility of Mn in Cu at elevated temperatures (T > 700°C) [Ref. 29] forming an FCC γ-phase. Figure 1.4 is a phase diagram of this alloy system. The γ-phase can be retained to room temperature by quenching in water from solution treatment in the single-phase region.

For alloys containing greater than 80 w/o Mn, the FCC γ-phase transforms to a metastable FCT martensitic structure in the as-quenched state of the diffusionless type. The temperature at which the FCC——> FCT transformation occurs upon quenching varies approximately linearly with Mn content (i.e., $T_{fcc\text{-}fct}$ increases with Mn content) [Refs. 12,27,30]. Basinski and Christian [Ref. 27] have shown that for as-quenched alloys with 76-88 w/o Mn the lattice constant varies inversely with the amount of Mn, while Worrell [Ref. 31] has reported that, when Mn is added to Cu, the lattice parameter (a_0) increases from 3.6147 A for pure FCC Cu (Type A1) to a maximum of about 3.76 Å for about 60% Mn with a minimum at about 80 w/o Mn.

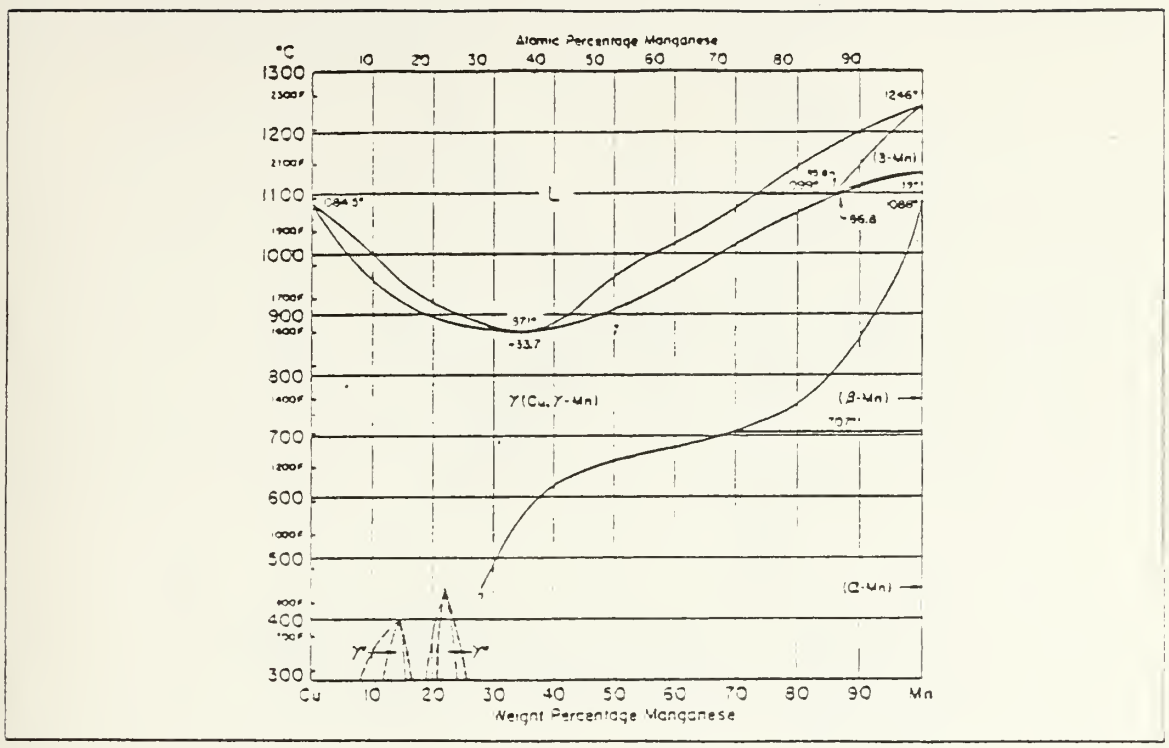

Figure 1.4 Phase Diagram of Copper-Manganese Binary System.

Increasing the Mn content above 80 w/o, the as-quenched (from γ-phase) structure becomes tetragonal [Ref. 27]. This corresponds to the martensite which forms during a room-temperature quench from the γ-phase field for alloys with 80 w/o Mn and greater. The FCC——> FCT transformation temperature, $T_{fcc\text{-}fct}$, is also called the martensite start temperature, M_s. For alloys of less than 80 w/o Mn, M_s decreases linearly below room temperature and approaches liquid nitrogen temperature ($-197°C$) as Mn content decreases to about 55 w/o. Sugimoto, et al [Ref. 12:p. 106], correlated their research with those of previous works [Refs. 30,32] showing the variation of M_s with Cu concentration (Figure 1.5). The M_s temperature is also associated with a minimum in Young's modulus [Ref. 30:p. 4855].

Several workers [Refs. 12,30,33,34,35] have shown that various Cu-Mn alloys with greater than 50 w/o Mn are antiferromagnetic upon quenching from the γ-phase to room temperature. The initiation of antiferromagnetism on cooling is associated with another concentration-dependent temperature, the Neel temperature, T_N. When antiferromagnetic ordering occurs, the degree of ordering increases with Mn content when quenched below T_N from the γ-phase, forming domains. The formation of these

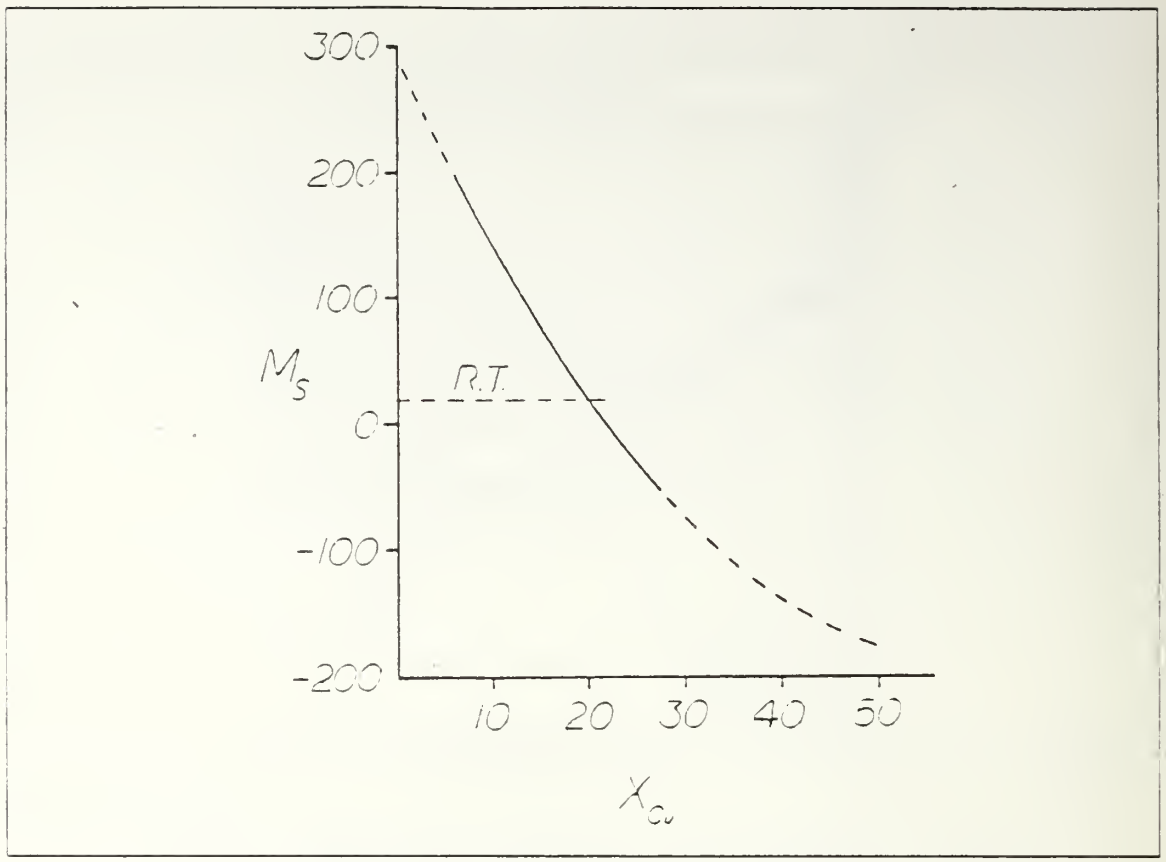

Figure 1.5 Variation of Martensite Start Temperature (M_s) with Copper Concentration (X_{Cu}).

domains are caused by the presence of an antiferromagnetic coupling between Mn atoms as the Mn content becomes significant [Ref. 33:p. 134]. Vitek and Warlimont [Ref. 36:p. 11] aggregated the data of other researchers [Refs. 12,30,32] to display the relationship between T_N and Cu concentration (X_{Cu}). Figure 1.6 is a reproduction from Reference 36 and shows the inverse linearity between T_N and X_{Cu}.

Comparing the Mn composition from 80 to 95 w/o of both the Neel and FCC——> FCT transformation temperatures (T_N and M_s, respectively), Bacon, et al [Ref. 32:p. 227], and Street [Ref. 34:p. 311S] demonstrated that antiferromagnetic ordering precedes (occurs at higher temperature on cooling) the tetragonal martensite formation, but that the difference between T_N and M_s decreases as Mn content decreases. In Figure 1.7, the M_s temperature from Figure 1.5 is superimposed on the T_N from Figure 1.6. A decrease in $T_N - M_s$ is seen as Mn content decreases to 80 w/o. When a quenched alloy is reheated from below T_N, antiferromagnetic ordering

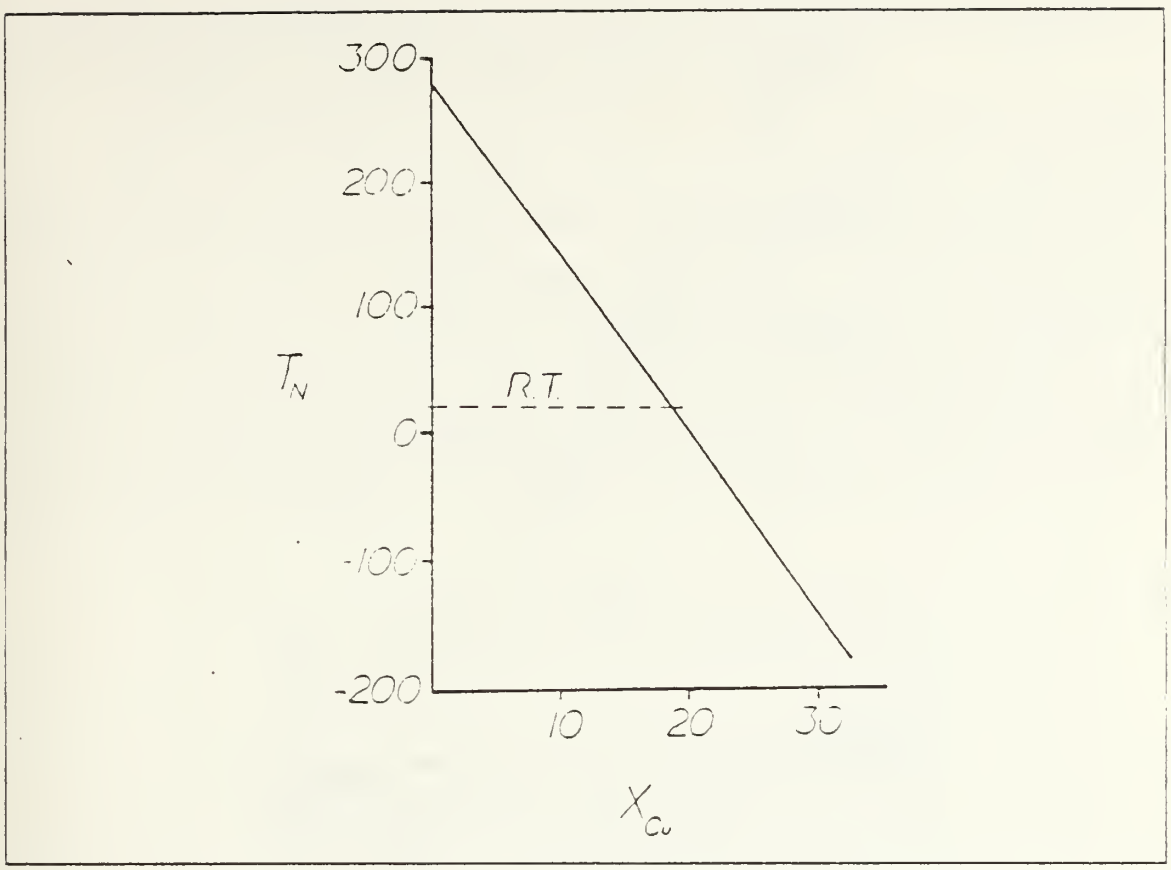

Figure 1.6 Variation of Neel Temperature (T_N) with Copper Concentration (X_{Cu}).

disappears for the reverse transformation (i.e., FCT——> FCC for alloys with > 80 w/o Mn); for these alloys, the antiferromagnetic ordering is long range. Street [Ref. 34:p. 314S] also found that, for alloys with less than 75 a/o Mn (about 73 w/o), no long-range, antiferromagnetic ordering occurs. Some short-range ordering could statistically occur with less than 50 a/o Mn, in small Mn clusters, but no definite T_N will exist due to the statistical distribution in cluster size [Ref. 34:p. 316S].

At the Neel temperature, on cooling, the magnetic moments of the Mn atoms are reoriented and aligned into antiferromagnetic (parallel and antiparallel) domains such that the net magnetism is zero. Neutron diffraction studies [Refs. 30,33,37:pp. 4855, 132, 104] have shown that antiferromagnetic ordering results in the occurrence of a (110) reflection, the intensity of which increases with Mn content. Continued quenching to below the M_s temperature causes a contraction to occur in the [100] direction, forming the FCT martensite with a twinning plane of (110). The moments of

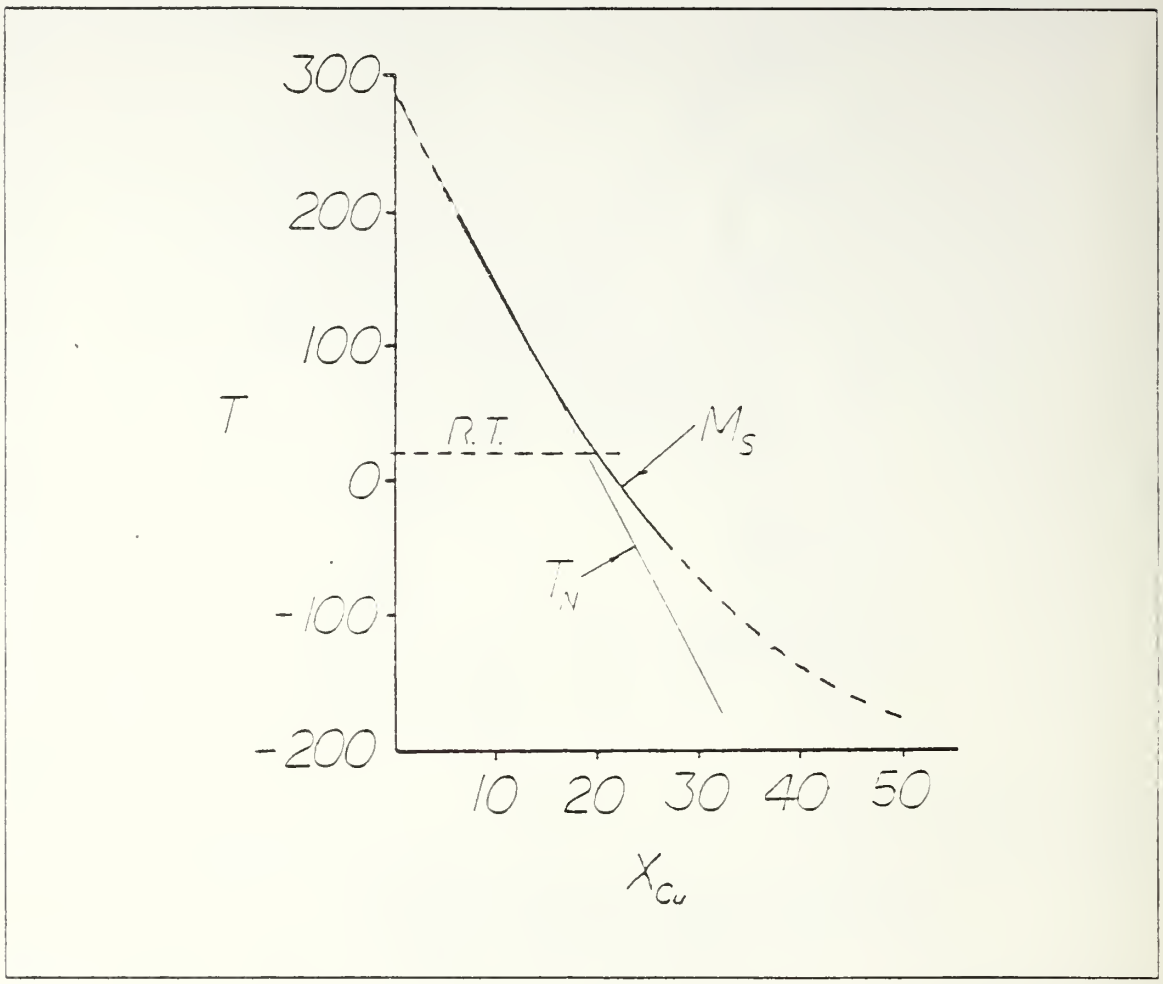

Figure 1.7 Variation of Martensite Start and Neel Temperatures with Manganese Content.

the Mn atoms in the martensite are parallel to the c-axis (i.e., one of the <110> directions) in the FCT structure [Ref. 33:p. 134]. Similar results are obtained in X-ray diffraction analysis, in that the ordering is represented by the appearance of peak splitting of the (200) and (220) reflections [Refs. 24,26,30:pp. 129, 2100, 4855]. The degree of tetragonality is expressed by the axial ratio, c/a, and the extent of (200)-(220) peak splitting reflects a decrease in the axial ratio for FCT Cu-Mn. Meneghetti and Sidhu [Ref. 33:p. 134] have concluded that no atomic ordering results because there are no superlattice reflections from neutron diffraction. It would appear from the data of Bacon, et al [Ref. 32:p. 227], that T_N and M_s coincide, at about 80 w/o Mn, at about 30°C and, that with lower Mn content, T_N becomes less than M_s. In fact, this would

tend to substantiate Street's [Ref. 34:p. 314S] observation that alloys of less than 75 a/o Mn do not show long-range, antiferromagnetic ordering.

Another characteristic of the Cu-Mn alloys is the existence of a miscibility gap, though there is some uncertainty about its exact location. Vintaykin, et al [Ref. 38], located this immiscibility between about 40 and 88 a/o (36 and 87 w/o) Mn at 700K (427°C) with a curve maximum at 60 a/o Mn at about 875K (600°C). (The data of Vintaykin, et al, is plotted on a phase diagram in Figure 1.8.) They used two methods to verify the position of the miscibility gap: (1) integral intensity data of neutron diffraction reflections of aged alloys [Ref. 38:p. 97] and (2) a recovery phenomenon at the temperature of transformation from a two-phase to a single-phase structure [Ref. 38:pp. 97-98].

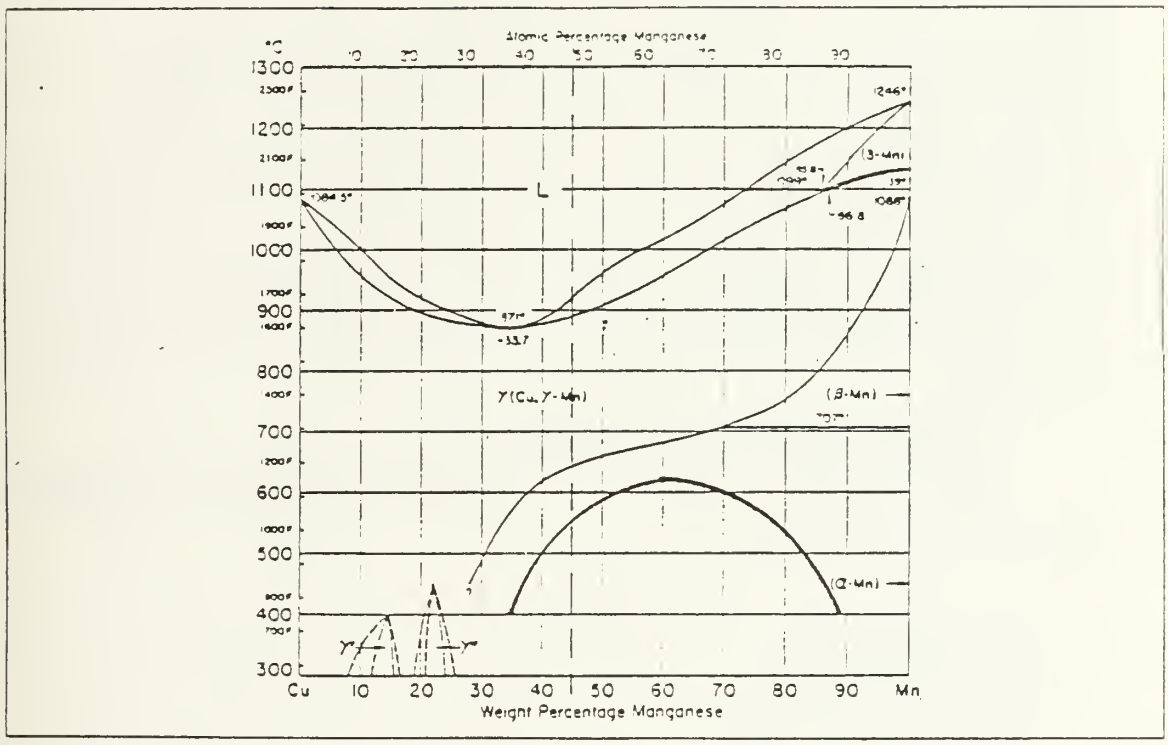

Figure 1.8 Phase Diagram of Copper-Manganese Binary System with Miscibility Gap.

Vitek and Warlimont [Ref. 36] used age-hardening data to determine the miscibility gap, based on the fact that an alloy aged within the gap will be harder due to the two-phase structure. If no major change in hardness was observed before and after aging, it was concluded that the aged alloy fell outside the miscibility gap, in the

single-phase region [Ref. 36:pp. 8,10]. The immiscibility region as delineated by Vitek and Warlimont is skewed toward the Mn-rich portion of the Cu-Mn phase diagram and occurs at slightly lower temperatures than Vintaykin's. The maximum of the Vitek and Warlimont curve occurs at about 78 a/o Mn at about 575°C (850K) [Ref. 36:p. 11]. An X-ray diffraction study by Venkateswarao and Chatterjee [Ref. 39:pp. 146, 148] found that the maximum of the miscibility gap is in agreement with Vintaykin, et al, with a Mn content of 66.6 a/o, but with a temperature of about 550°C (823K), closer to the Vitek and Warlimont data.

The importance of the miscibility gap is that it assists in explaining the initial decomposition reaction of the FCC phase, in which separable regions rich in Cu and rich in Mn form [Refs. 36,37,40:pp. 10, 106, 142]. Ultimately, growth of the Mn-rich regions would lead to the equilibrium α-Mn phase[3] [Ref. 37:pp. 105-106]. However, the effects of interest here occur at relatively early aging times, where the fine-scale composition modulations apparently create a high localized driving force (ΔT) for antiferromagnetic ordering and martensitic formation when quenched to room temperature from an aging temperature within the miscibility gap. This is because T_N and M_s are effectively raised locally in the Mn-rich regions, so that quenching to room temperature may give rise to the FCC——> FCT transformation. Based on the nominal composition of INCRAMUTE, it was expected that this alloy just falls within the miscibility gap at 400°C, and so should undergo similar two-phase decomposition upon aging.

2. Damping Properties of Cu-Mn Alloys

High damping materials can be classified on the basis of the predominant internal friction mechanisms:

- composite materials
- ferromagnetic alloys
- twinned microstructures

---

[3] α-Mn has a Type A-12 structure [Ref. 41:p. 2] (Pearson symbol cI58) with a lattice parameter (a_0) of 8.9139 Å [Ref. 42:p. 740]. Initially, it preferentially precipitates at grain boundaries and then within the grains satisfying a Kurdjumov-Sachs orientation relationship with the matrix [Ref. 26:p. 2101]:

$$(111)_{matrix} \,//\, (101)_{\alpha Mn}$$
$$[110]_{matrix} \,//\, [111]_{\alpha Mn}$$

with the rod longitudinal direction of $[110]_{\alpha Mn}$ or $[111]_{matrix}$ [Ref. 28:p. 451].

The copper-manganese alloy system falls into the twin category. The development of high damping capacity in Cu-Mn alloys has often been attributed to the formation of a tetragonal martensitic twin structure [Refs. 8,24,26,28:pp. 43, 137, 2104, 451]. Because of the necessity of antiferromagnetic ordering to effect the FCC——> FCT transformation, the room temperature damping capacity, or internal friction, of as-quenched Cu-Mn is high for alloys with a Mn content greater than 82 a/o [Refs. 8,12:pp. 42, 105]. Since alloys with less than 82 a/o do not form a complete tetragonal structure when quenched to room temperature from an FCC γ-phase solution treatment [Refs. 27,28,36,39,43,44,45,46:pp. 662, 451, 8, 140, C5-973, 109, 113-114, 109], relatively low damping occurs [Refs. 10,12:pp. 126,105]. Additionally, no FCT structure whatsoever forms with a room temperature quench for less than 50% Mn alloys [Refs. 45,46:pp. 114,109]. These as-quenched Cu-Mn alloys are characterized by high ductility and low strength.

However, aging of as-quenched alloys of less than 82 a/o Mn concentration greatly enhances their damping capacity. This is due to the decomposition of the single-phase γ-FCC structure into regions rich in Cu and in Mn within the miscibility gap, effectively raising T_N and M_S. Quenching to room temperature then enables the aged alloy to form the tetragonal structure for compositions between 50 and 80 w/o Mn since $T < M_S < T_N$. This can be seen in Figure 1.9, taken from reference 45 [p. 113]. Isothermal aging causes M_S to increase and more of a volume fraction of the matrix is transformed to martensite especially at room temperature; this is especially important with regard to allowing martensite formation in low Mn alloys. It would appear that, for the three aging temperatures considered (i.e., 350°C, 400°C, and 450°C), tetragonality reaches a lower bound for a Mn content of about 50 a/o (47 w/o) at room temperature. The aging time to achieve this bound varies inversely with temperature (i.e., 120 hours at 350°C, 20 hours at 400°C, and 2 hours at 450°C). It is also evident that the band of FCC——> FCT transition temperatures (i.e., M_S and the martensite finish temperature, M_f) gradually becomes narrower as the aging time increases at any of the aging temperatures. Since INCRAMUTE lies near the middle of the compositional abscissa of the phase diagram, it may show the thermodynamic properties of either a Cu-rich or a Mn-rich alloy.

The presumed mechanism by which damping occurs in partially tetragonal alloys of < 80 w/o Mn is a cooperative realignment of the FCC matrix with the FCT martensitic twins which formed from the age-quench sequence, and/or movement of

aging time for both alloys at 400°C (i.e., 2 hours for 57 w/o and 2.5 hours for 65 w/o). Similar room temperature results can be inferred from the data presented by Bichinashvili, et al [Ref. 45:p. 114], for a 78.5 a/o Mn alloy isothermally aged at 400°C.

Damping in Cu-Mn has been studied to determine its dependency on the following:

a. aging condition [Refs. 7,8,10,11,13,24,39,44,47] – Aging effects on damping are similar to the aging effects on other mechanical properties (i.e., strength, hardness, etc.). Damping capacity should increase with aging time to a maximum condition after which an overaged condition occurs where the damping will decrease to preaged values.
b. cold work [Refs. 7,9,11] – Cold work typically has a detrimental effect on damping. Except for very light working (< 5% cold work), cold worked specimens show a drastic reduction in damping when compared to unworked material. Cold working creates a high dislocation density, thereby impeding twin boundary mobility.
c. composition [Refs. 6,10,12,13,39,47] – In as-quenched alloys, the damping does not vary considerably with Mn content. However, for equivalent aging conditions, alloys with greater Mn content will achieve higher damping values. The lower Mn alloys will achieve equivalent damping when aged for longer times or at higher temperatures for equal or shorter times.
d. test temperature [Refs. 6,7,8,10,12,13,24,26,44,47,48,49] – The effect of test temperature will depend on its value relative to the Neel temperature, T_N. For high damping capacity to be achieved, T_N must be greater than T_{test}. This is a necessary condition for damping. For alloys of greater than 80 w/o Mn content, this is easily achieved in the as-quenched condition where T_N is above room temperature. But alloys within the miscibility gap must be aged to raise T_N sufficiently where room temperature testing is below T_N. Excessive aging can cause damping to decrease due to excessive twin boundary density effectively pinning or limiting twin boundary mobility.
e. strain or stress [Refs. 8,10,11,24,44,48] – In general, damping capacity increases with applied stress or strain. However, the degree of influence stress has on damping depends on the alloy's thermomechanical history. Additionally, damping will reach a maximum value with stress beyond which further stressing will lower damping values.

Even though they did not use the term "tweed" at all, Butler and Kelly noted a directionality to their observed mottling along the [110] direction with a modulation associated with it. This modulation varied with the aging conditions and appeared to be small rods or plates (about 300 x 70 Å) in the [110] direction when the 70% Mn was aged at 425°C for 2 hours [Ref. 26:p. 2101]. Both research efforts [Refs. 26,36] found that twin formation more readily occurred in the aged alloys of higher Mn concentration or in the alloys of lower Mn aged for longer times.

Hedley's research [Ref. 24] into the aging effects on a 57 w/o Mn alloy found that a noticeable "tweed" structure occurred when aged at 400°C for about 2 hours. Microtwins progressively formed and grew on continued aging at 400°C [Ref. 24:pp. 130-131]. Their boundaries were parallel in {110} planes. His X-ray diffraction results for the aged 57 w/o Mn alloy show the tweed appeared when the lattice tetragonality commenced (i.e., 2-hour aging time at 400°C) [Ref. 24:p. 132].

Both Hedley [Ref. 24:p. 132] and Vitek and Warlimont [Ref. 36:p. 11] concluded that the formation of the mottled and tweed structures provides verification of the development of a two-phase structure upon aging within the miscibility gap of the Cu-Mn alloy system. Similar structures have been found in a variety of other alloy systems, such as Cu-Be [Ref. 50], Ni_2V [Ref. 51], β-brass [Refs. 52,53], Ti-Ni [Refs. 54,55], Cu-Al-Ni [Ref. 53], V_3Si [Refs. 56,57], Fe-Pd [Ref. 58], Ti-Al-Nb [Ref. 59], and $Ni_{58}Al_{42}$ [Ref. 60]. Work has also been attempted, with excellent results, in simulating the Cu-Be tweed structure in a two-dimensional computer model [Ref. 61]. Mottled and tweed structures have been linked with several different categories of phase transitions:

- order-disorder transformations in Hume-Rothery and stoichiometric alloys
- ω-phase formation
- FCC-FCT transformations

Considerable attention has been given to the relationship of mottled and tweed effects to the subsequent formation of martensitic twins. In this regard, mottled images effect, softening of the elastic shear constant or modulus [i.e., $C' = (C_{11} - C_{12})/2$], diffuse spots and satellite spots in diffraction patterns, and internal friction peaks, are all representative of anomalous behavior prior to martensite formation and have been variously termed "premartensitic", "pretransformation", "pretransitional", or "premonitory" effects.

II. OBJECTIVES

Material damping in Cu-Mn alloys has been known for over 40 years. Yet most of the research has occurred in the past 25 years, concentrating on the alloys with greater than about 60 w/o Mn.

During this period, INCRA, Inc., directed commercial research and development of INCRAMUTE, a high damping alloy with less than 50 w/o Mn. The purpose of this current research was to attempt to extend the observations and theories of damping characteristics and properties of the alloys with greater than 60 w/o Mn to INCRAMUTE with 40 w/o Mn. The following goals guided this research:

- to determine the relationship of room temperature damping properties to applied strain (or stress) under random vibrations for various aging times at 400°C
- to metallographically characterize the microstructures associated with high damping in INCRAMUTE
- to propose a theory for INCRAMUTE's damping mechanism

III. EXPERIMENTAL PROCEDURE

Sample material of the alloy INCRAMUTE (nominal composition of 58 w/o Cu, 40 w/o Mn, 2 w/o Al) was supplied by the International Copper Research Association (INCRA) in the form of a rolled plate (0.25 inch x 5.75 inch x 8.75 inch). The actual composition, as determined by Anamet Laboratories, Inc., of Berkeley, California, was:

	Cu	Mn	Al	Zn	Si	Fe	Cr	Remainder
w/o	53.1	44.8	1.61	0.1	0.08	0.06	0.05	0.20

All specimens were solution treated at 800°C for 2 hours in evacuated quartz tubes, followed by a water quench to room temperature. Aging was done at 400°C for 1, 2, 4, 8, 16, 32, and 64 hours in Pyrex tubes sealed under vacuum. Finally, the samples were quenched in water from the aging temperature. Based on the work of Butler and Kelly [Ref. 9], all specimens were stored in a freezer maintained at −22°C until they were required for testing or observation to prevent any room temperature aging which might affect the damping properties or microstructural characteristics. Additional specimens for X-ray diffractometry and electron microscopy were given an 128-hour aging treatment.

A JEOL JEM-100CX II electron microscope operated at 120kV was used for all transmission electron microscopy (TEM). Foils were prepared by rolling a section of the as-received plate to 0.0155-inch thickness. Warm rolling was required to prevent cracking. After each aging treatment, 3-mm (0.118-inch) diameter discs were punched from the foil. The discs were then jet polished using a solution of 50% H_3PO_4 and 50% H_2O with a 40-volt potential for 35-40 seconds. Static polishing was accomplished in a magnetically-stirred saturated solution of CrO_3 and H_3PO_4 at 8-13 volts, depending on the aging time. Preferential grain boundary etching occurred after jet polishing. However, this did not adversely affect TEM analysis. The average grain size, as observed in an optical microscope, was about 40 μm (Figure 3.1). Figure 3.2 shows the surface of a TEM specimen after jet polishing of as-quenched INCRAMUTE observed in the scanning electron microscope (SEM). While a jet-polished TEM specimen of INCRAMUTE aged at 400°C for 8 hours is seen in Figure 3.3.

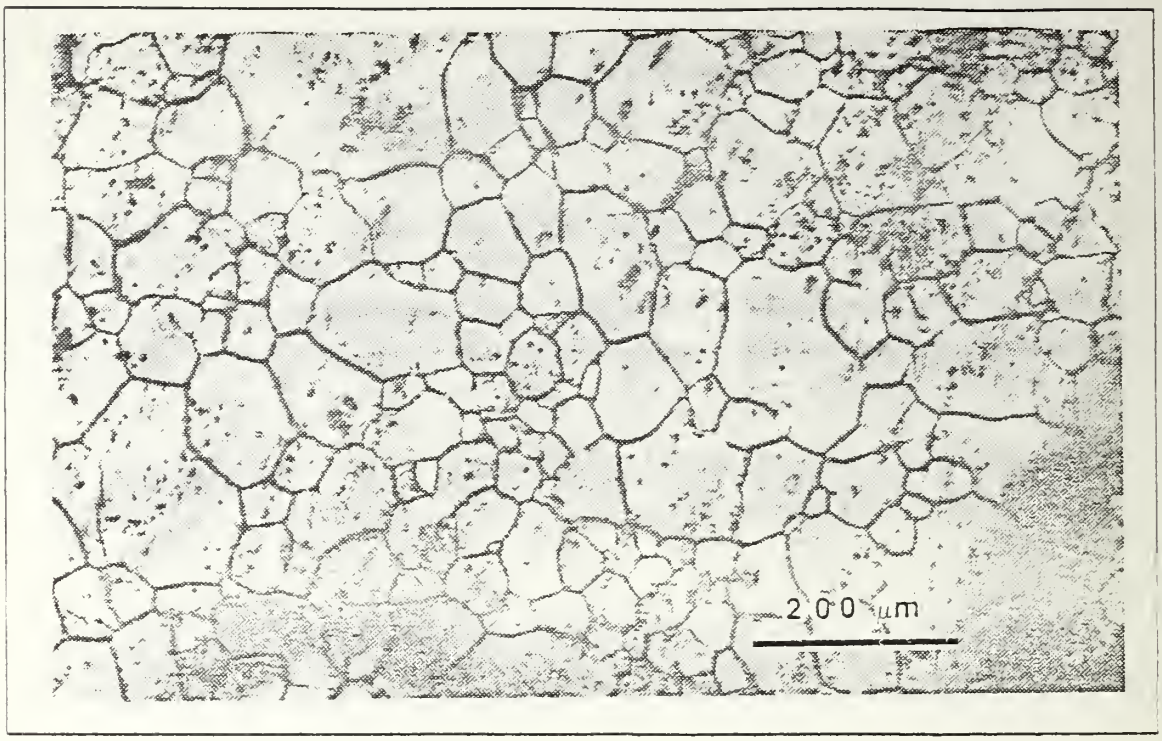

Figure 3.1 40 µm grain size in INCRAMUTE aged at 400°C for 8 Hours.

Reduced size tensile specimens were cut in accordance with Reference 62 from the as-received plate. Tensile specimens had a gage length of 1 inch with a cross section of about 0.25 inch x 0.25 inch. Post-aging tensile tests were conducted on an Instron Universal Testing Instrument Model TTD at a strain rate of 3.33×10^{-3} sec^{-1}. The tensile specimens of the as-quenched and of four of the aged conditions (1, 4, 16, and 64 hours) were tested to fracture to establish the mechanical properties of INCRAMUTE. The other tensile specimens aged for 2, 8, and 32 hours were alternately loaded and unloaded to correspond to the observed stress levels during the damping experiments which coincided with each aging treament's pseudoelastic region. Rockwell B (R_B) hardness readings were taken after tensile testing, using a Wilson Rockwell Hardness Tester Model IJR.

Specimens of 0.049-inch thickness were made to use in an optical microscope to observe the martensitic surface relief in quenched specimens from solutionizing and aging treatments. These were mechanically and, then, electrolytically polished in a solution of 50% H_3PO_4 and 50% H_2O and mounted in a cantilever-stressing jig to provide an edge-on view to the objective. Thus, both compressive and tensile loading

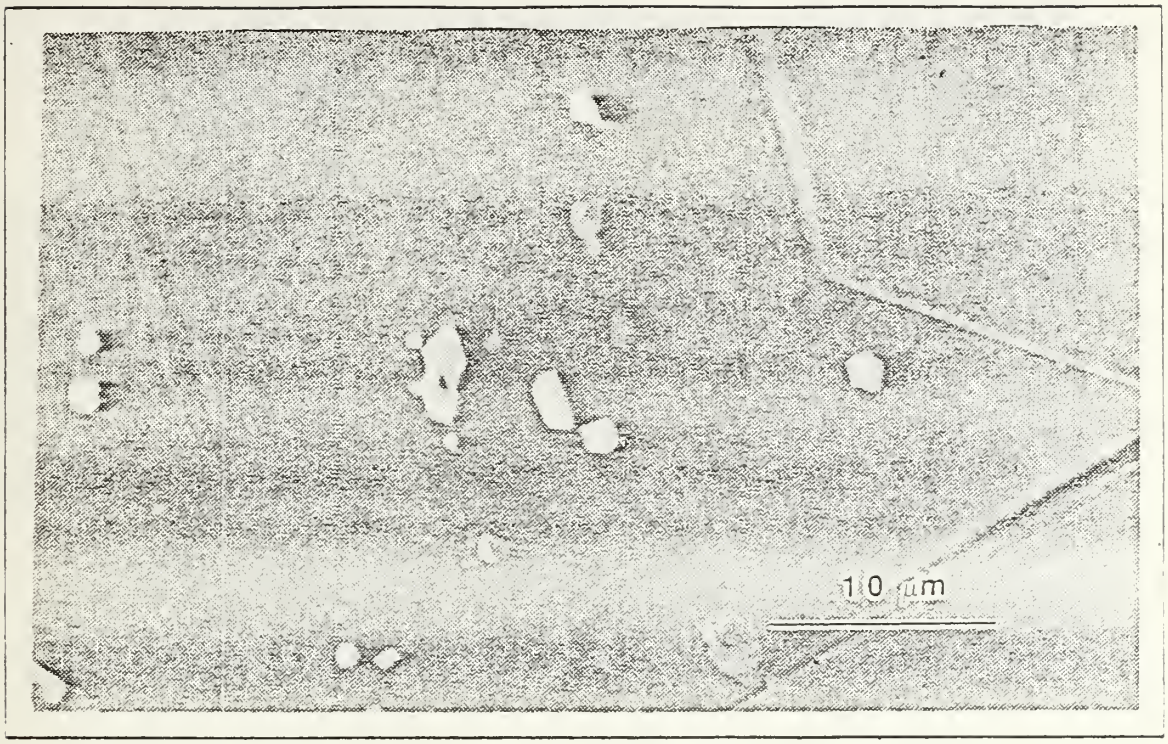

Figure 3.2 Jet-Polished TEM Specimen of As-Quenched INCRAMUTE Observed in a Scanning Electron Microscope (SEM).

effects on the twinned microstructure could be observed simultaneously under polarized light. The stressing jig is shown in Figure 3.4.

Lattice parameters were determined for the as-quenched and each aged condition. The Philipps XRG-3100 X-ray diffractometer was used with an emission of $K_{\alpha 1}$ for Cu at a wavelength (λ) of 1.5405 Angstrons ($\mathring{A}$) at a scan rate of 2°/minute.

The mass density (ρ) for each heat treatment condition was determined using the specimens for the X-ray diffraction analysis.

Damping measurements were done at room temperature in air using the resonant apparatus as described in Reference 14. The original technique involved using an optical microscope with a reticle to measure the cantilever beam tip displacement with the aid of a strobe light. A random, vibrational load is applied at the beam root and is measured by an accelerometer mounted on the grip.

The research group directed by Professor Y.S. Shin of the Naval Postgraduate School in Monterey, California, modified this arrangement by replacing the microscope and strobe light with a second accelerometer mounted at the beam tip. The signals

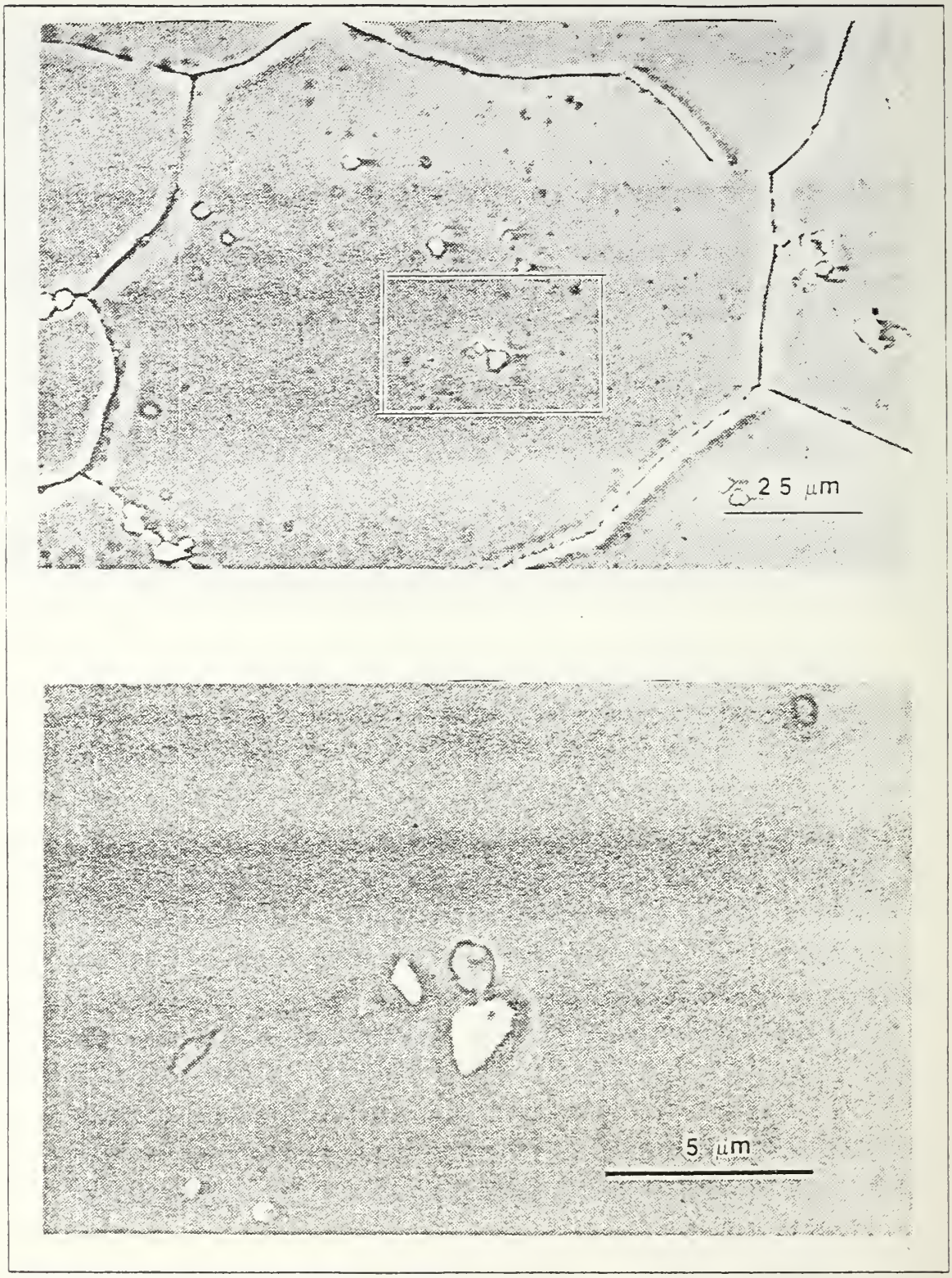

Figure 3.3 Jet-Polished TEM Specimen of INCRAMUTE Aged at 400°C for 8 Hours Observed in a Scanning Electron Microscope (SEM).

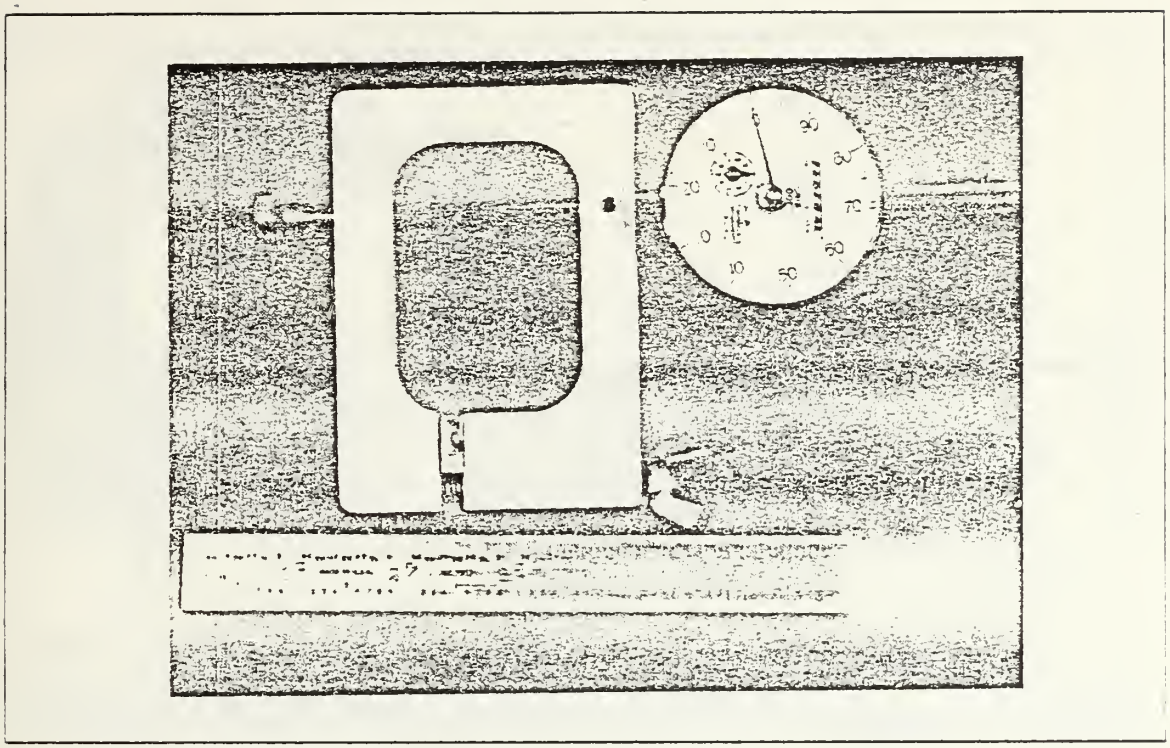

Figure 3.4 Optical Microscope Stressing Jig.

from both accelerometers are compared by a Hewlitt-Packard HP-3582A Spectrum Analyzer to produce the transfer function frequency response for the beam under random vibration. A block diagram of the system is shown in Figure 3.5 with individual components. Figure 3.6 is a photograph of the shaker and amplifier arrangement with a specimen in the grip.

The resonant frequency of the vibrating cantilever beam is a function of the specimen's Young's modulus (E), density (ρ), thickness (h), and vibrating length (L_v):

$$f_n = (h/2\pi)(C_n / L_v)^2(32\ E/\rho)^{1/2} \qquad \text{(eqn 3.1)}$$

where C_n is a constant depending on the modal response, i.e.,

Mode(n)	C_n
1	1.8751
2	4.6941
3	7.8548

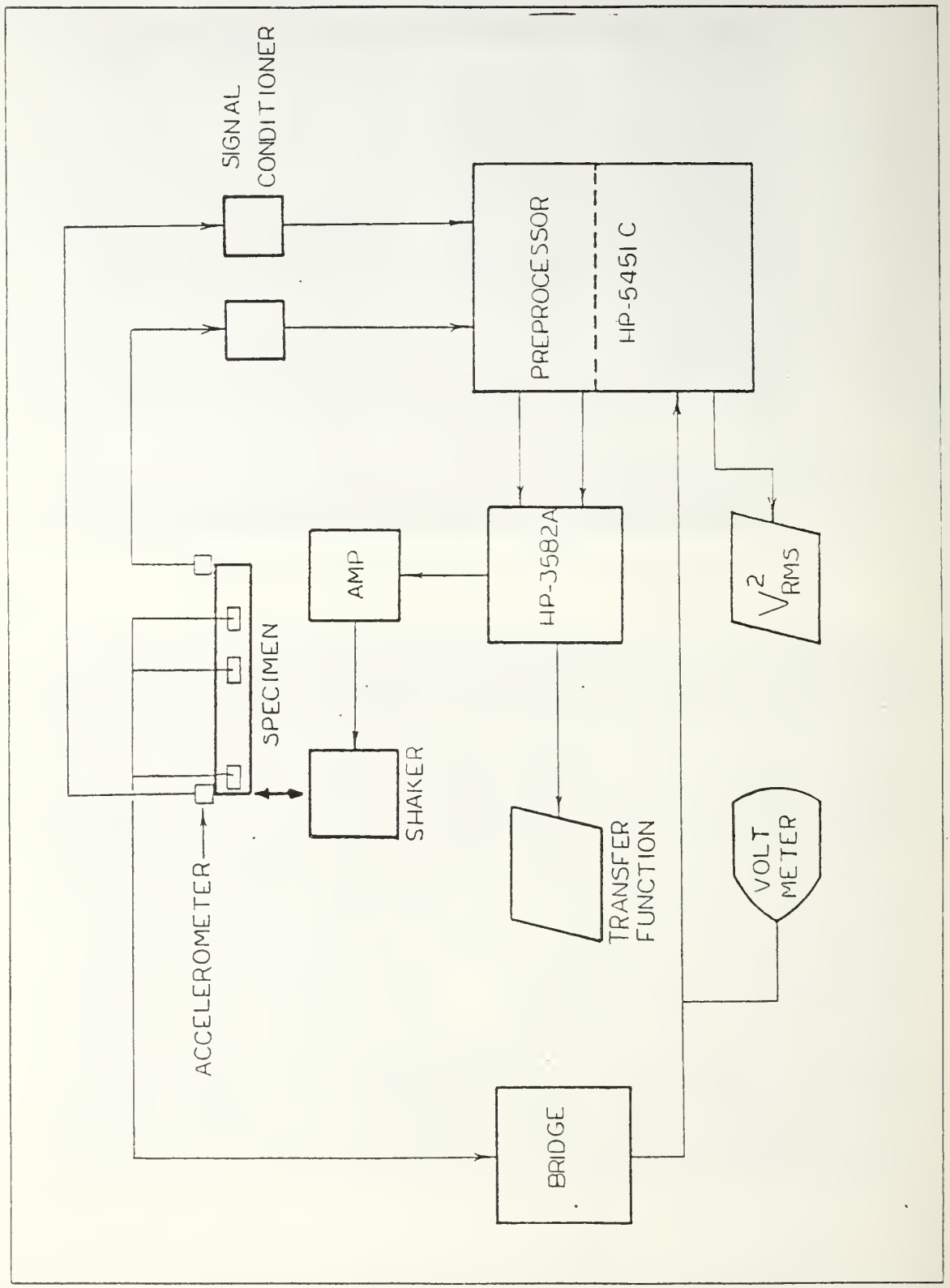

Figure 3.5 Block Diagram of Damping Experiment Components.

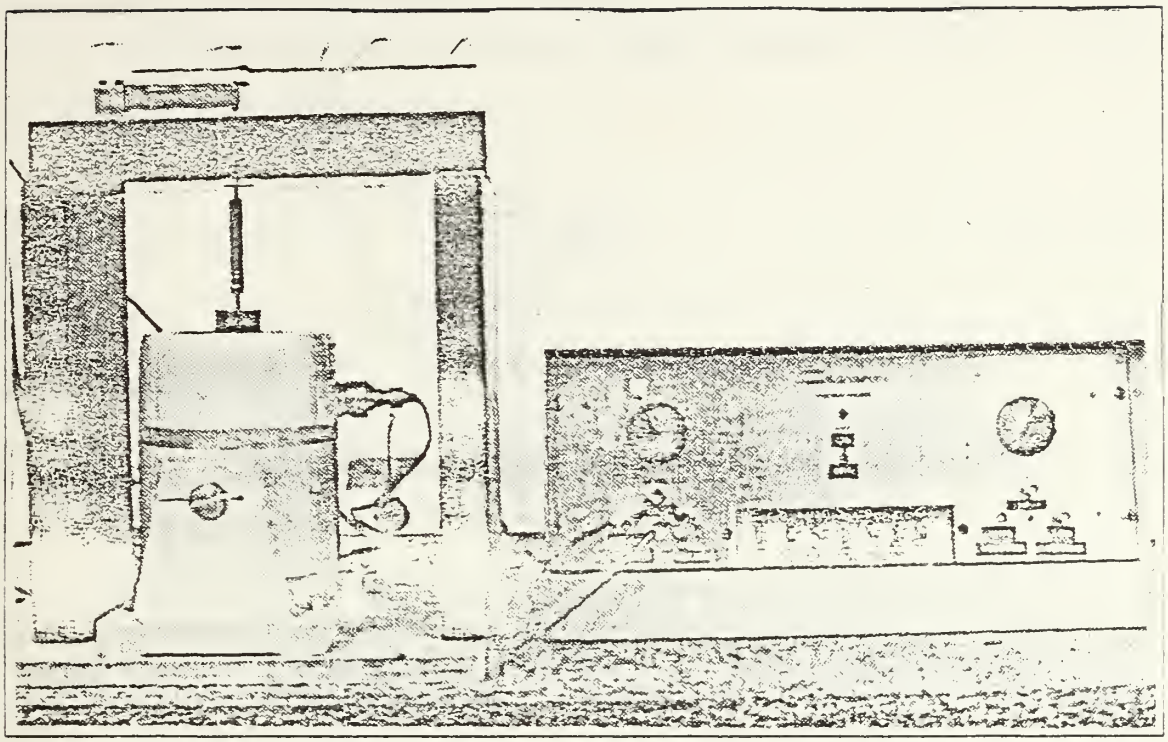

Figure 3.6 Electromagnetic Shaker Used in Damping Experimentation.

The mode 1 resonant frequency is termed the natural frequency. Each mode has a characteristic response in vertical deflection. These are shown below in Figure 3.7.

The absolute maximum stress (or strain) occurs at the root for any mode. Local maxima occur at the peaks of the modal deflection curves, or where $\partial y/\partial x = 0$. Thus, for each mode n, there are $n-1$ local maxima. Assuming a prismatic beam the vertical response of the cantilever beam is:

$$y(x) = A_n [(\sin\beta_n L_v - \sinh\beta_n L_v)(\sin\beta_n x - \sinh\beta_n x) + \quad \text{(eqn 3.2)}$$

$$(\cos\beta_n L_v + \cosh\beta_n L_v)(\cos\beta_n x - \cosh\beta_n x)]$$

where A_n is the amplitude. β_n is defined by

$$\beta_n^2 = \omega_n (m/EI)^{1/2} \quad \text{(eqn 3.3)}$$

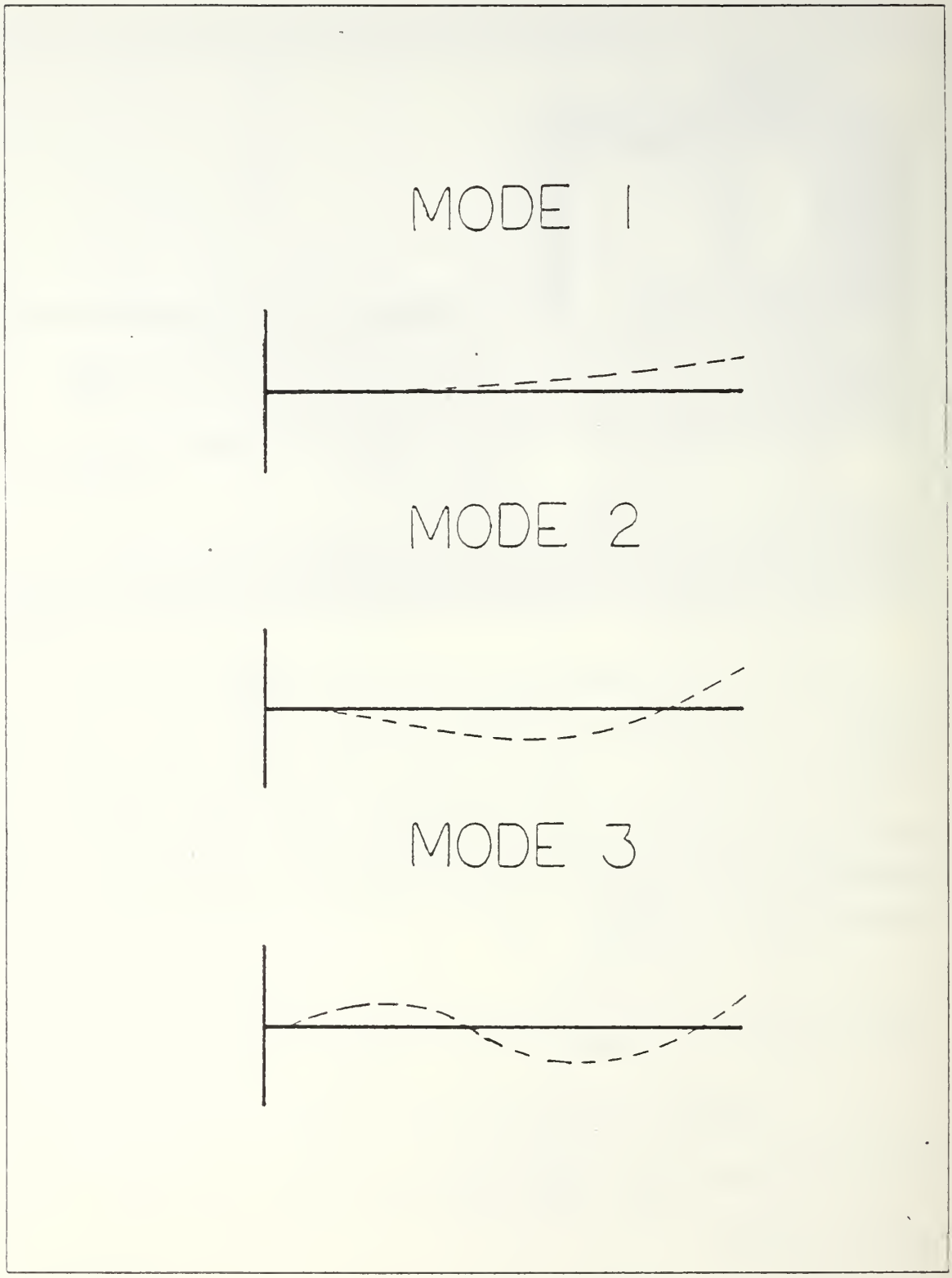

Figure 3.7 Characteristic Response of Cantilever Beam to First Three Modes of Excitation.

such that ω_n is the resonant frequency of mode n, m is the beam mass per unit length, E is Young's modulus, and I is the area moment of inertia of the beam. Using the resonant frequency definition of

$$\omega_n = C_n^2(EI/mL_v^4)^{1/2} \qquad \text{(eqn 3.4)}$$

β_n may be simplified to

$$\beta_n = C_n/L_v \qquad \text{(eqn 3.5)}$$

Normalizing the distance from the root, x, to x/L_v, the positions of the beam local maxima are found to be:

n	x/L_v
1	0.00
2	0.53
3	0.31 and 0.71

For mode 3 vibration, the supremum of the maxima occurs at $x/L_v = 0.71$. Three foil strain gages[4] were mounted at the longitudinal positions corresponding to the suprema of the maxima for each of the three modes (i.e., $x/L_v = 0.00, 0.53$, and 0.71).

Damping specimens were cut to the specifications for the resonant dwell method of Figure AIII-1 of Reference 14 and is reproduced in Figure 3.8 herein. The variable dimensions of thickness and vibrating length were selected as approximately 1/16 inch and 4.85 inches, respectively. This corresponds to a nominal mode 1 resonance at 59.42 Hz. Modes 2 and 3 resonant frequencies for these dimensions are calculated to be 372.38 Hz and 1042.74 Hz, respectively. Some interference in frequency response curves was experienced from the 60-Hz electrical source during Mode 1 excitation, though this effect diminished with increasing the applied loading. The actual specimen dimensions prior to testing are provided in Table I.

---

[4]Resistive-type strain gages (Type CEA-13-250UN-350), manufactured by Measurements Group, Inc., were used with a gage factor of $2.12 \pm 0.5\%$ and a resistance of $350\ \Omega \pm 0.3\%$.

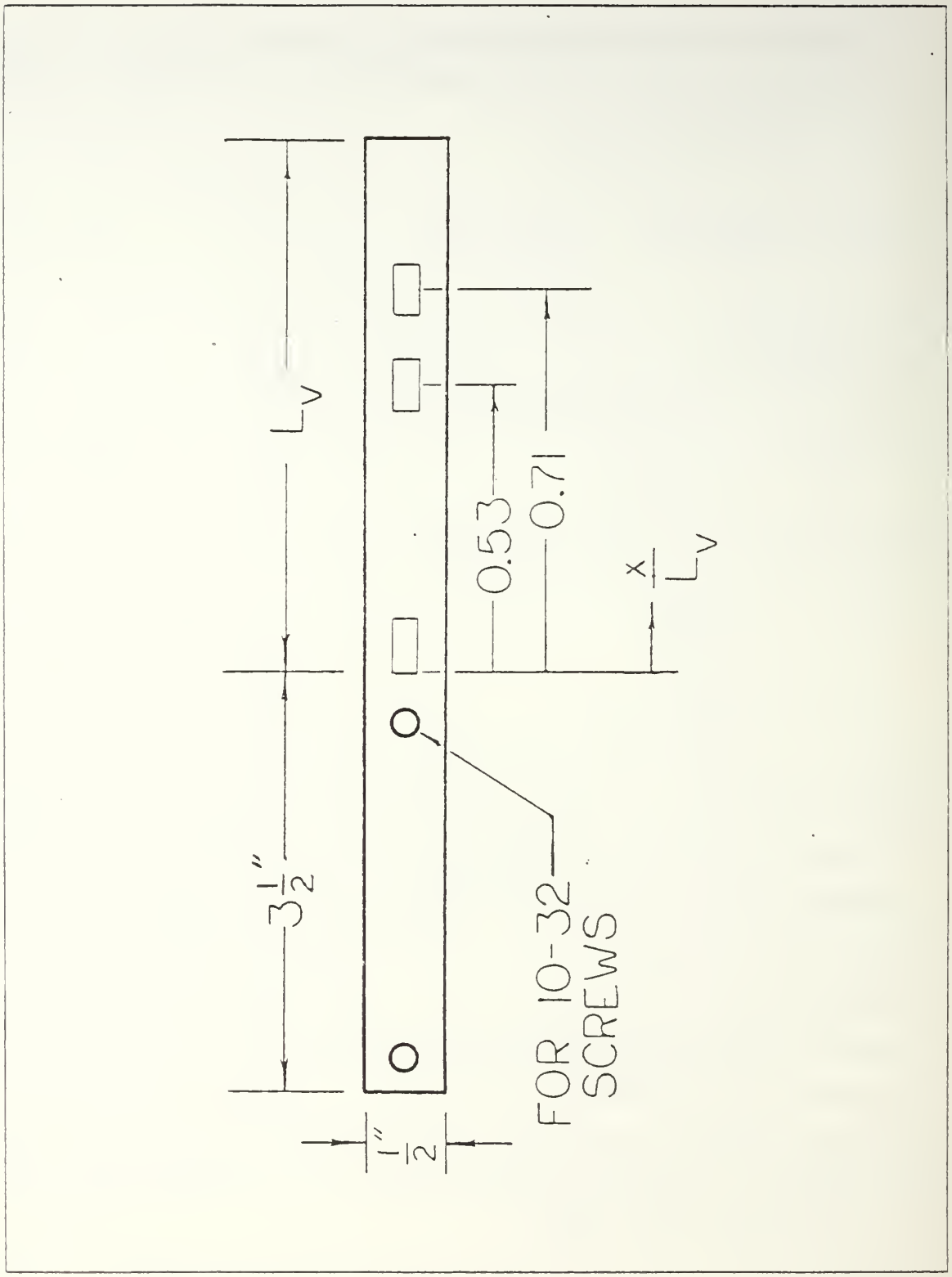

Figure 3.8 Specifications for Resonant Dwell Method Damping Specimens.

TABLE I

DAMPING SPECIMEN DIMENSIONS PRIOR TO TESTING

Heat Treatment	Thickness (inch)	Vibrating Length (inch)
STQ	0.0642667	4.8671875
Aged for 1 hour	0.0634333	4.84375
Aged for 2 hours	0.06333	4.828125
Aged for 4 hours	0.0639333	4.828125
Aged for 8 hours	0.0645	4.828125
Aged for 16 hours	0.0634	4.828125
Aged for 32 hours	0.0632333	4.828125
Aged for 64 hours	0.0632	4.8125

For each mode and loading condition, the spectrum analyzer averaged 128 data samples from the beam root and tip accelerometers to produce a frequency response. With the half-power method at resonance, Equations 1.5 and 1.11 were used to determine the specific damping capacity (SDC) from the frequency response curve for each loading and each mode of excitation. The strain was determined from the resistive voltage generated by the strain gage and amplified by the Wheatstone bridge. The HP-5451C Fourier Analyzer sampled the strain voltage for 5 seconds and a result in V_{RMS}^2 was obtained with the analyzer's algorithm. This was then converted to average peak strain, ε_{peak}, using the bridge conversion factor of 2000 $\mu\varepsilon$/V. Thus, strain- or stress-dependencies were found. The stress developed by placement of the accelerometer at the beam tip could not be ignored since this tended to decrease the resonant frequency as the mass loading was increased.

Additionally, a damping specimen of untreated 1020 steel was prepared to a natural frequency of 50 Hz to compare the damping of INCRAMUTE to that of a known poor damper. The results for the 1020 steel specimen are contained in Appendix B.

IV. RESULTS AND DISCUSSION

A. MECHANICAL PROPERTIES OF INCRAMUTE

Figure 4.1 is a composite stress-strain diagram for the as-quenched and for the 1-, 4-, 16-, and 64-hour aged tensile specimens of INCRAMUTE. The curves show the typical characteristics of precipitation hardening with aging.

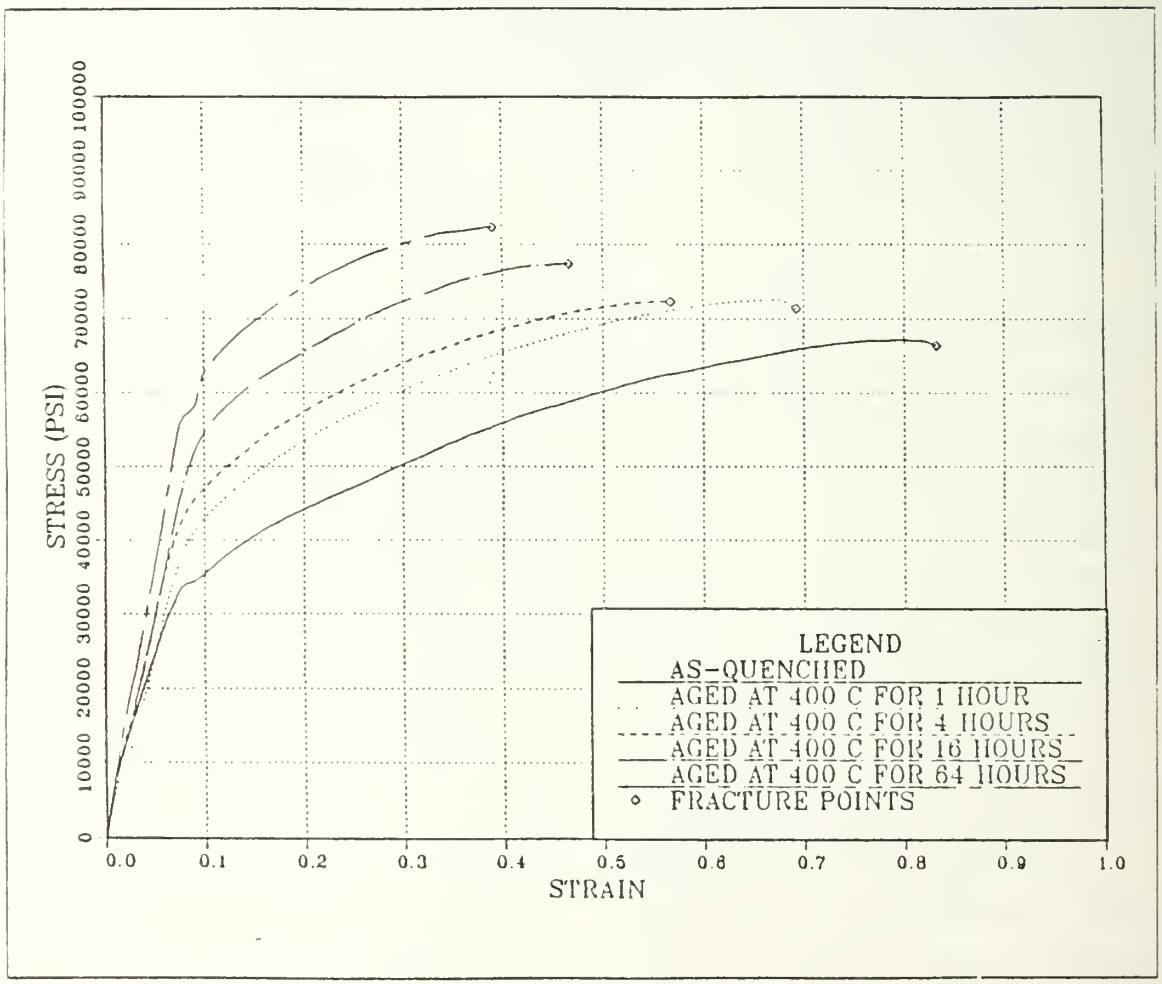

Figure 4.1 Stress-Strain Curves for Fractured Tensile Specimens.

There is a concomitant decrease in toughness, while the strength increases as aging progresses. Hardness and elongation results are provided in Table II. These

hardness values follow the same trend and are plotted[5] with the hardness data from Vitek and Warlimont [Ref. 36:p. 8] in Figure 4.2. The evolution of hardness in aged INCRAMUTE is seen to fall into the compositional pattern defined by the data of Vitek and Warlimont and exhibits a maximum hardness when aged for about 64 hours.

TABLE II

HARDNESS AND ELONGATION DATA
FROM TENSILE TESTS OF INCRAMUTE

Heat Treatment	Hardness (R_B)	Final Gage Length (inch)	Elongation (%)
AQ	72	1.453125	45.3
1-Hour Age	78	1.375	37.5
2-Hour Age*	75		
4-Hour Age	79	1.296875	29.7
8-Hour Age*	80		
16-Hour Age	85	1.265625	26.6
32-Hour Age*	88		
64-Hour Age	89	1.234375	23.4
128-Hour Age*	86		

* NOTE: Hardness readings for these aging conditions were taken after tensile hysteresis tests. Specimens were not fractured nor plastically deformed. Hardness for the 128-hour aging was determined from the XRD specimen.

Appendix A contains scanning electron microscope (SEM) photographs of the fracture surfaces of each tensile specimen. It can be seen that ductile rupture characteristics decrease with aging and a marked brittle character is quite evident in the specimen aged for 64 hours. Also, no inclusions existed in the dimple-type rupture features of the as-quenched INCRAMUTE, though small second-phase particles appear in the aged specimens. It was noted that occasionally these particles appeared at the tips of cracks which had developed interior to the specimen. This would attest to the hardening characteristics of the aging process in INCRAMUTE.

[5]Rockwell B (R_B) hardness values were converted to Vickers hardness (H_V) using Table 4 for cartridge brass (70% Cu - 30% Zn) from Reference 63 [p. 334].

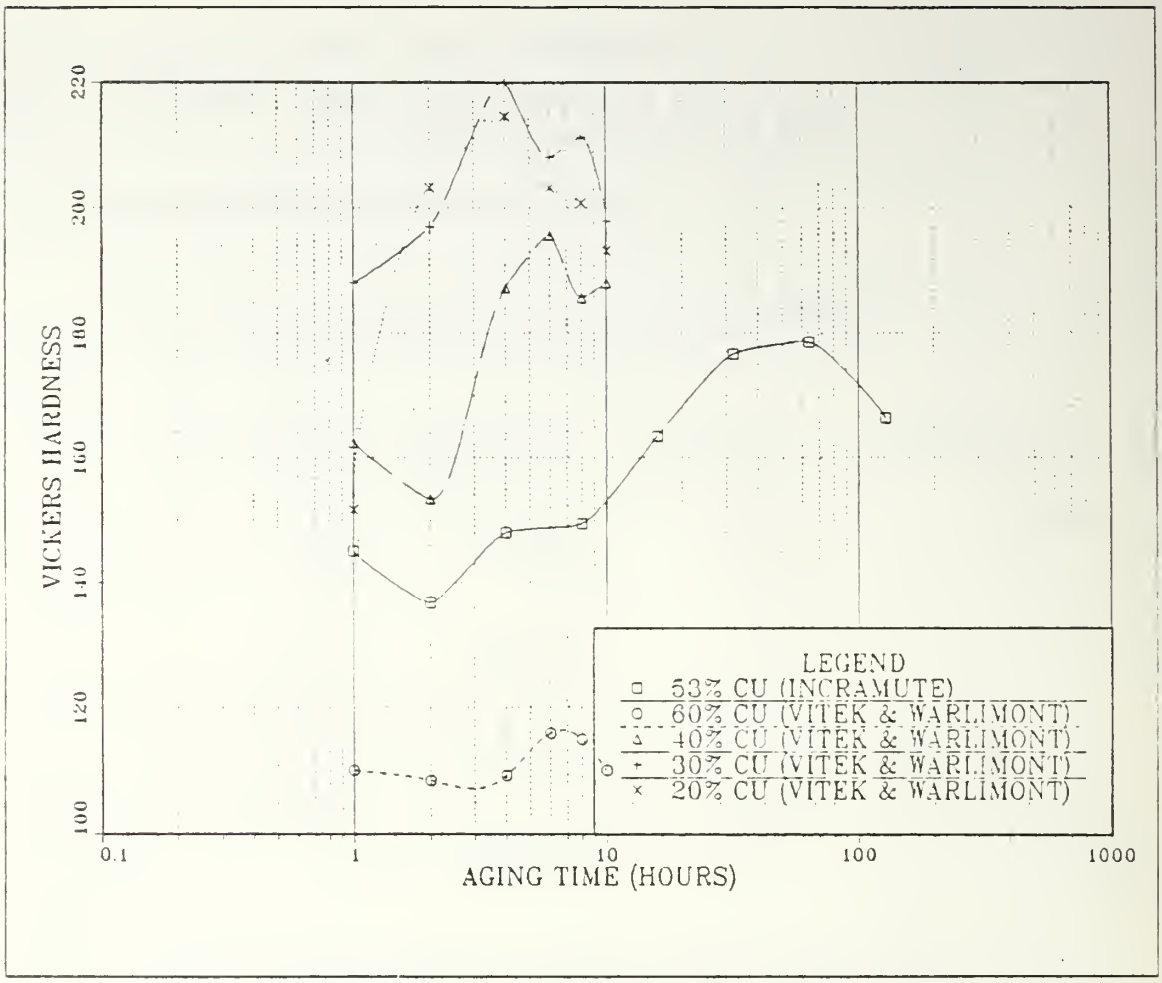

Figure 4.2 Effect of Alloy Composition on Aging Response.

It was expected that the pseudoelastic behavior described previously would exhibit a more pronounced shift, or "jog", in the elastic region as the aging progressed to a condition of maximum damping, as explained in Section I.C. and seen in Figure 1.3. However, it is evident and consistent with usual precipitation hardening effects that the linear elastic region of the curve becomes more distinct, with an evident increase in both Young's modulus and yield points with aging.

Cyclic hysteresis tests were conducted in tension for specimens aged for 2, 8, and 32 hours. Loading to and unloading from 500, 750, 1000, and 1500 lbs for each specimen are shown in Figures 4.3, 4.4, and 4.5, respectively. The loading is normalized for each respective reduced cross sectional area. Unloading is typified by anelasticity such that subsequent loading forms a narrow loop representing the energy absorbed.

Each of these hysteresis responses are pseudoelastic in nature. Comparing the corresponding loops generated among the three heat treatments reveal that nearly all are of approximately equal area. The 32-hour aged sample shows a loop nearly double in area than the other two for the condition of loading to 750 lbs subsequent to unloading from 500 lbs. It is also evident that increasing the aging time in INCRAMUTE increases the strain experienced for equivalent stress levels. The 32-hour aged specimen showed the greatest strain or the most pronounced pseudoclastic behavior.

Figures 4.6 through 4.9 represent the previous hysteresis loading unloading data replotted for each loading condition (i.e., Figure 4.6 for 500 lbs, 4.7 for 750, 4.8 for 1000, and 4.9 for 1500). The graphs compare the loading response for each aging condition (2, 8, and 32 hours). All curves exhibit a characteristics of hysteresis, i.e., energy dissipation, and display a residual strain.

It appears that for the lowest loading condition at 500 lbs (Figure 4.6) the 8- and 32-hour aged specimens display similar energy loss traces, while the 2-hour one is somewhat less. The loading portion for each of these are nearly identical. In Figures 4.7 and 4.8 at 750- and 1000-lb loadings, respectively,the 8- and 32-hour aged specimens now diverge more from the 2-hour aged specimen, such that the hysteresis mechanism for these two is more enhanced. The curve shapes for the 8- and 32-hour aged specimens in Figures 4.7 and 4.8 (loading and unloading) are quite similar indicating that the same mechanism is now at work in them. This shape is distinct from the one displayed by the 2-hour aged specimen in Figures 4.7 and 4.8. Lastly, each specimen reacts identically when loaded to and unloaded from 1500 lbs (Figure 4.9), but the area mapped out is directly related to the aging time.

It can also be seen in each of the loading diagrams, the point corresponding to point 2 in Figure 1.3 has a distinct characteristic in that the loading curve abruptly changes direction; this feature is observed under all loadings of the 32-hour aged specimen and commencing for upwards of the 750-lb loading for the 8-hour aged one. This same mechanism for the 2-hour aged specimen is not energized until it is loaded to 1500 lbs.

The following summarizes the tensile hysteresis tests conducted on INCRAMUTE:

a. The parent phase Young's modulus did not vary with aging time (Figure 4.6).

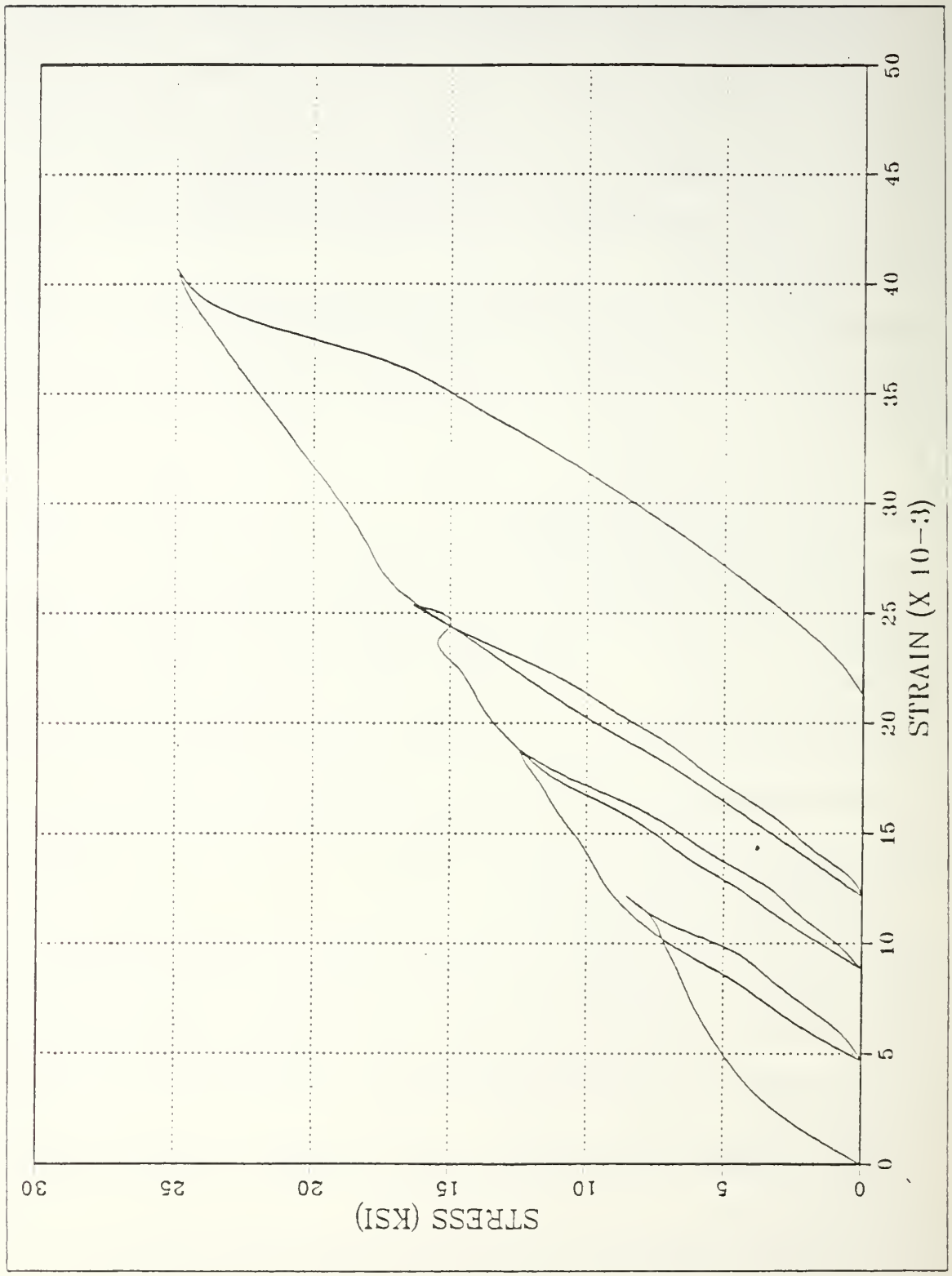

Figure 4.3 Hysteresis Response of 2-Hour Aged Tensile Specimen of INCRAMUTE Cyclically-Loaded in Pseudoelastic Region.

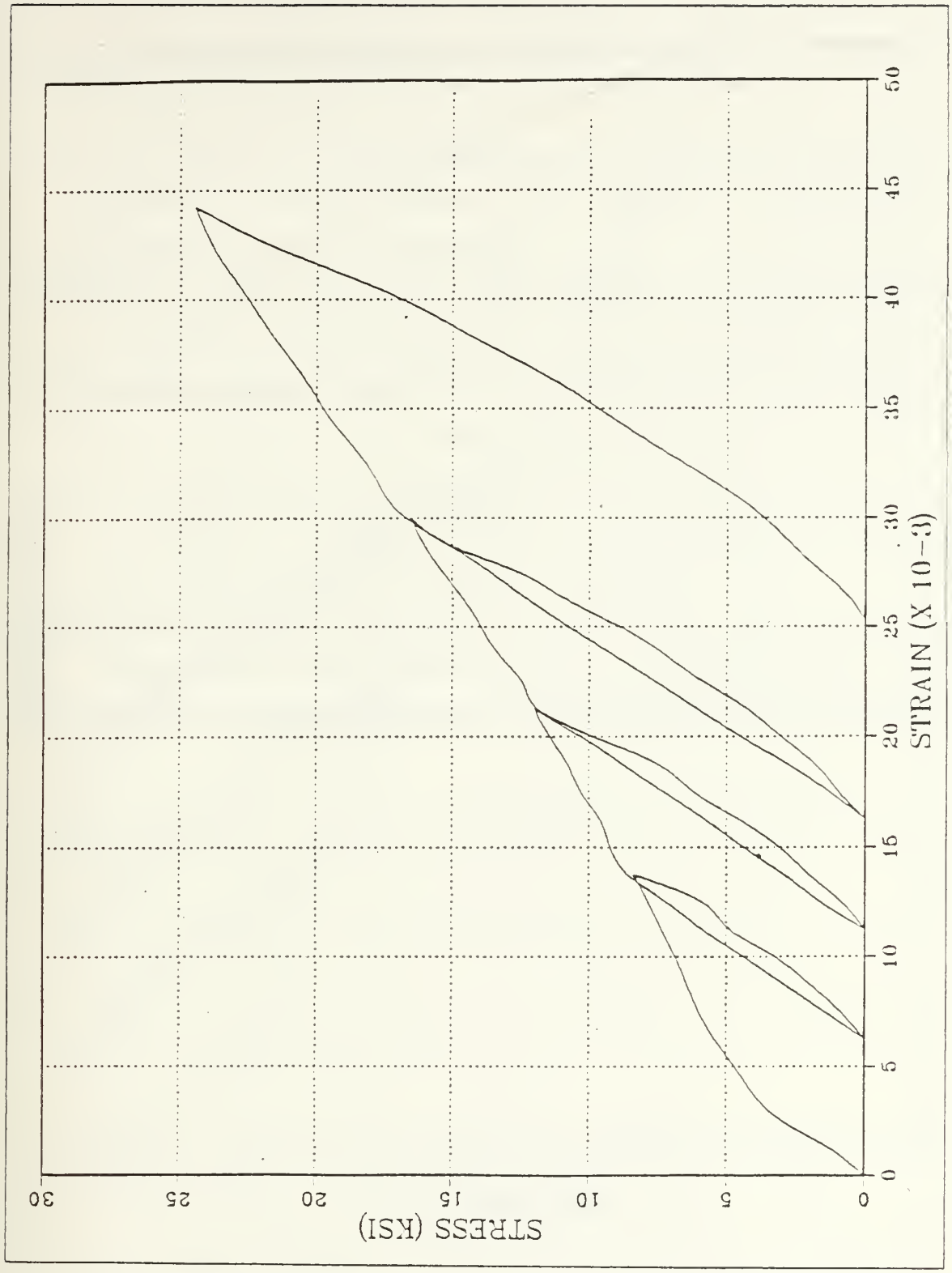

Figure 4.4 Hysteresis Response of 8-Hour Aged Tensile Specimen of INCRAMUTE Cyclically-Loaded in Pseudoelastic Region.

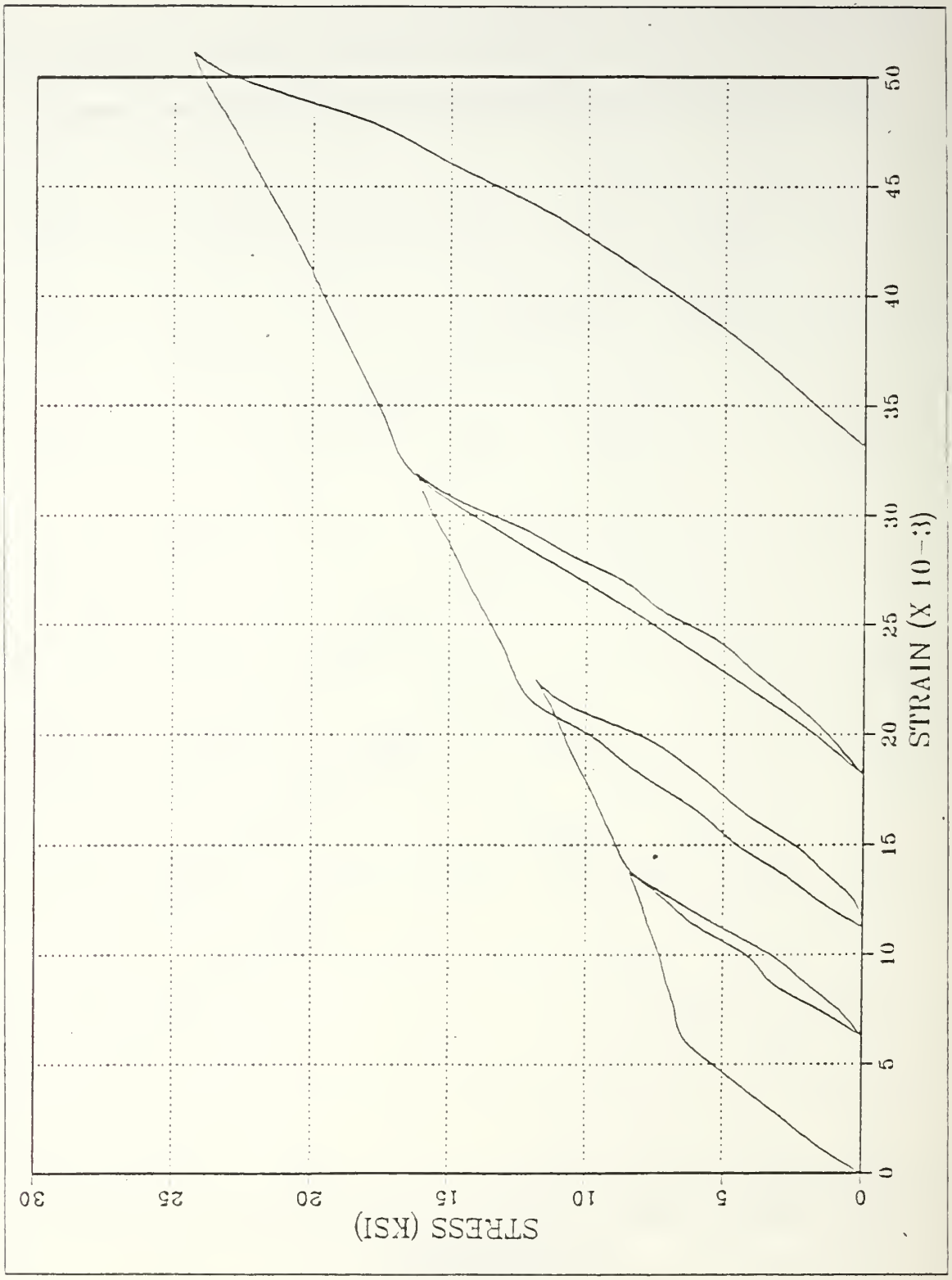

Figure 4.5 Hysteresis Response of 32-Hour Aged Tensile Specimen of INCRAMUTE Cyclically-Loaded in Pseudoelastic Region.

b. At very low stresses (i.e., 500-lb applied load), the martensitic formation and austenitic retransformation rates are approximately the same for each aging time, but the 2-hour aged specimen had the least energy absorption.

c. Austenitic retransformation upon unloading proceeded at the same rate as the elastic loading of the parent phase regardless of aging time. This implies that a relaxation, or recovery, modulus, equal in magnitude to Young's modulus, governs the austenitic retransformation.

d. Based on the shapes of the loading portions of the hysteresis curves, INCRAMUTE should be partially martensitic upon quenching from the aging condition. This can be inferred from the slopes of the curves from the martensite nucleation stress to the full load condition (i.e., slope of hysteresis curve from points 2 to 3 in Figure 1.3). Aged-and-quenched INCRAMUTE may, on the other hand, be saturated with martensitic twins due to the limited Mn content. Then the pseudoelasticity is a consequence of twin growth from the reorientation of the FCC austenitic phase to the FCT structure of the twins. This is called elastic twinning [Ref. 21:pp. 1538-1539].

e. The same mechanism is activated for the 8- and 32-hour aged specimens for any loading condition, while the 2-hour aged one must be highly loaded to achieve the same curve shape corresponding to the mechanism in longer aging times.

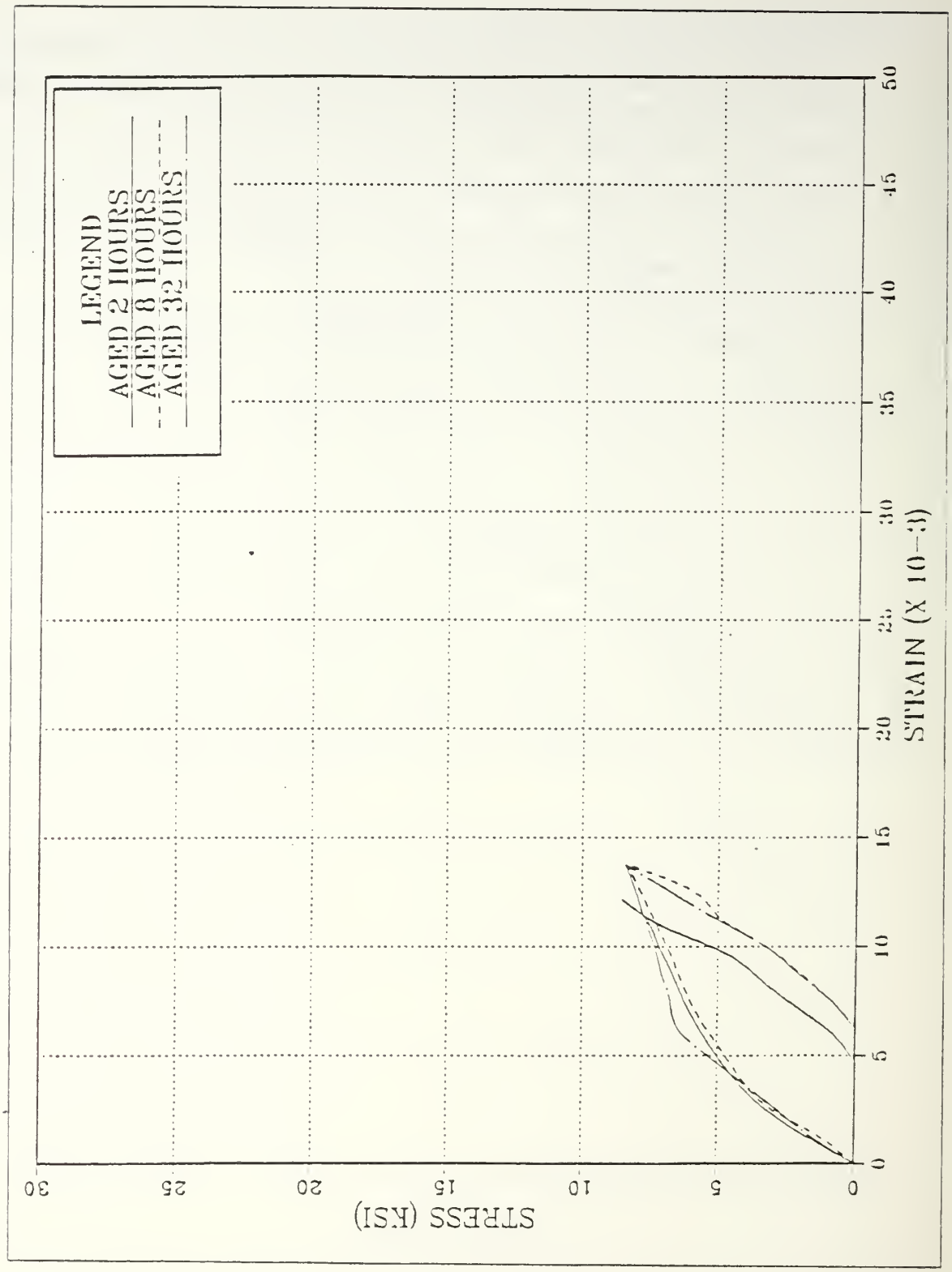

Figure 4.6 Hysteresis Characteristic Developed by Specimens Tested in Tension to 500 lbs.

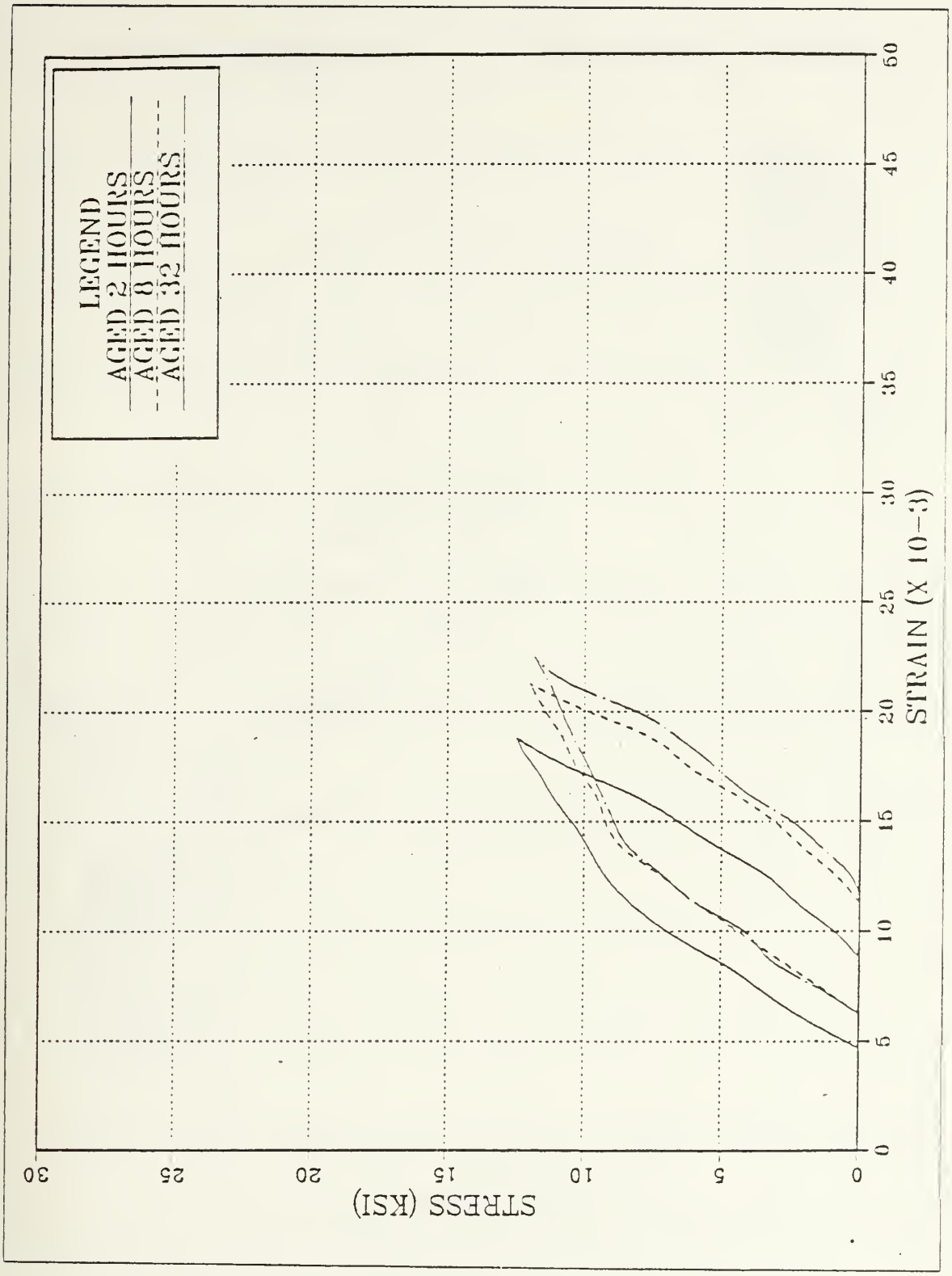

Figure 4.7 Hysteresis Characteristic Developed by Specimens Tested in Tension to 750 lbs.

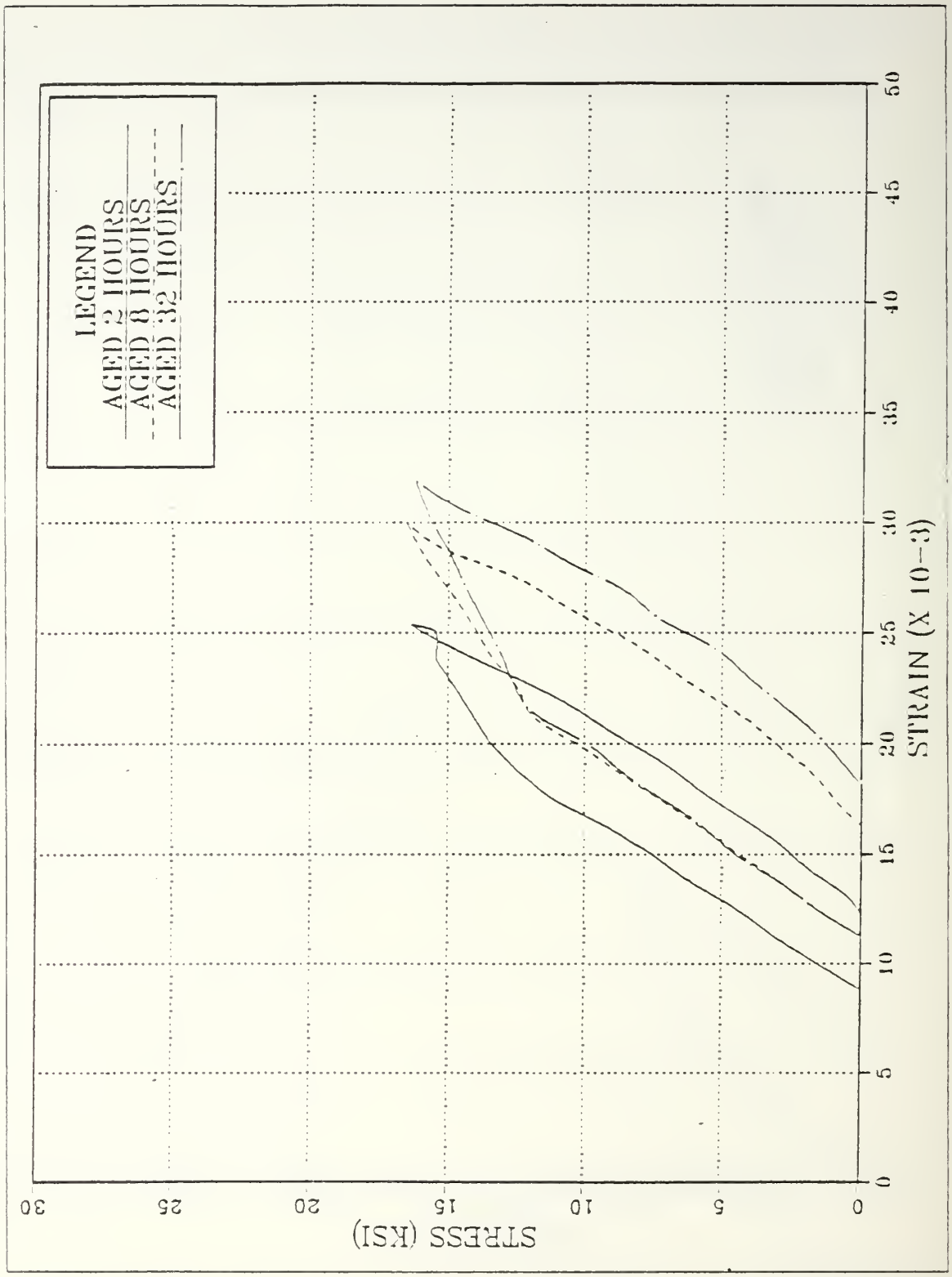

Figure 4.8 Hysteresis Characteristic Developed by Specimens Tested in Tension to 1000 lbs.

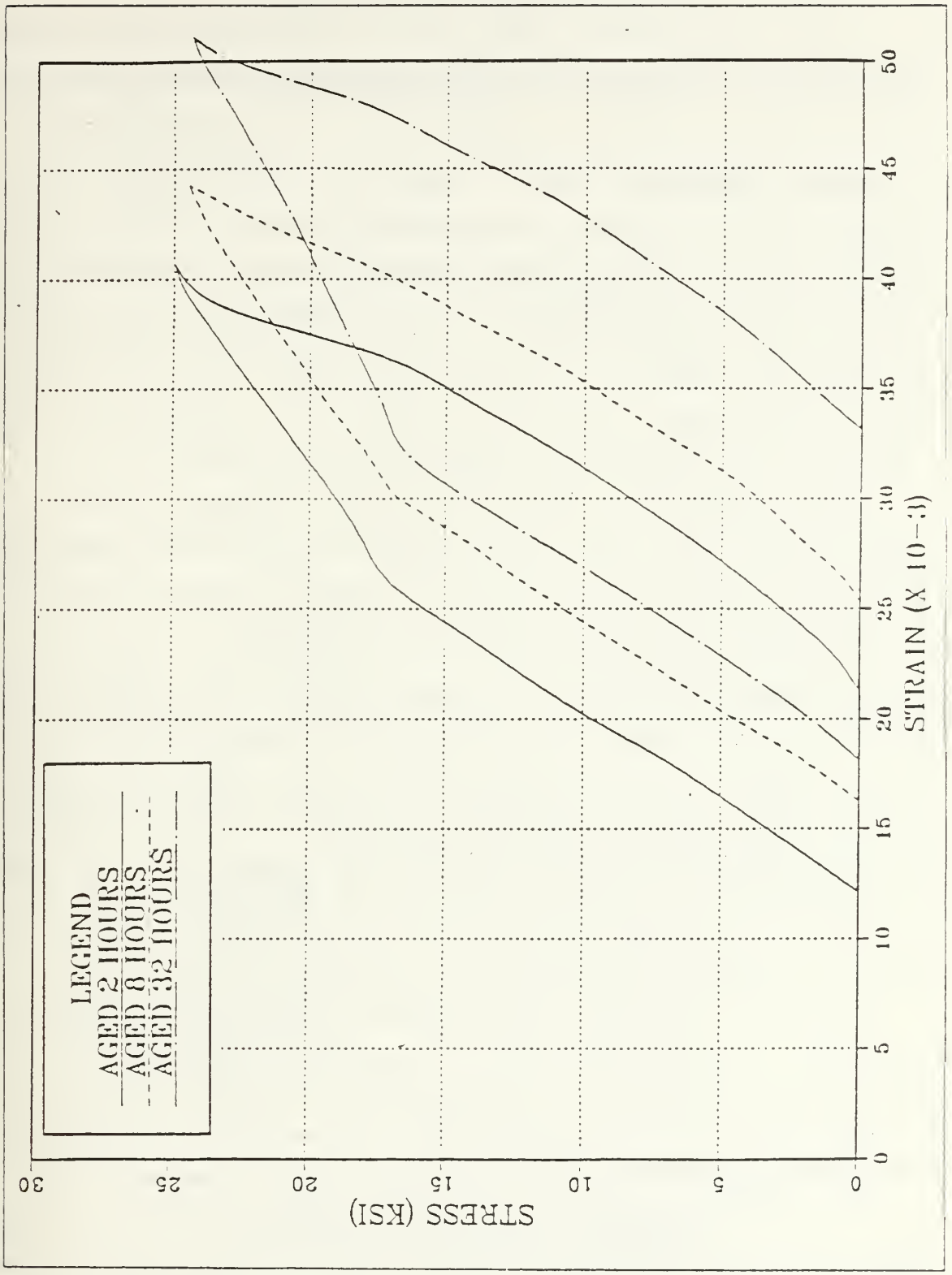

Figure 4.9 Hysteresis Characteristic Developed by Specimens Tested in Tension to 1500 lbs.

B. DAMPING CHARACTERISTICS OF INCRAMUTE

Specific damping capacity (SDC) values for INCRAMUTE for each mode and heat treament condition are plotted versus the average peak strain, ε_{peak}, in Figures 4.10, 4.11, and 4.12. For Mode 1 resonance, appreciable strain-dependence does not occur until INCRAMUTE has been aged for 4 hours; for aging times higher than this, a significant dependence of SDC on strain is seen. The damping is relatively strain-independent, or constant, for the as-quenched condition and for the specimens aged for 1 and 2 hours. The as-quenched specimen exhibited the lowest SDC values at about 9% throughout the loading range. The largest damping levels were achieved by the 16-hour aged specimen with SDC_{max} = 68% at $\varepsilon_{peak} = 2.27 \times 10^{-3}$. Damping fell off with further aging where it appeared that both the 32- and 64-hour agings had about the same damping levels. Even for these apparently "overaged" conditions, SDC values of about 30% were observed at moderate to high strain levels.

Examining Figures 4.11 and 4.12, which show the resonance for Modes 2 and 3, respectively, very little, if any, strain dependence is seen; the same approximate damping and the same relative damping levels are preserved between the various aged conditions; this is true for both Mode 2 and Mode 3 resonances.

The 16-hour aging condition exhibits some interesting features. When the second and third harmonics were observed, the specimen reversed its relative position to the other heat treament conditions (i.e., it showed the lowest damping levels in Modes 2 and 3). However, as strain is increased (the right side of Figure 4.11), a greater strain-dependence than other heat treatment conditions is displayed. In fact, this specimen was the only one to show a monotonically increasing SDC with applied strain over the strain range of Mode 3 and Mode 2; as can be seen in Figures 4.12 and 4.11, all other heat treatment conditions were relatively constant or decreased with strain. (Note especially the trend of the 8-hour aged specimen in Mode 3.)

In Figures 4.13-4.20, each heat treatment's strain-dependence is plotted by incorporating all three harmonic modes of vibration on one graph. Even though the data are discontinuous from mode to mode, the ΔSDC in overlapping strain regions is not more than about 10% (i.e., $\zeta = 0.016$). Thus, it is assumed that strain-dependent damping can be considered continuous in these regions of overlapping strain.

It is apparent in comparing the damping levels among the as-quenched specimen (Figure 4.13) and the 1- (Figure 4.14), 2- (Figure 4.15), and 4-hour (Figure 4.16) aged specimens do not show any significant strain dependency. In fact, SDC is relatively

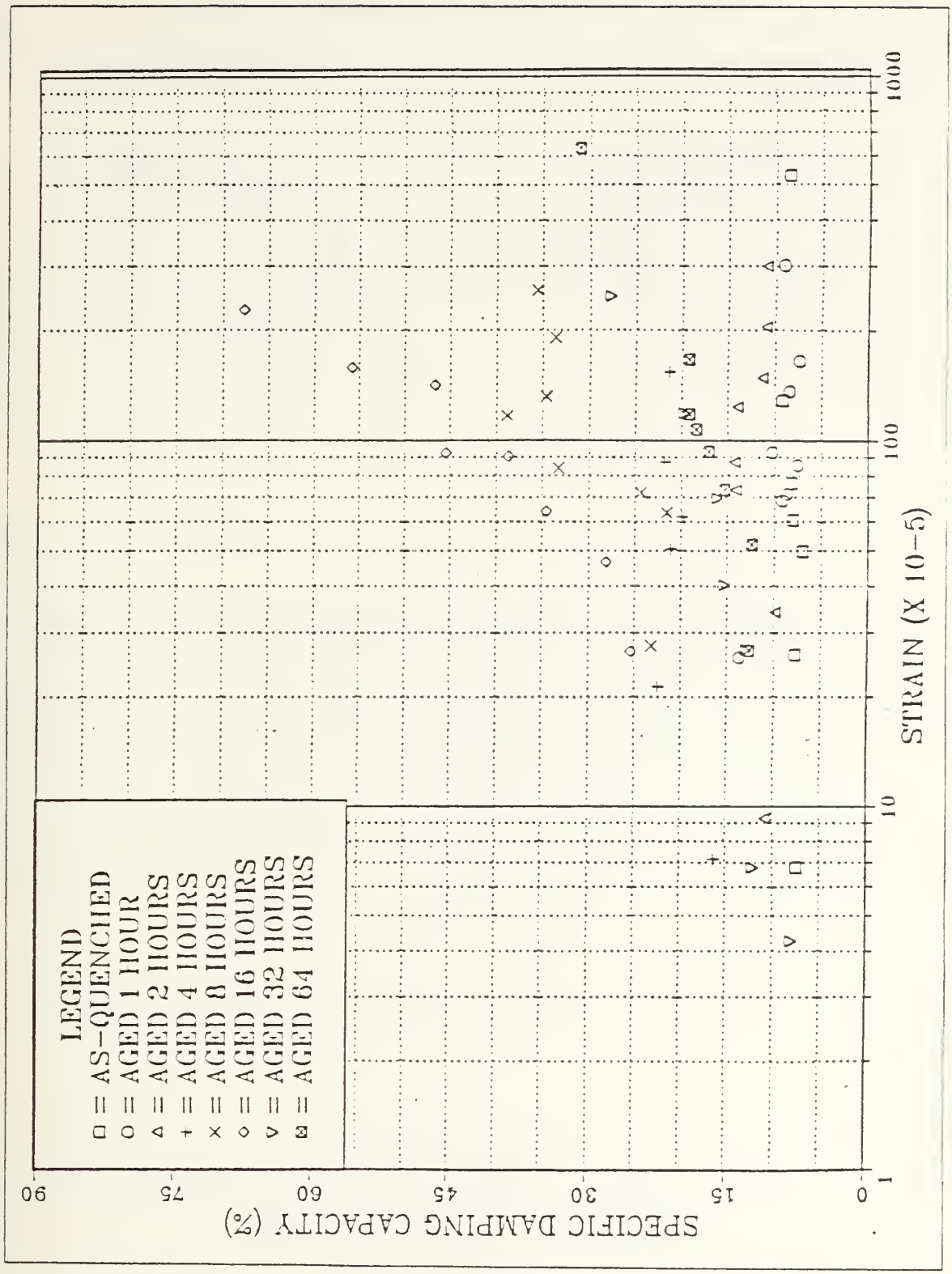

Figure 4.10 Mode I Damping Characteristics of INCRAMUTE for Various Heat Treatments and Strain Levels.

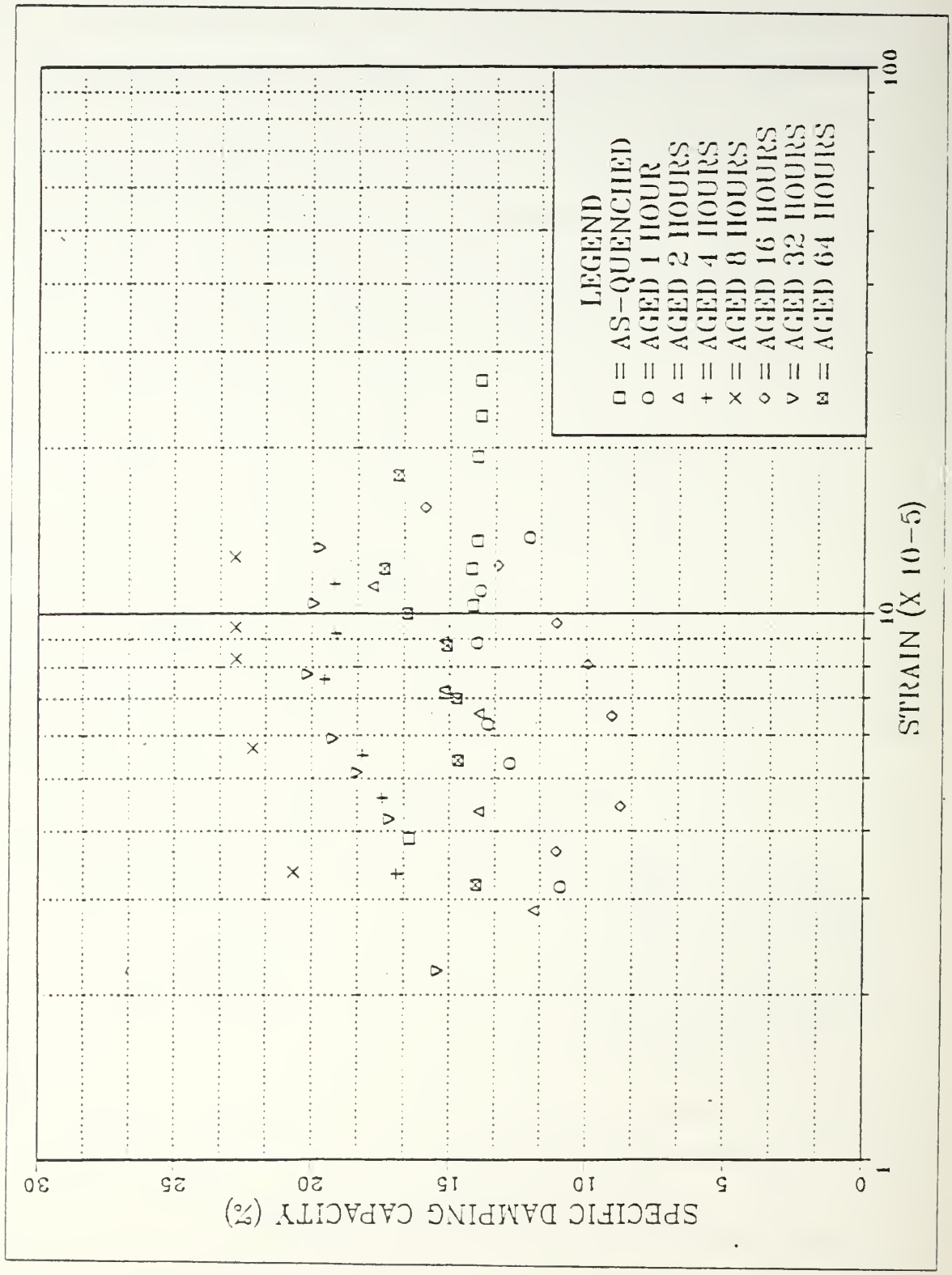

Figure 4.11 Mode 2 Damping Characteristics of INCRAMUTE for Various Heat treatments and Strain Levels.

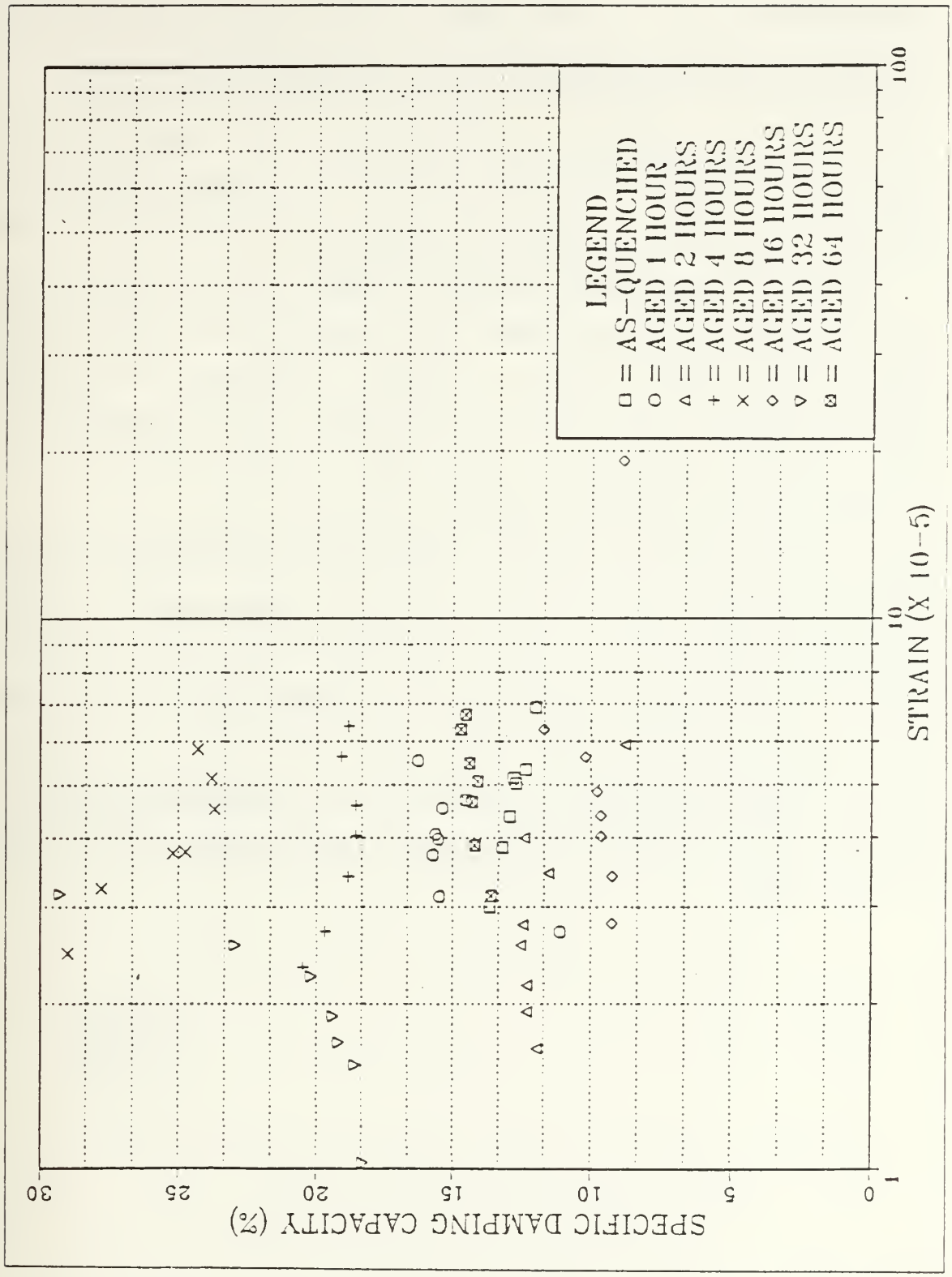

Figure 4.12 Mode 3 Damping Characteristics of INCRAMUTE for Various Heat Treatments and Strain Levels.

constant throughout the applied strain range. The damping is about the same for the as-quenched and the 1- and 2-hour agings. The 4-hour aged specimen exhibited an uniform increase in SDC to about 20% throughout the strain range.

It is not until INCRAMUTE is aged for 8 hours at 400°C that any significant strain relationship to damping is evidenced (Figure 4.17). SDC begins to increase at $\varepsilon_{peak} \sim 7.2 \times 10^{-4}$ and reaches maximum in SDC ~ 39% at $\varepsilon_{peak} \sim 11.67 \times 10^{-2}$, after which SDC leveled off at a value of about 35%. This would signify for this aging condition, INCRAMUTE's damping capacity becomes saturated.

The 16-hour aged specimen (Figure 4.18) shows a strain continuity between modes and displays a significant increase in SDC above $\varepsilon_{peak} \sim 1.0 \times 10^{-4}$. This aging condition did not exhibit a plateau, or saturation, but appeared to monotonically increase with applied strain. Since this is highly unlikely, it must be assumed that the strain required to saturate the 16-hour aged specimen was not attained ($\varepsilon_{saturate} \geq 2.27 \times 10^{-3}$ where SDC ~ 68%).

Figures 4.19 and 4.20 show the relationship of SDC to ε_{peak} for the 32- and 64-hour aged specimens, respectively. They show nearly identical damping relationships to strain. These two can be considered overaged conditions of damping where the SDC values are about one-half of the 16-hour aging's. Both of these two aging conditions show a marked increase in SDC at ε_{peak} of about 7.0×10^{-4}. Since the SDC curve for the 64-hour aged specimen did not decrease below the values for the 32-hour aging, it would appear that overaging does not cause a damping relaxation to the SDC values of as-quenched INCRAMUTE. But an overaged-limiting value for damping may be a premature conclusion since damping specimens were not aged beyond 64 hours.

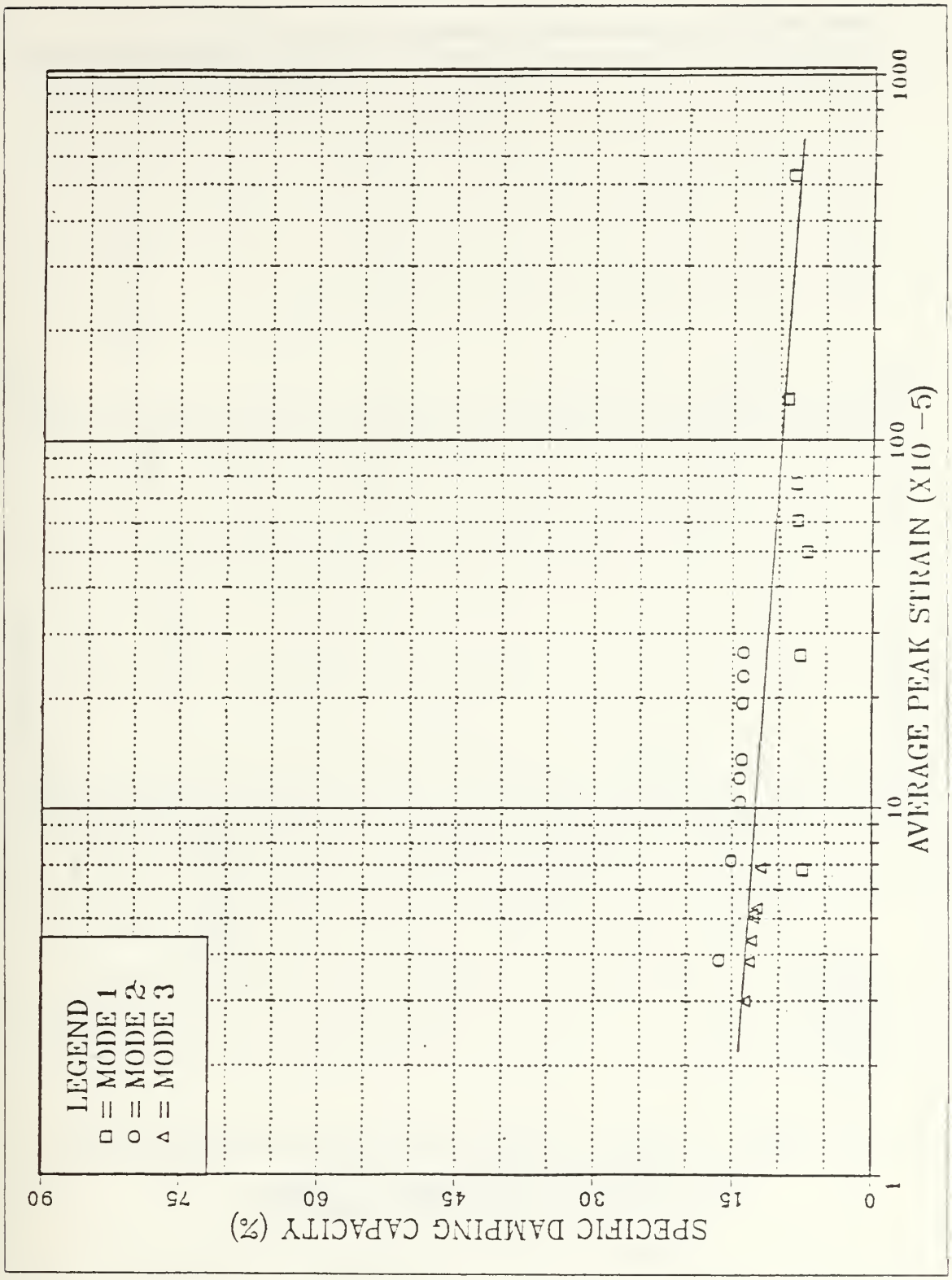

Figure 4.13 SDC-Strain Relationship for As-Quenched INCRAMUTE Under the First Three Harmonic Modes.

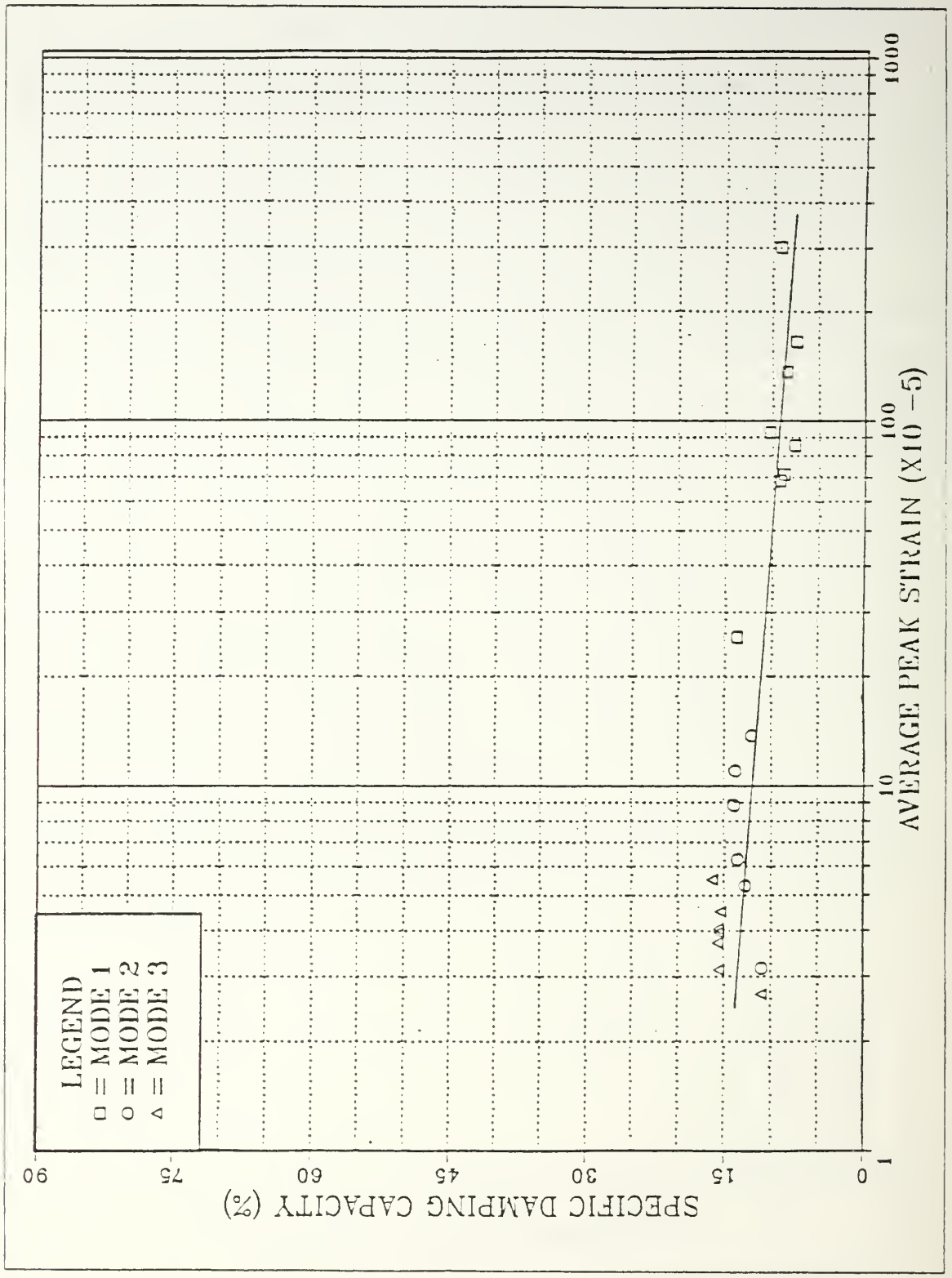

Figure 4.14 SDC-Strain Relationship for INCRAMUTE Aged at 400°C for 1 Hour Under the First Three Harmonic Modes.

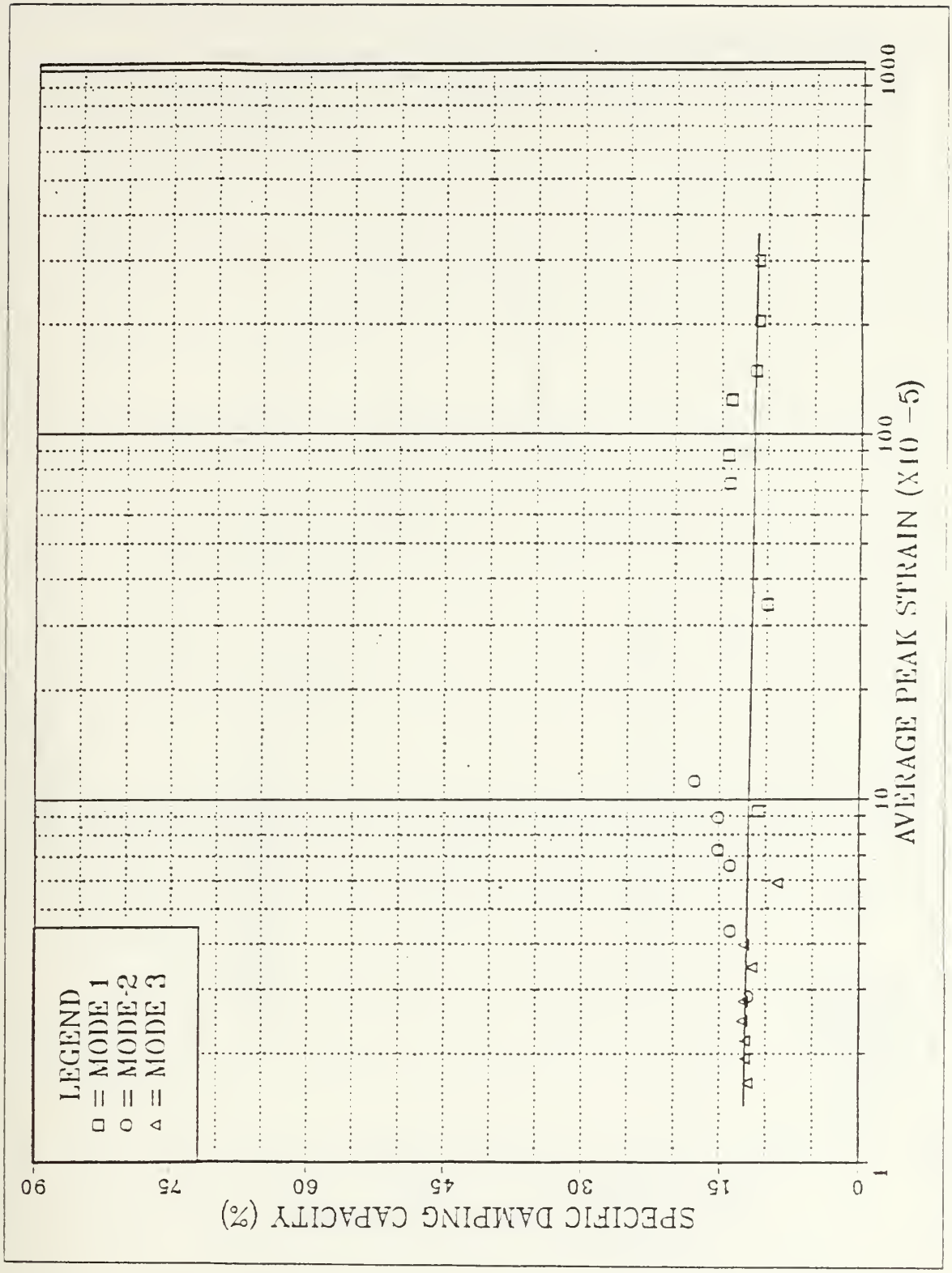

Figure 4.15 SDC-Strain Relationship for INCRAMUTE Aged at 400°C for 2 Hours Under the First Three Harmonic Modes.

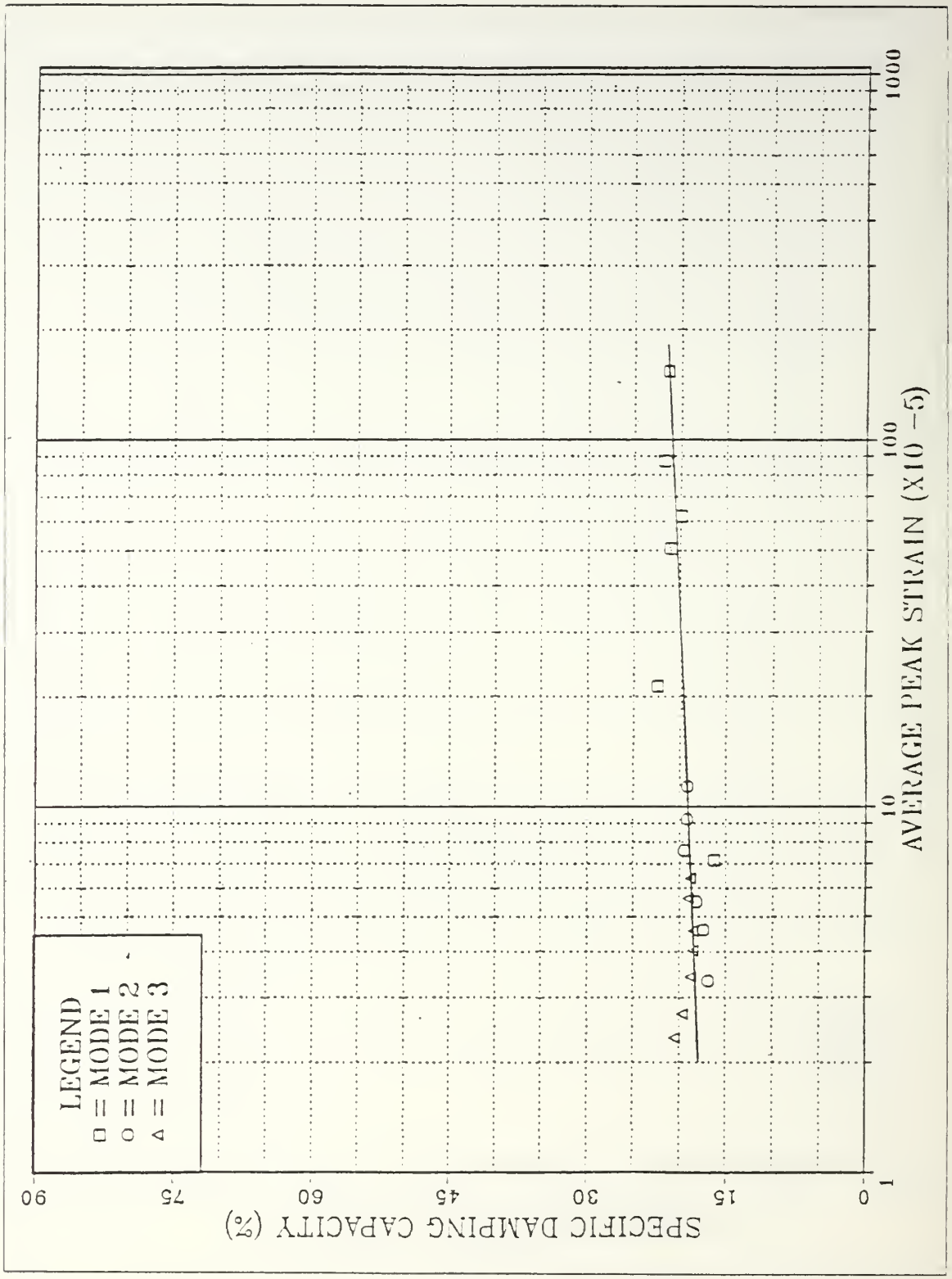

Figure 4.16 SDC-Strain Relationship for INCRAMUTE Aged at 400°C for 4 Hours Under the First Three Harmonic Modes.

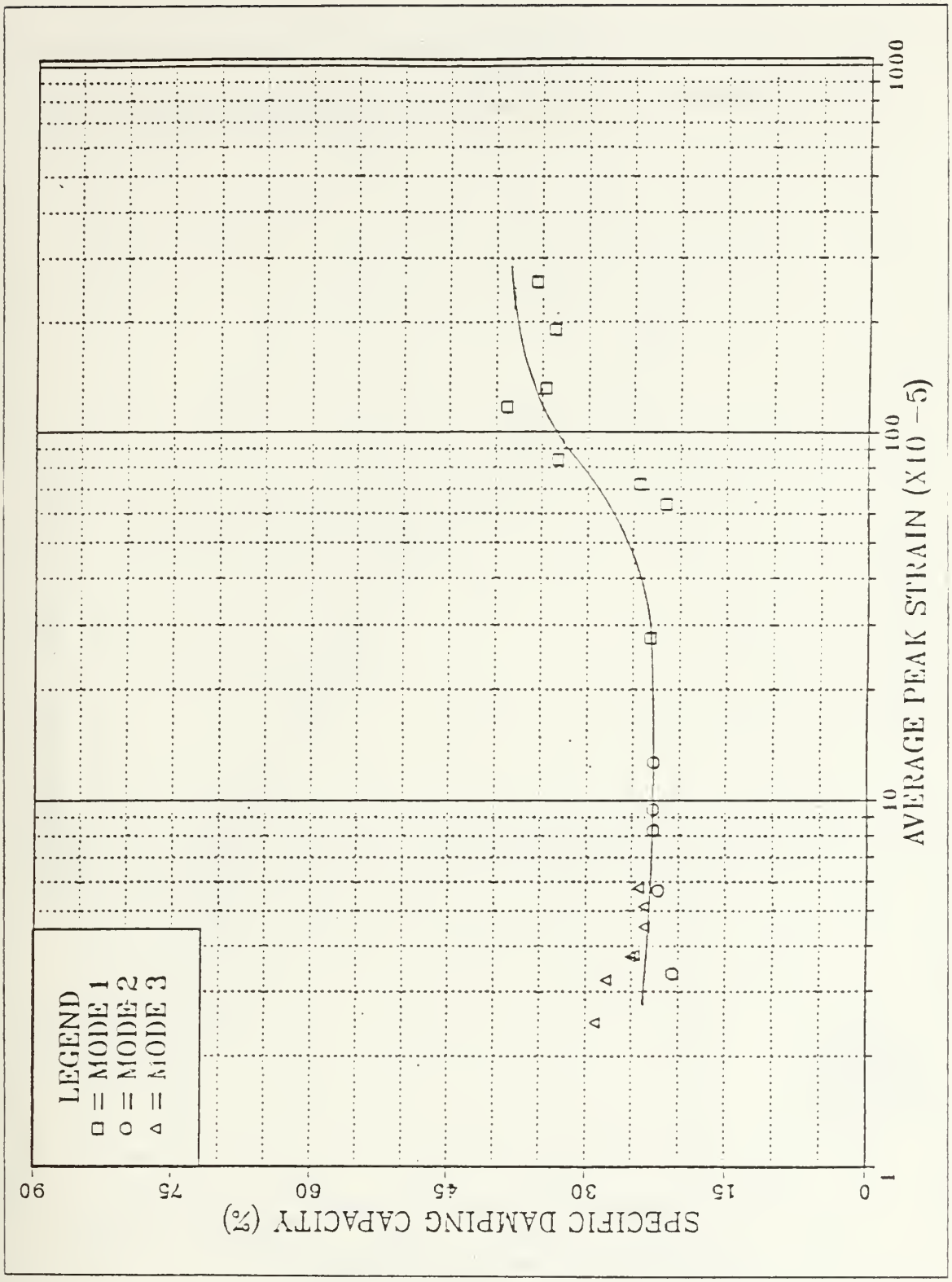

Figure 4.17 SDC-Strain Relationship for INCRAMUTE Aged at 400°C for 8 Hours Under the First Three Harmonic Modes.

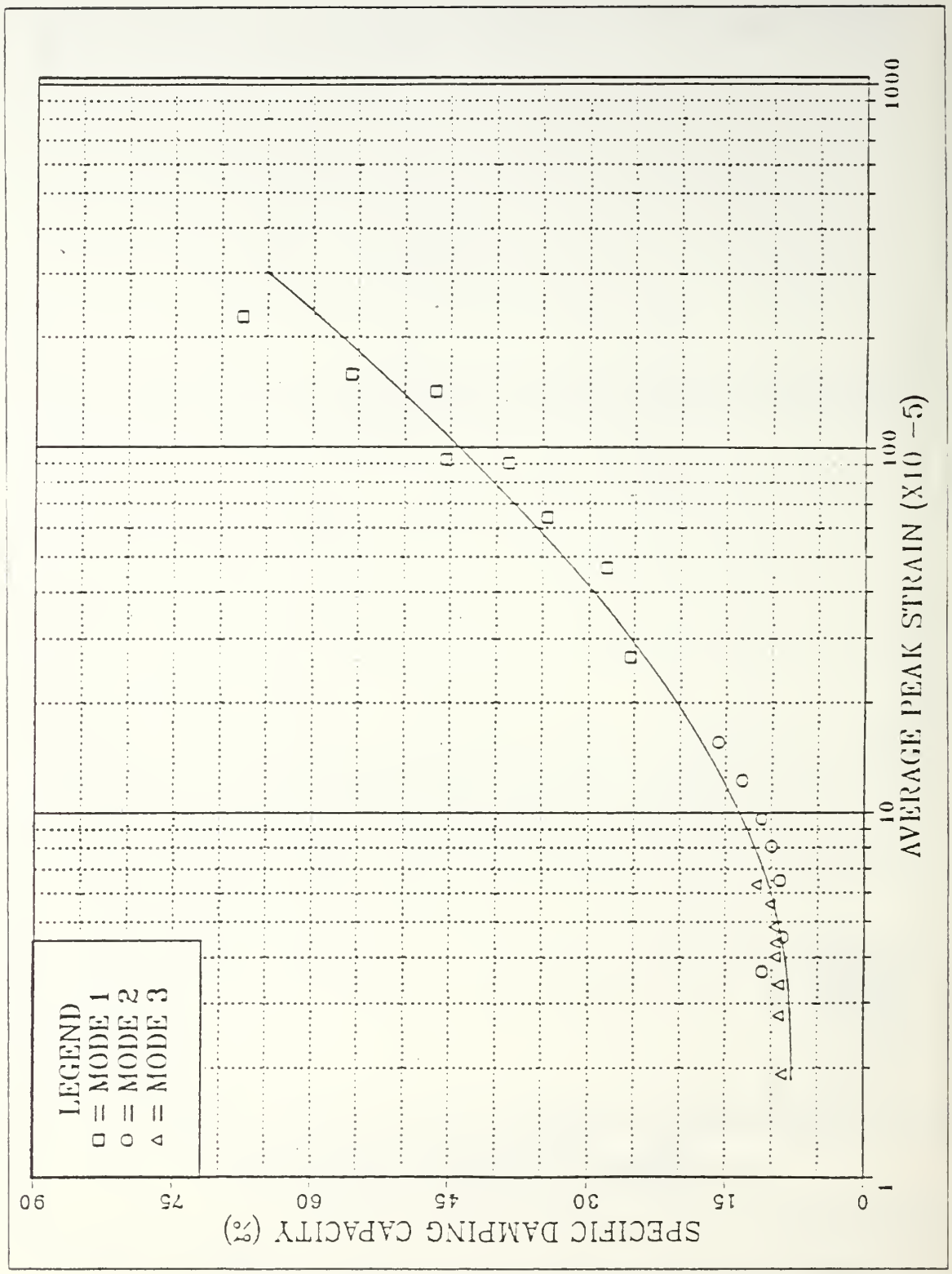

Figure 4.18 SDC-Strain Relationship for INCRAMUTE Aged at 400°C for 16 Hours Under the First Three Harmonic Modes.

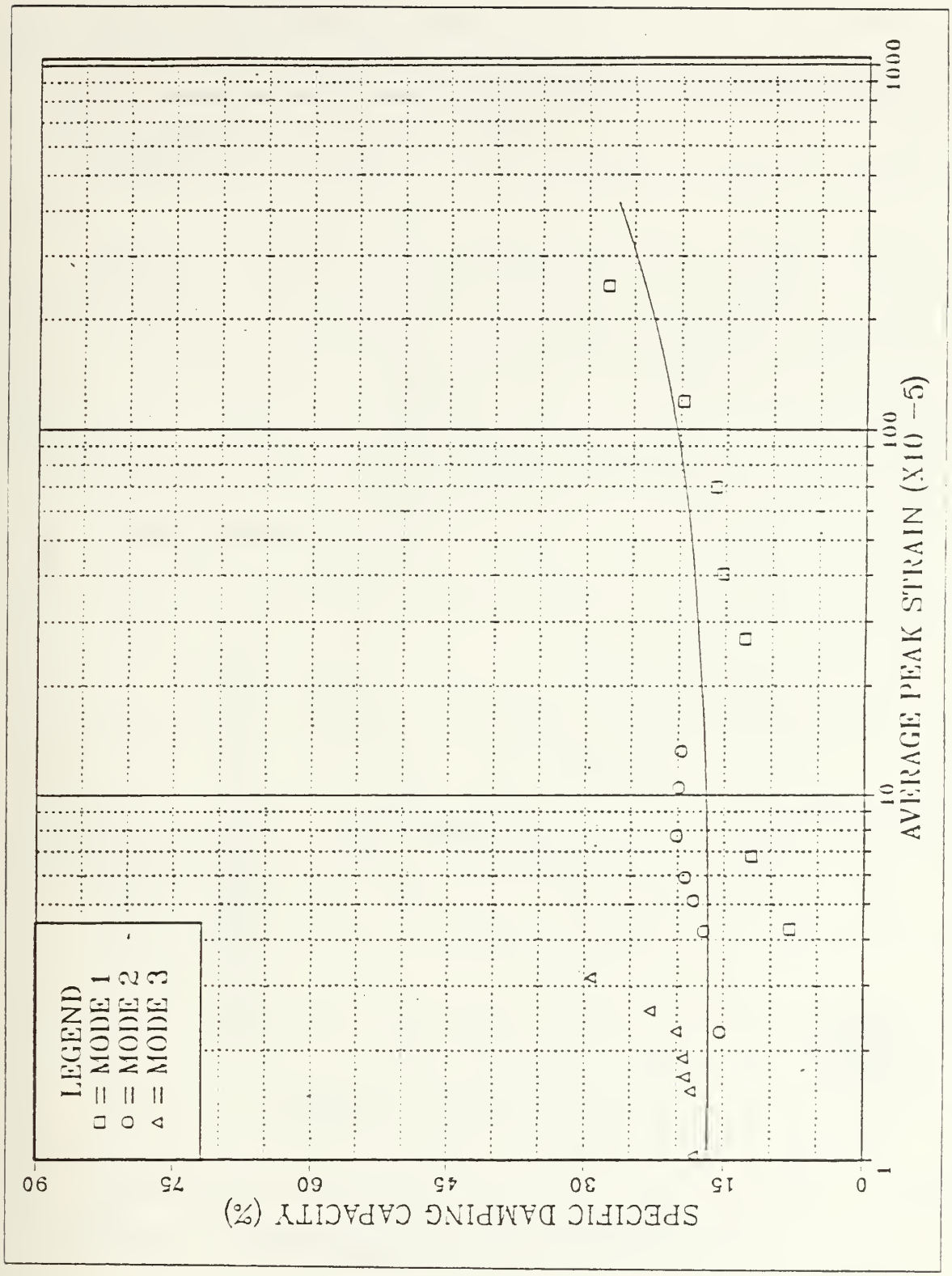

Figure 4.19 SDC-Strain Relationship for INCRAMUTE Aged at 400°C for 32 Hours Under the First Three Harmonic Modes.

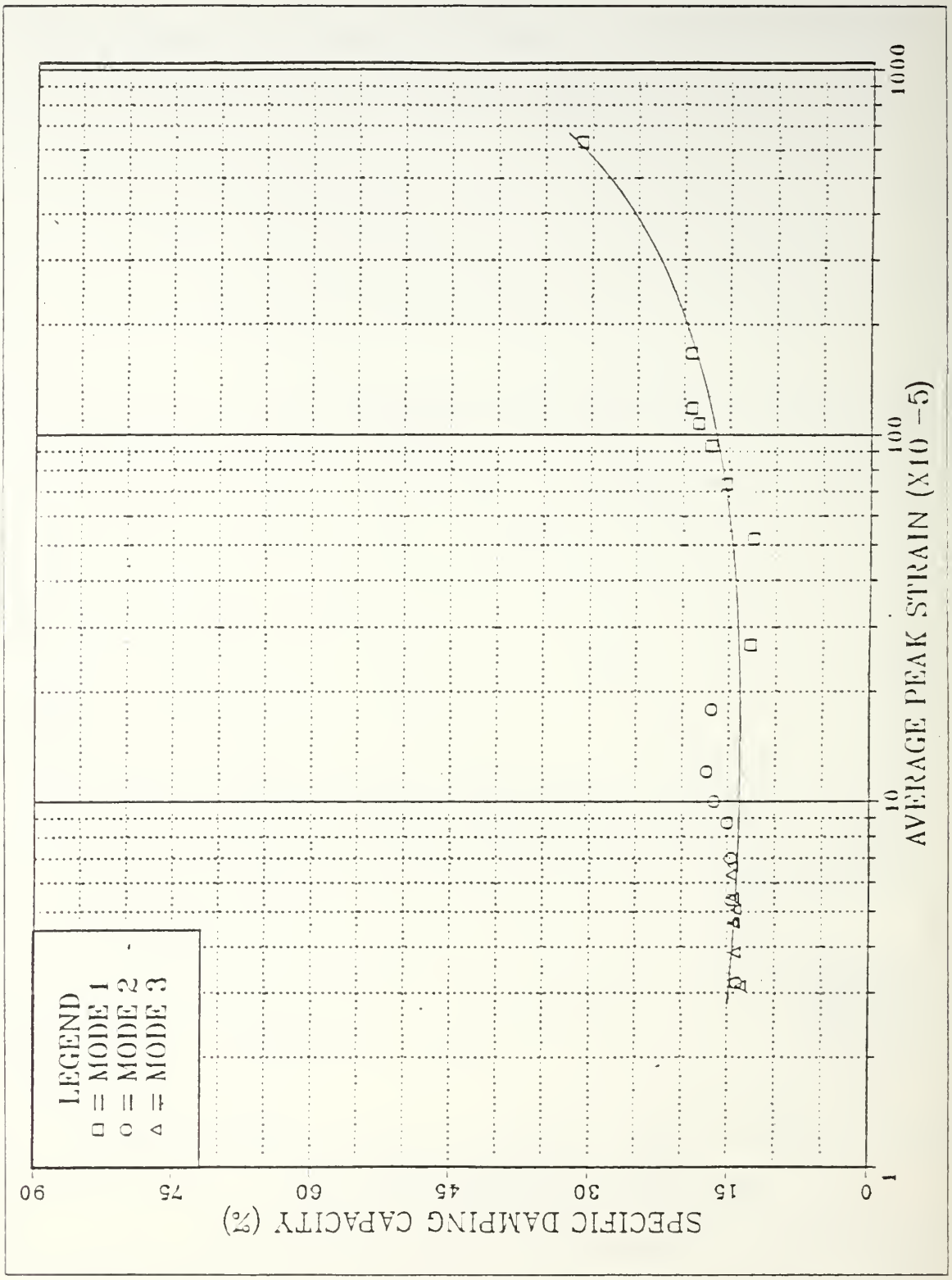

Figure 4.20 SDC-Strain Relationship for INCRAMUTE Aged at 400°C for 64 Hours Under the First Three Harmonic Modes.

C. X-RAY DIFFRACTION RESULTS

The Mn composition of INCRAMUTE just lies within the miscibility gap proposed by Vintaykin, et al [Ref. 38:p. 96]. Therefore, it is not clear whether the process of decomposition will occur at 400°C, so that it is also uncertain whether antiferromagnetic ordering and/or martensitic twinning will occur on a subsequent quench.

INCRAMUTE can be expected to have an as-quenched FCC lattice parameter of between 3.74 and 3.75 A, based on the data presented by Birchon, et al [Ref. 8:p. 42], and by Worrell [Ref. 31:p. 929]. Its tetragonality can be inferred from Figure 4.21, which is taken from Butler and Kelly [Ref. 26:p. 2100], where INCRAMUTE, with a 45/53 Mn-to-Cu ratio, would be expected to have a very slight degree of tetragonality, probably less than 1% (i.e., $c/a > 0.99$) for a 2-hour, 400°C age. This figure also shows an increasing axial ratio (i.e., decreasing tetragonality) as the Mn content is lowered and as the aging temperature is raised.

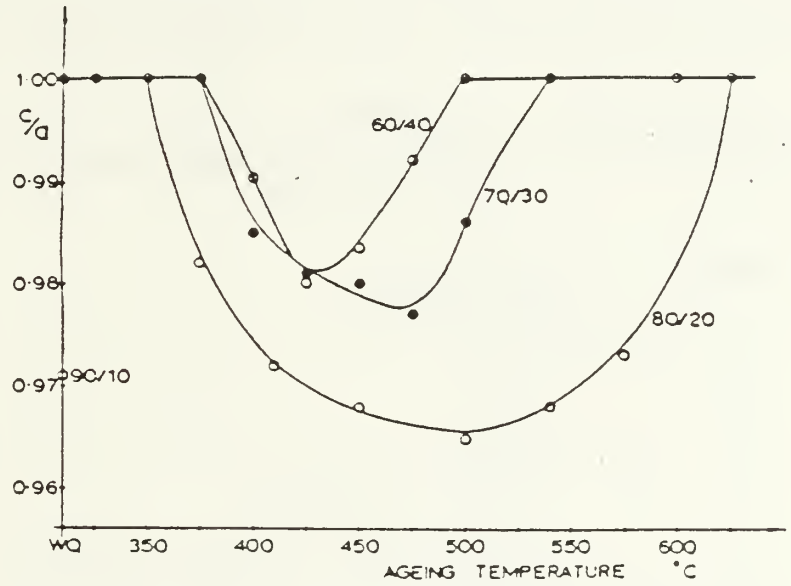

Variation in c/a ratio for 60/40, 70/30, and 80/20 Mn-Cu alloys aged for 2 hr at different temperatures.

Figure 4.21 Tetragonality as a Function of Copper-Manganese Composition and Aging Temperature.

As-quenched INCRAMUTE was found to have an FCC structure with a lattice parameter of 3.7484 Å. X-ray diffraction patterns did not show peak splitting of (200) nor of (220) reflections for INCRAMUTE aged at 400°C for times up to 128 hours. For all aging times, very weak intensity peaks were observed which corresponded to secondary reflections of an undetermined crystal structure with a lattice parameter of about 4.45 Å. Because of the weak intensities and somewhat inconsistent reflections with aging time, it was assumed that these are not second-phase α-Mn particles precipitated during aging, but rather are a transition phase, probably consisting of zones rich in Mn, which precede α-Mn precipitation ($a_{\alpha Mn}$ = 8.9139 Å).

Table III shows the lattice parameters for INCRAMUTE as determined by X-ray diffraction. This data is also graphically presented in Figure 4.22 along with Hedley's data on the lattice parameters for 57 w/o and 65 w/o Mn alloys aged at 400°C [Ref. 24:pp. 132-133]. It can be seen that the tetragonality decreases as Mn content is reduced and, more importantly, that room temperature tetragonality does not occur in INCRAMUTE aged at 400°C. Therefore, it may safely be surmised that the FCC——> FCT transformation for aged-and-quenched alloys within the miscibility gap must necessarily vanish for Mn contents somewhere between 45 w/o and 57 w/o.

TABLE III

LATTICE PARAMETERS FOR EACH HEAT TREATMENT CONDITION OF INCRAMUTE

Heat Treament	Lattice Parameter (Angstrons)
AQ	3.7484
1 Hour Age	3.737864
2 Hour Age	3.739308
4 Hour Age	3.736943
8 Hour Age	3.734718
16 Hour Age	3.737543
32 Hour Age	3.732213
64 Hour Age	3.732848
128 Hour Age	3.734585

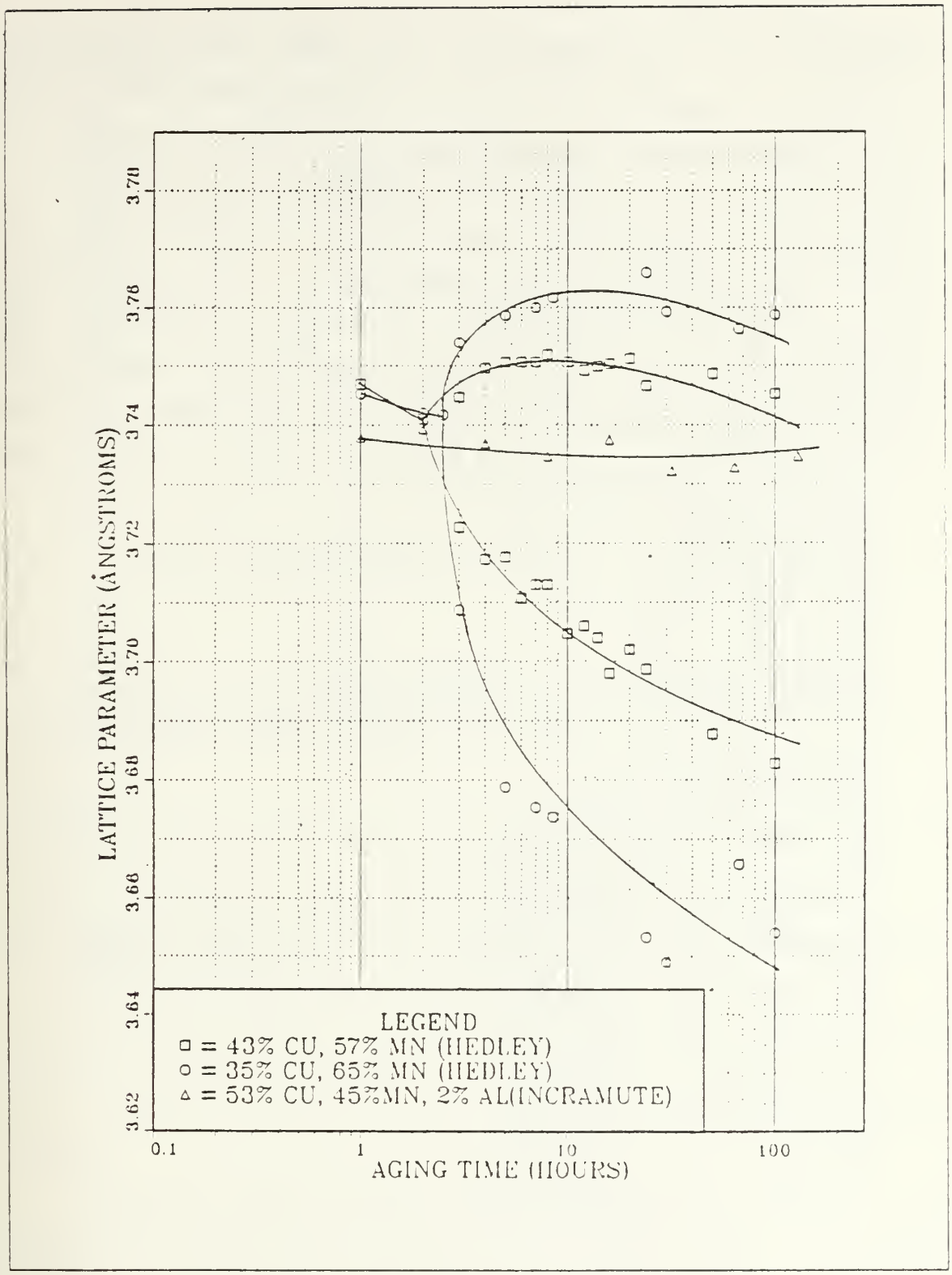

Figure 4.22 Lattice Parameter Comparison for INCRAMUTE and Two Copper-Manganese Alloys Aged at 400°C for Various Times.

Examining Figure 1.9 again, one can conclude that INCRAMUTE does not form martensitic twins upon quenching from a 400°C age or for any aging treatment. INCRAMUTE does exhibit a lattice contraction with aging time at 400°C, but the Mn content is not sufficient enough to form martensite after aging at this temperature. It may be possible that with a higher aging temperature (say, by aging at 450°C or 500°C), enough of a driving force may be imparted to the INCRAMUTE to cause localized twin formation due to the relatively low Mn content. From Figure 1.9, quenching to room temperature causes the aged alloy to form the tetragonal structure only for compositions between 50 w/o and 80 w/o Mn since $T < M_S < T_N$. It would appear that, for the three aging temperatures considered by Bichinashvili, et al [Ref. 45:p. 113], (i.e., 350°C, 400°C, and 450°C), tetragonality reaches a lower bound where the Mn content is about 50 a/o (47 w/o) at room temperature. The aging time to achieve this bound varies inversely with temperature (i.e., 120 hours at 350°C, 20 hours at 400°C, and 2 hours at 450°C).

The mass densities (ρ) for each heat treatment condition are provided in Table IV and plotted in Figure 4.23, below.

TABLE IV

DENSITY VARIATION IN INCRAMUTE WITH HEAT TREATMENT

Heat Treatment	Density (lbs/in^3)
AQ	0.2551659172
1 Hour Age	0.2583756429
2 Hour Age	0.2581812562
4 Hour Age	0.2609508549
8 Hour Age	0.2610323978
16 Hour Age	0.2616710417
32 Hour Age	0.2618871758
64 Hour Age	0.2601768922
128 Hour Age	0.2615068165

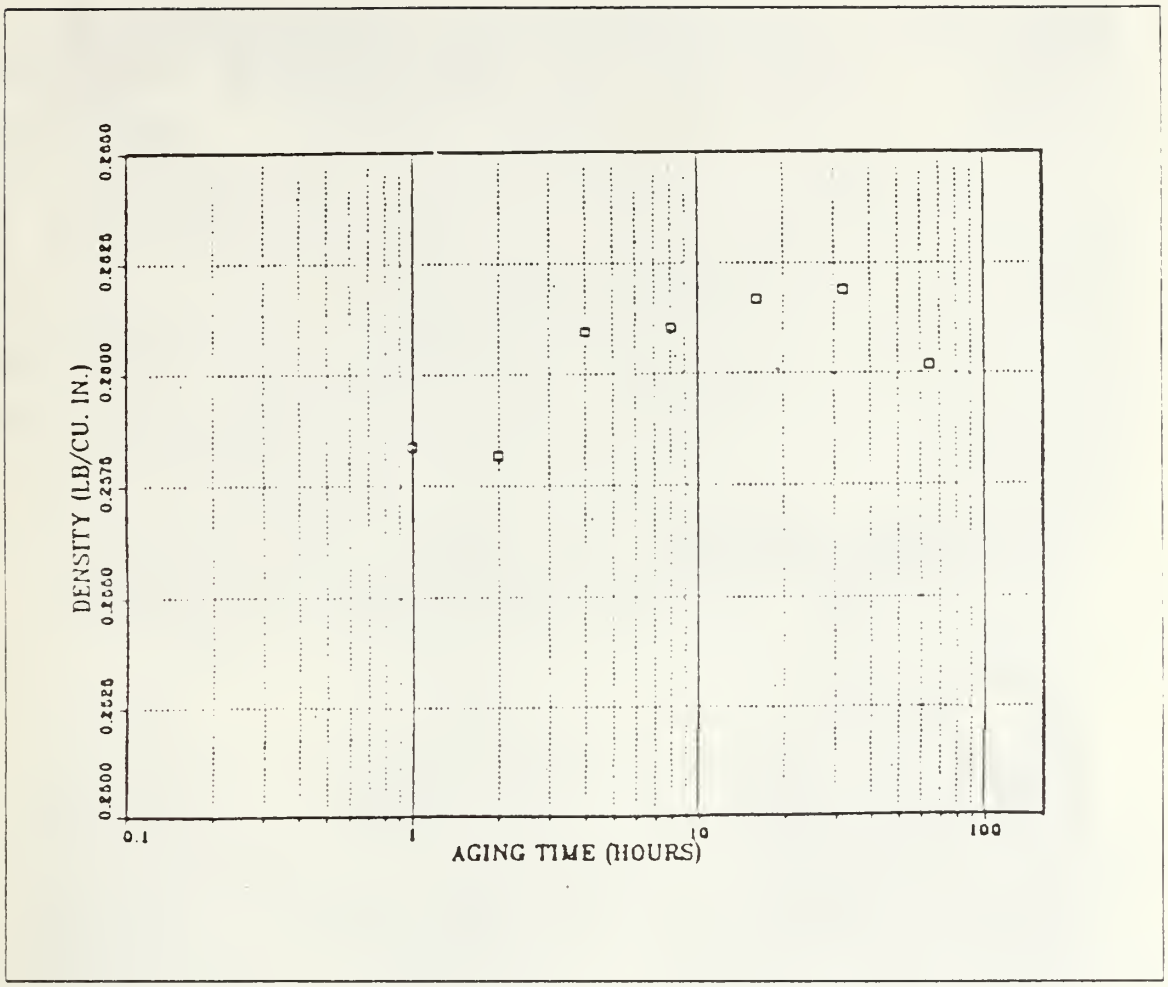

Figure 4.23 Mass Densities of INCRAMUTE Aged at 400°C.

D. TRANSMISSION ELECTRON MICROSCOPIC (TEM) EXAMINATION OF INCRAMUTE

Figures 4.24 through 4.33 represent bright field TEM images with inset diffraction patterns for the as-quenched condition and for 400°C agings from 1 through 128 hours, respectively. None of the specimens displayed martensitic twin structures. However, either a mottled or a tweed structure is clearly evident in all conditions examined.

Specifically, mottling without marked directionality is observed in the as-quenched specimen and in those aged for 1, 2, and 4 hours. The associated diffraction patterns for these thermal conditions exhibit the typical characteristics of the so-called premartensitic structure. Figures 4.24 to 4.27 show diffuse diffraction and

satellite spots. These may be indicative of the elastic strain contrast associated with the early stages of decomposition within the miscibility gap. During aging, the initially homogeneous γ-phase of INCRAMUTE decomposes and forms Cu-rich and Mn-rich clusters with coherent interfaces. These interfaces, because they are coherent, have elastic lattice distortion associated with them. It can also be seen in comparing these micrographs that, as aging progresses to 4 hours, the mottled contrast becomes more pronounced and coarser. If it is appropriate to associate the image effect with elastic strains, then it must be concluded that aging increases the elastic distortion in the lattice [Ref. 64:p. 199].

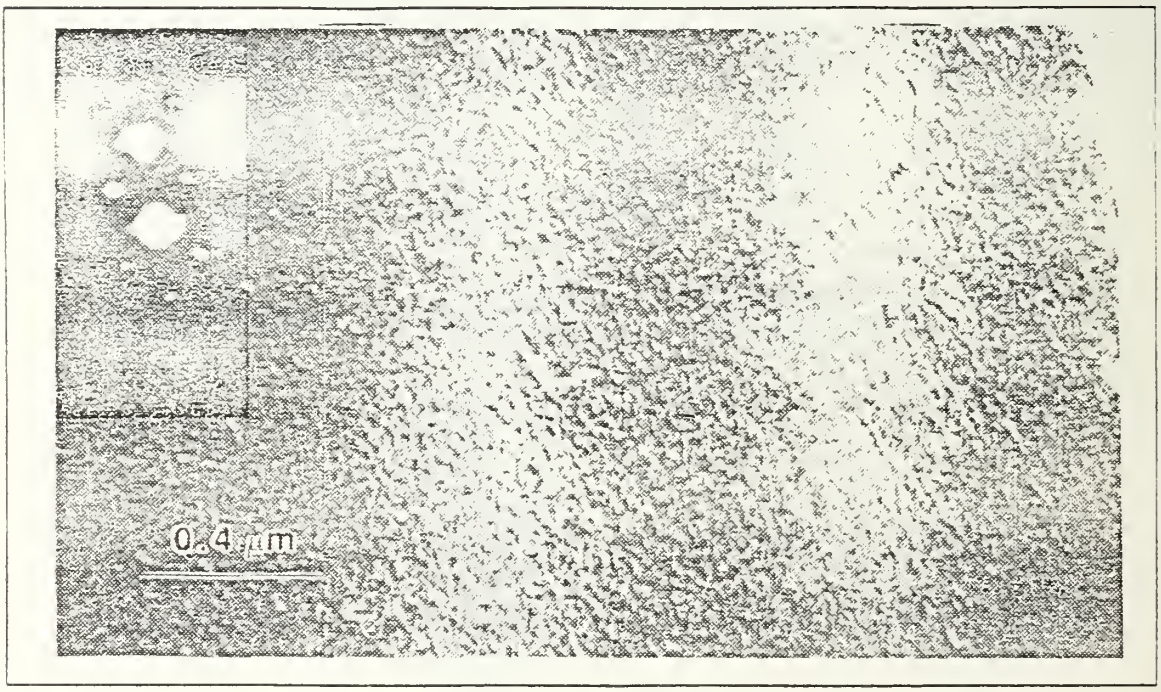

Figure 4.24 Transmission Electron Micrograph of As-Quenched Foil of INCRAMUTE.

In the electron micrographs for the 8- and 16-hour aged foils of INCRAMUTE (Figures 4.28 and 4.29), the mottled appearance is supplanted by a directional structure, or "tweed". The strain energy associated with the tweed's misfit has relaxed or been minimized such that now semi-coherent or possibly incoherent interfaces exist [Ref. 64]. This is supported by the disappearance of diffuse diffraction images in Figures 4.28 and 4.29. Examination of these and other micrographs for these aged foils reveals that the tweed pattern delineates <110> directions. Occasionally, an indistinct

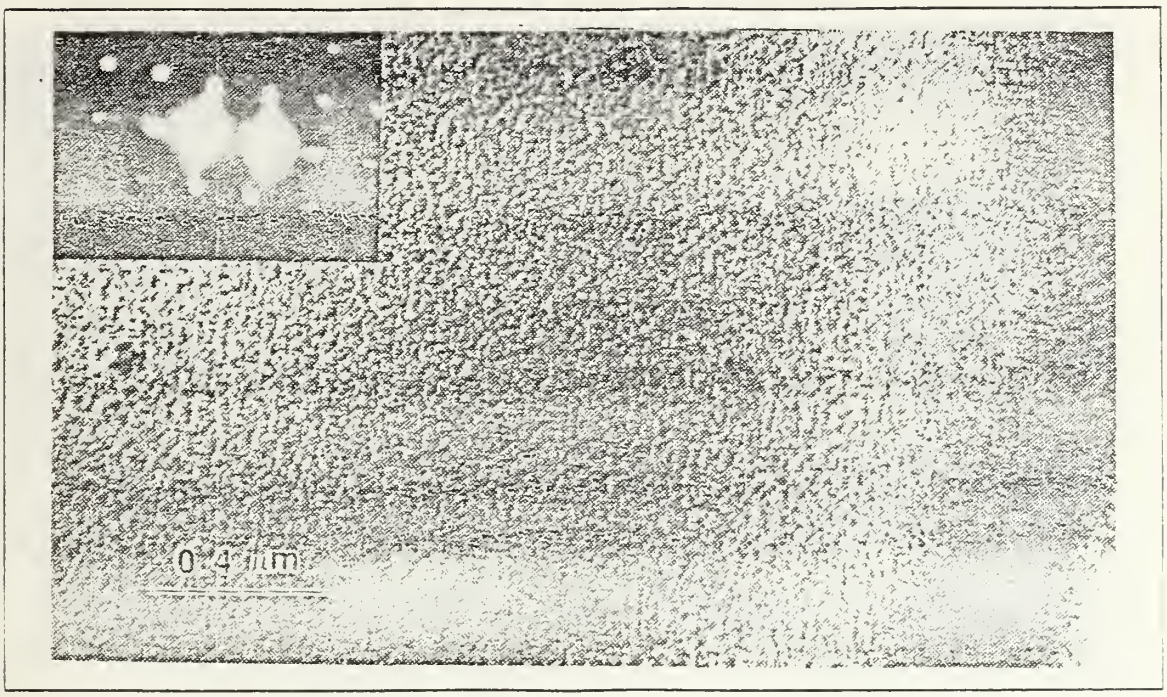

Figure 4.25 Transmission Electron Micrograph of INCRAMUTE Foil Aged at 400°C for 1 Hour.

"banding" occurred in the 16-hour aged foil (Figure 4.30). This banding may represent a preliminary condition to the formation of martensitic twins. From the micrographs of the 8- and 16-hour aged specimens, modulation values for the tweed structure were obtained as 85-140 Å and 175-300 Å, respectively. Even though the 32-hour aged specimen (Figure 4.31) displayed some evidence of a tweed character, a modulation was not determined because the tweed was rather indistinct in order to differentiate the boundaries between light and dark regions properly. The modulation values measured herein represent the average width of the light or dark regions of the tweed pattern.

Micrographs of 32-, 64-, and 128-hour aged foils of INCRAMUTE are contained in Figures 4.31, 4.32, and 4.33, respectively. With prolonged aging, the tweed structure coarsens (i.e., 32 hours) and eventually disappears and is replaced by a mottled structure (i.e., 64 and 128 hours). Recalling that maximum hardness was obtained in INCRAMUTE when aged to 64 hours, certain conclusions can be drawn with respect to damping and TEM observations. The tweed structure is a highly strained region of fine coherent precipitation. The damping levels achieved by the 8-, 16-, and 32-hour aged specimens are consistent with this. Aging to maximum hardness produces a

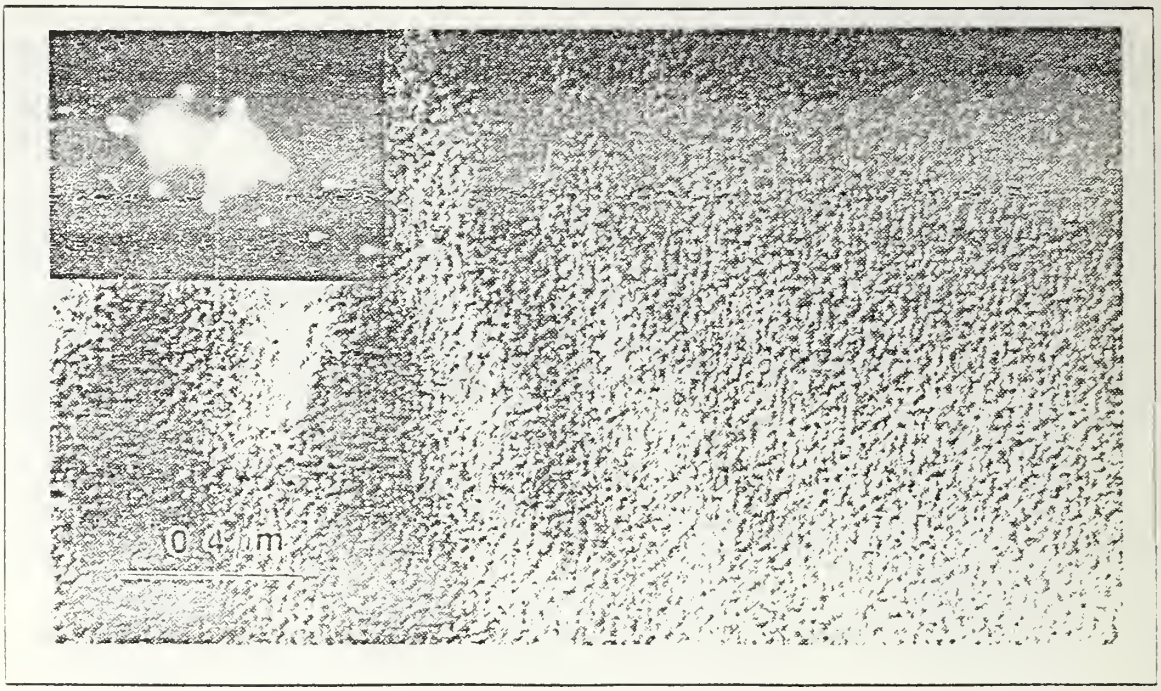

Figure 4.26 Transmission Electron Micrograph of INCRAMUTE Foil Aged at 400°C for 2 Hours.

structure of semi-coherency associated with relaxed, or minimized, strain energy and with a concomitant deterioration in damping capacity. Thus, the tweed structure is the necessary requirement for the production of high damping in INCRAMUTE. Overaging to 128 hours, then, produces a less hard structure associated with an incoherent structure.

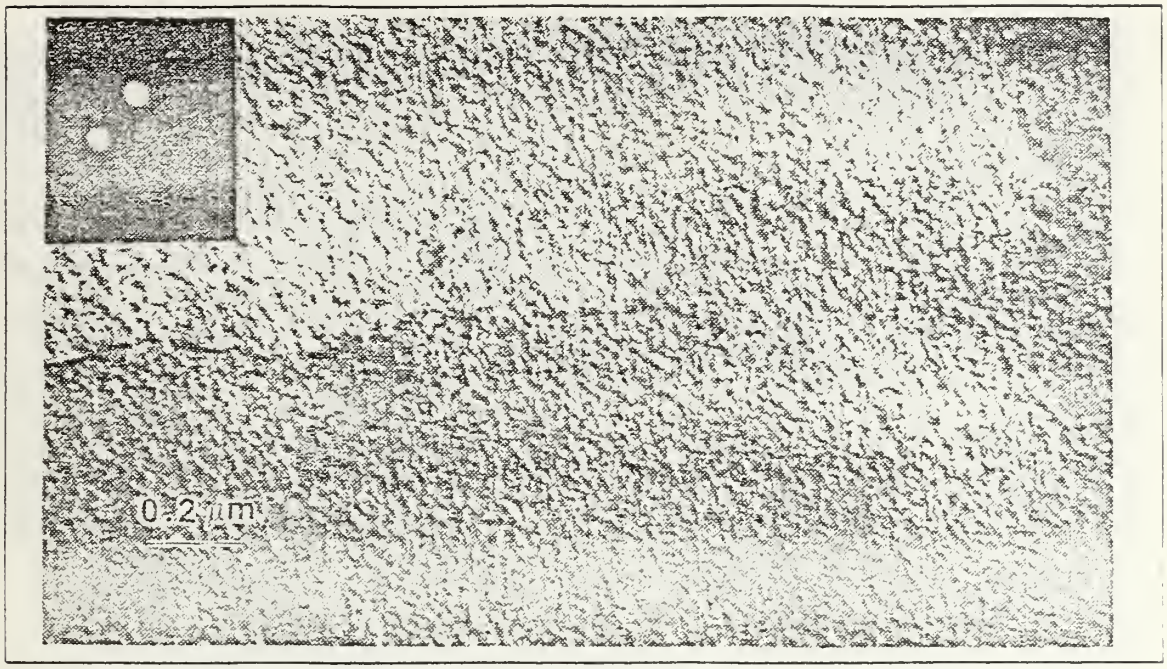

Figure 4.27 Transmission Electron Micrograph of INCRAMUTE Foil Aged at 400°C for 4 Hours.

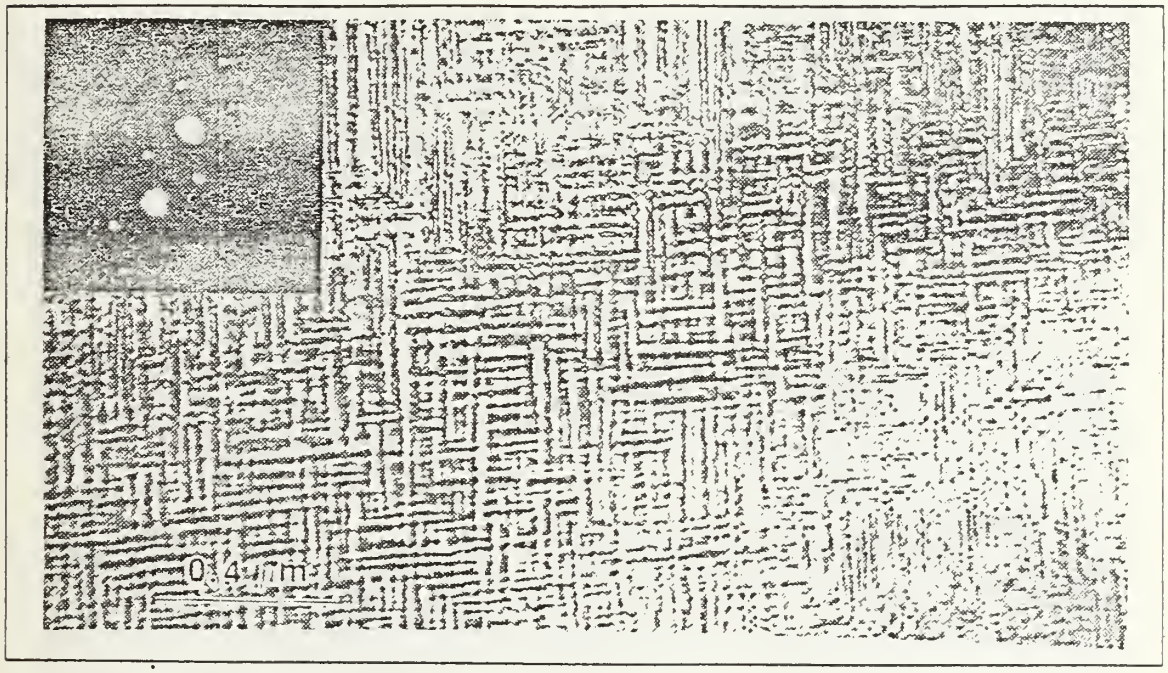

Figure 4.28 Transmission Electron Micrograph of INCRAMUTE Foil Aged at 400°C for 8 Hours.

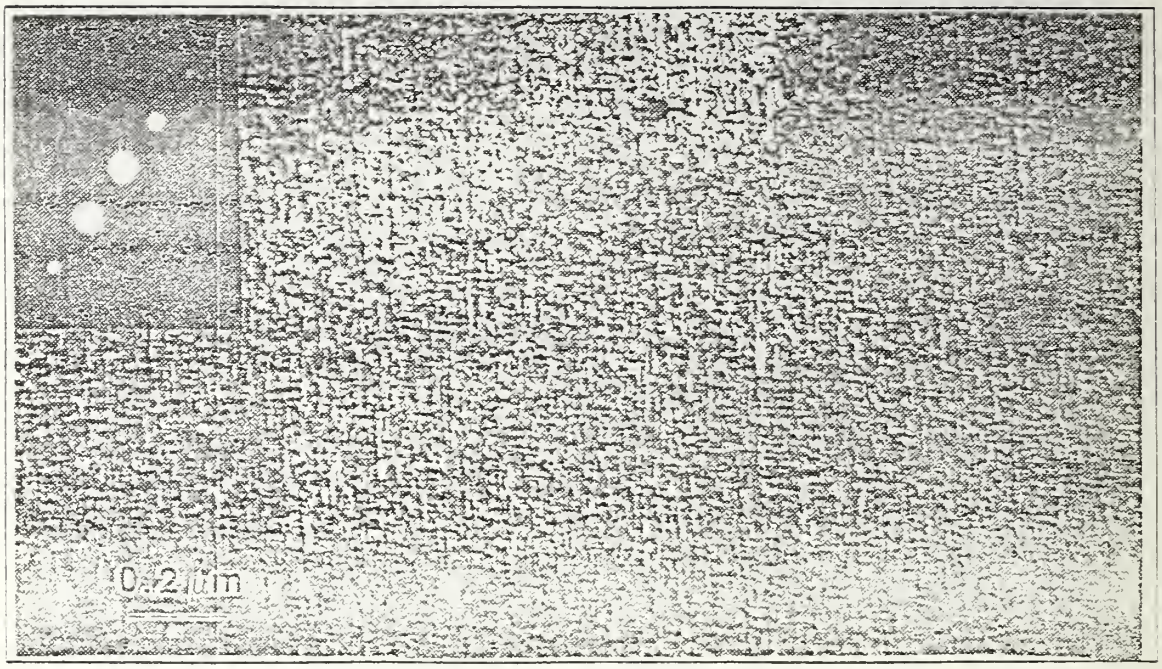

Figure 4.29 Transmission Electron Micrograph of INCRAMUTE Foil Aged at 400°C for 16 Hours.

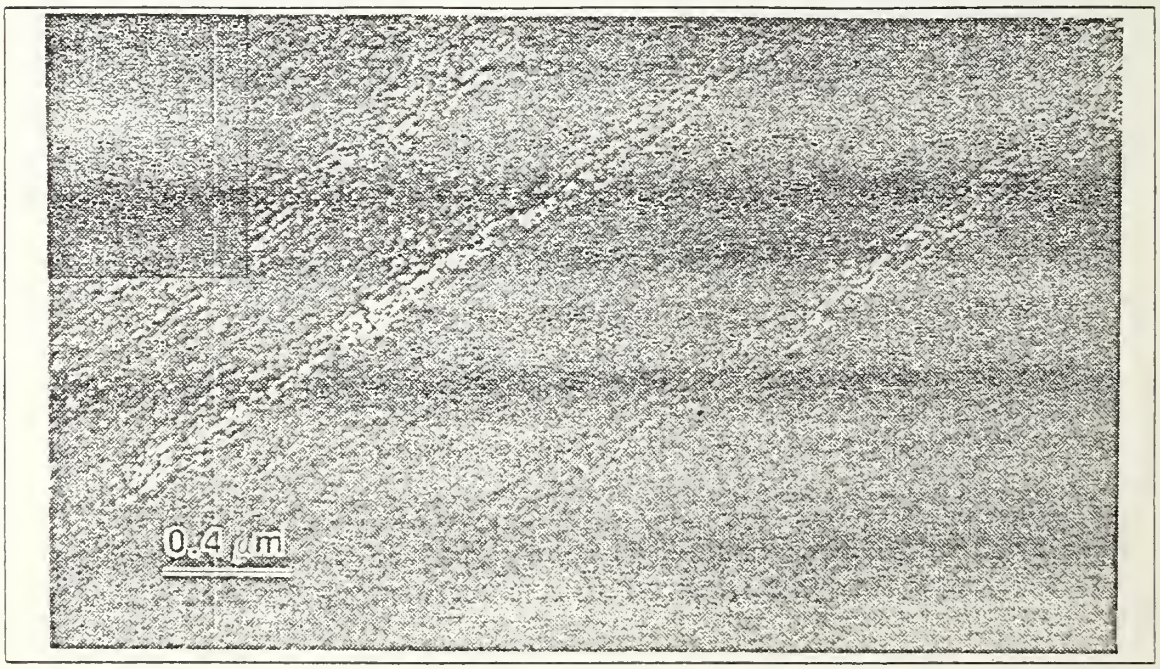

Figure 4.30 Transmission Electron Micrograph of INCRAMUTE Foil Aged at 400°C for 16 Hours.

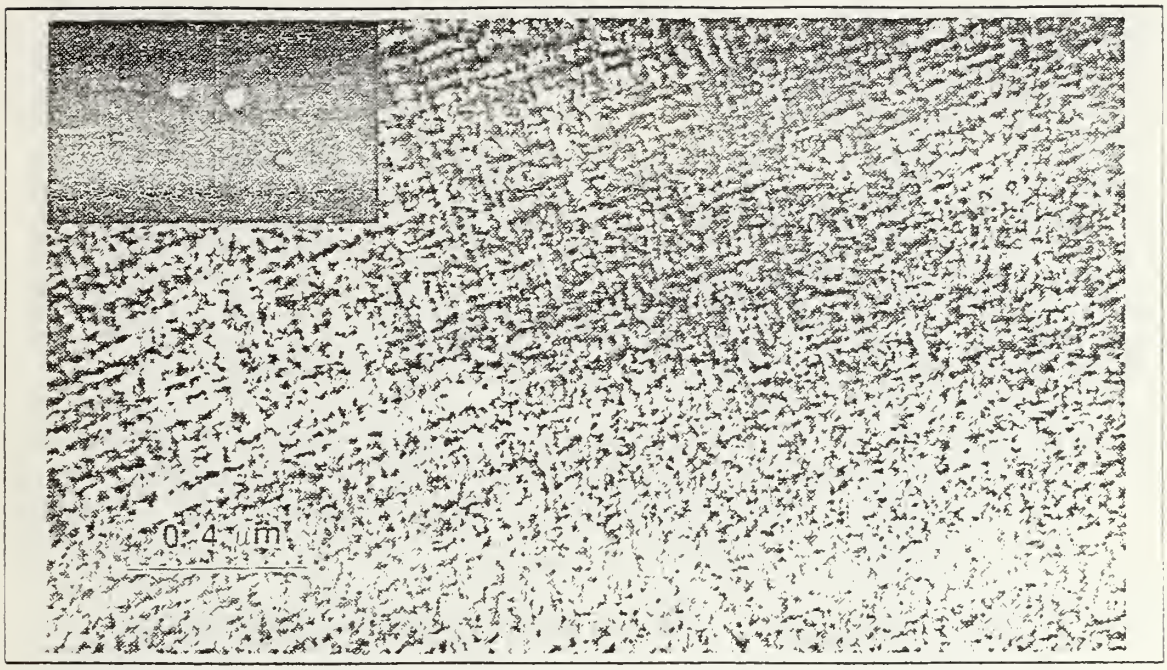

Figure 4.31 Transmission Electron Micrograph of INCRAMUTE Foil Aged at 400°C for 32 Hours.

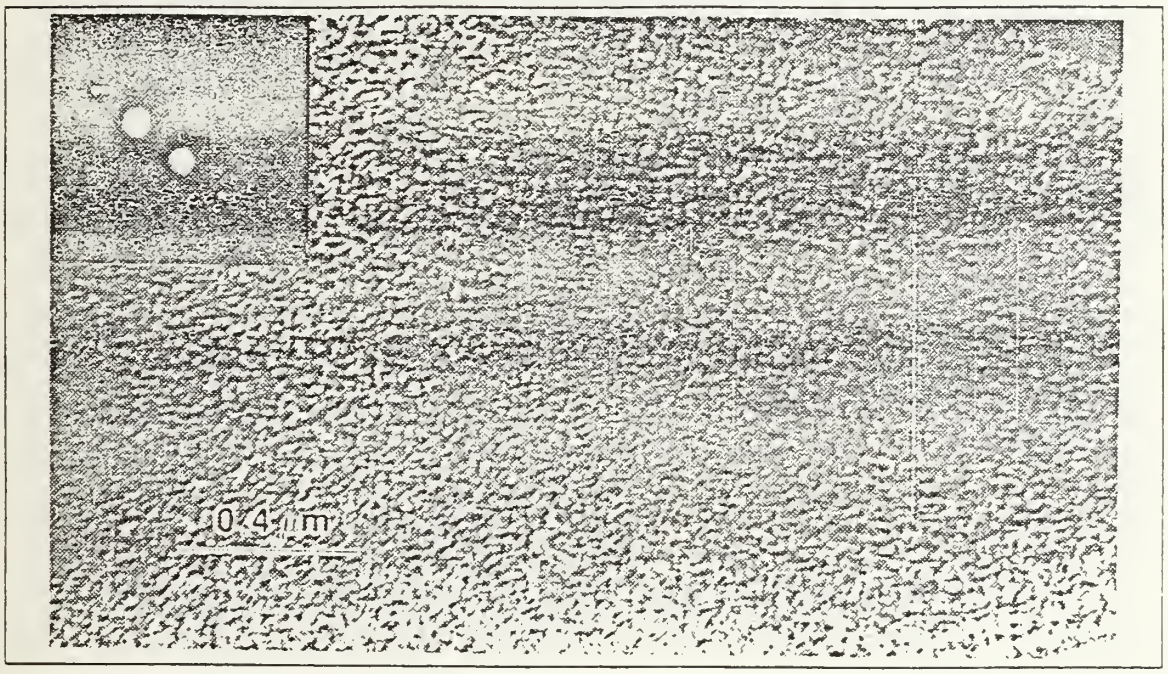

Figure 4.32 Transmission Electron Micrograph of INCRAMUTE Foil Aged at 400°C for 64 Hours.

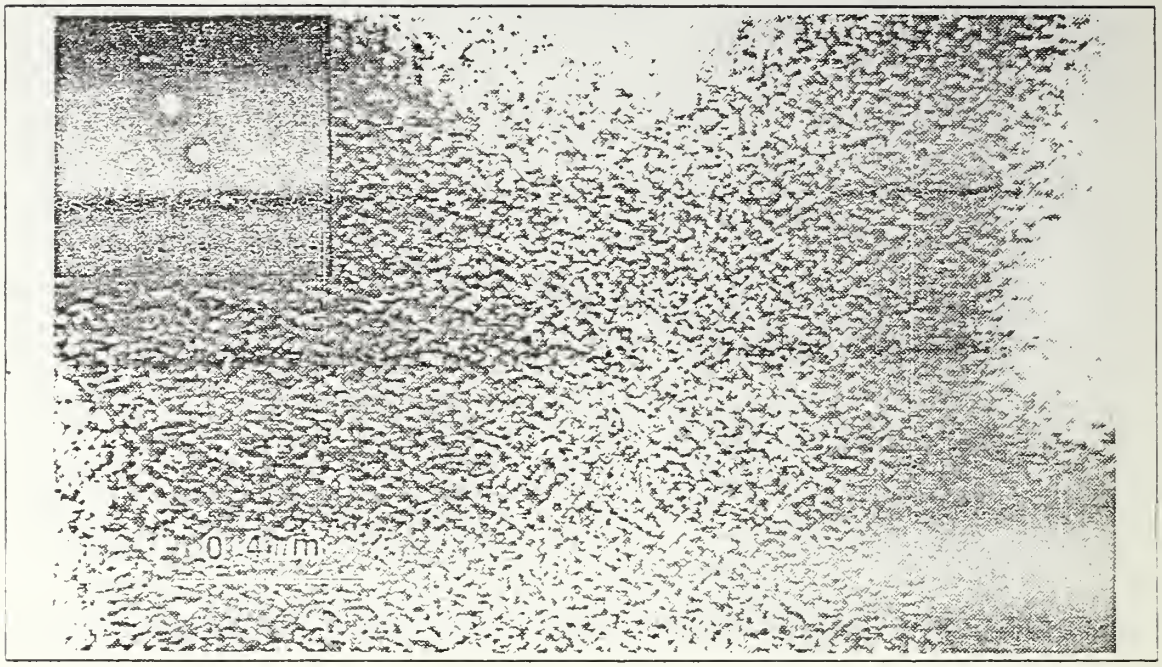

Figure 4.33 Transmission Electron Micrograph of INCRAMUTE Foil Aged at 400°C for 128 Hours.

E. OPTICAL MICROSCOPIC OBSERVATION

In order to verify the TEM results of the preceding section, two optical specimens (one in the as-quenched condition, the other aged for 16 hours) were polished and mounted in the cantilever stressing jig for observation under polarized light. It was anticipated that stress-induction of martensite could be observed in this way.

Figures 4.34 and 4.35 show micrographs of unstressed and stressed as-quenched INCRAMUTE at the tensile root of the specimen, respectively. Annealing twins can be clearly observed. As supported by the relatively strain-independent behavior of SDC (Figure 4.13), no difference is seen under polarized light when the as-quenched specimen is statically stressed to about 40 ksi, which has an associated strain of about $\varepsilon \sim 3.0 \times 10^{-3}$.

For comparison, a 16-hour aged specimen was stressed to the same levels as the as-quenched specimen, while being observed in the optical microscope. Figures 4.36 and 4.37 show the specimen's tensile root in the unstressed condition in normal and polarized light, respectively, magnified 425X. Stressing to various levels produced no visible twin contrast at the tensile root of the 16-hour aged specimen. This can be seen

Figure 4.34 Optical Micrograph of As-Quenched INCRAMUTE in the Unstressed Condition Under Polarized Light.

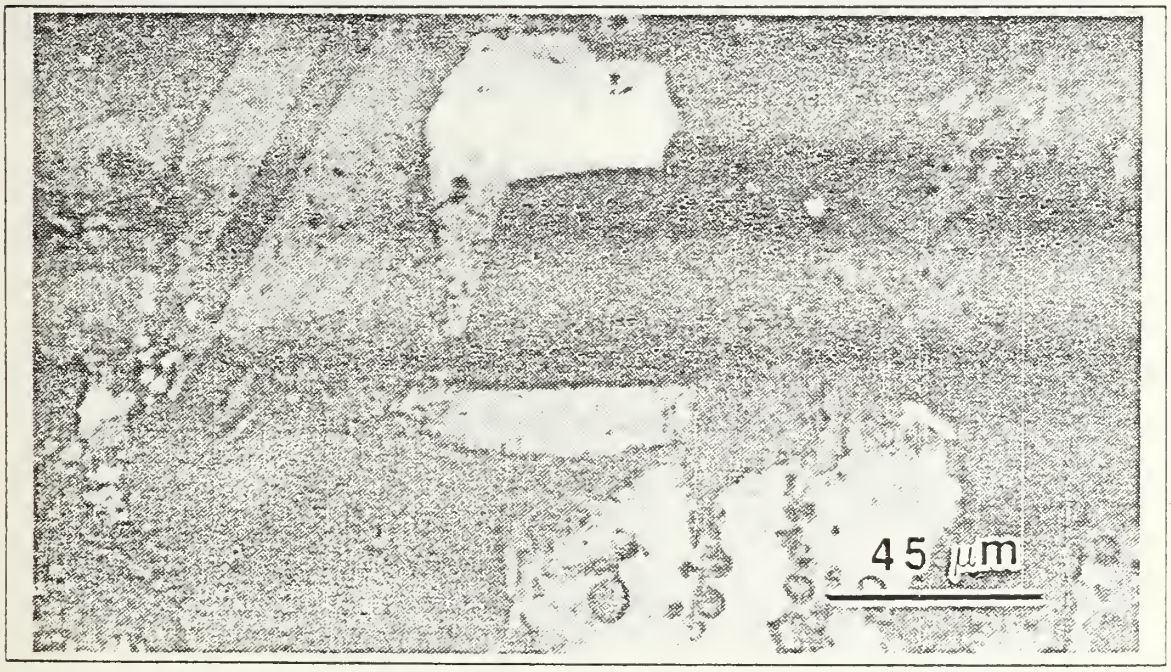

Figure 4.35 Optical Micrograph of As-Quenched INCRAMUTE in the Stressed to about 40 KSI Under Polarized Light.

in the optical micrographs of Figures 4.38 through 4.41, which are stressed to 25, 38, 51, and 64 ksi under polarized light at a magnification of 425X. Grain boundaries are clearly distinguishable, but there is no evidence of martensitic twins in the unstressed condition nor in any of the stressed conditions. These static stress levels correspond to the average peak strain levels associated with the 55-65% SDC values in Figure 4.18.

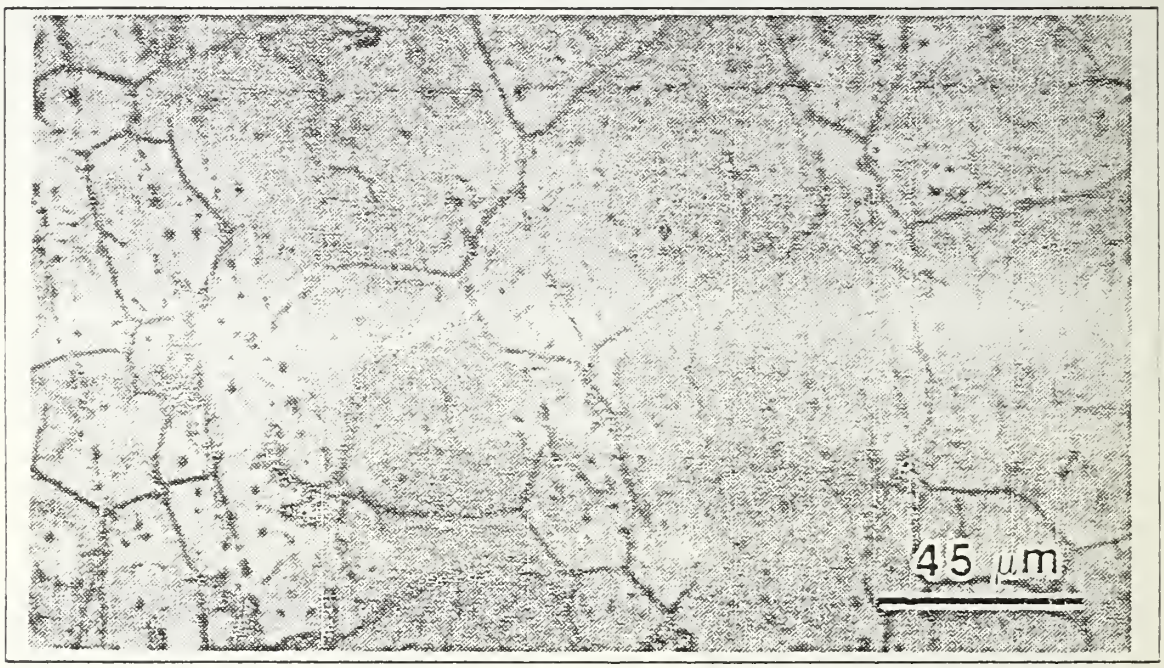

Figure 4.36 Optical Micrograph of 16-Hour Aged INCRAMUTE in the Unstressed Condition Under Normal Light.

Figure 4.37 Optical Micrograph of 16-Hour Aged INCRAMUTE in the Unstressed Condition Under Polarized Light.

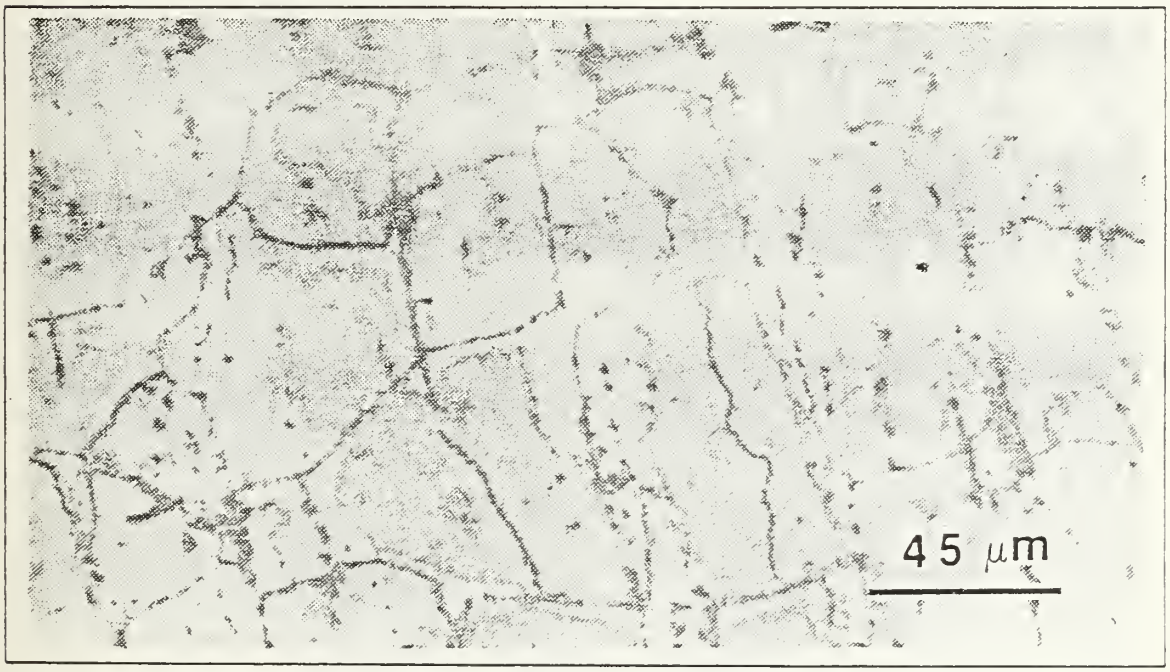

Figure 4.38 Optical Micrograph of 16-Hour Aged INCRAMUTE in the Stressed to about 25 KSI Under Polarized Light.

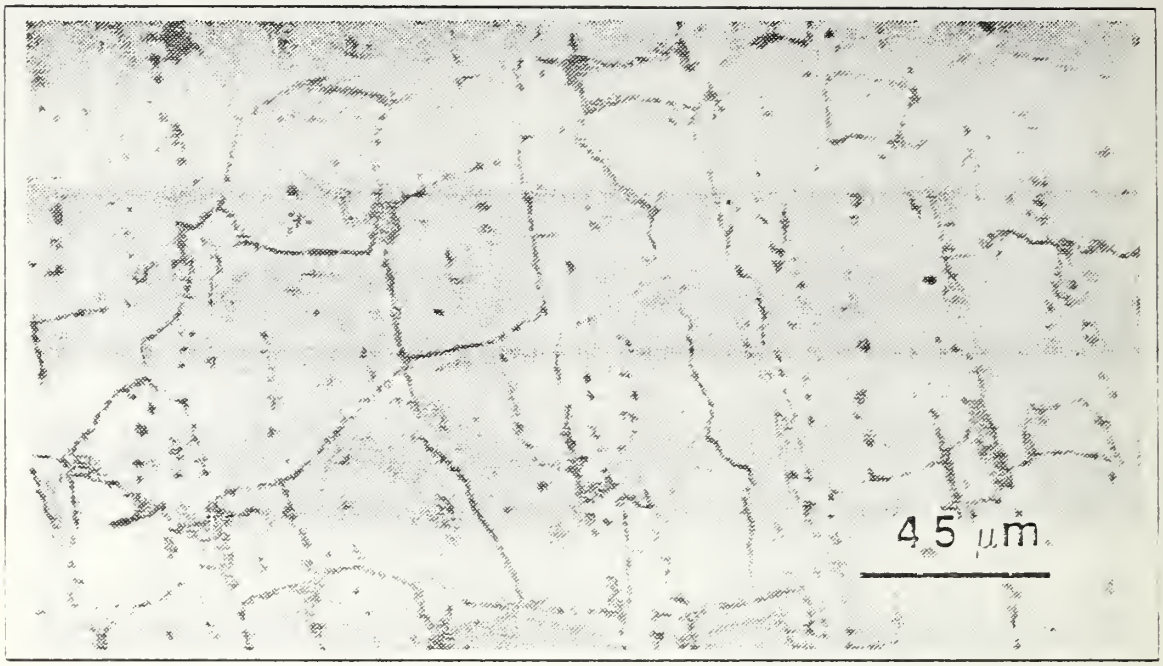

Figure 4.39 Optical Micrograph of 16-Hour Aged INCRAMUTE in the Stressed to about 38 KSI Under Polarized Light.

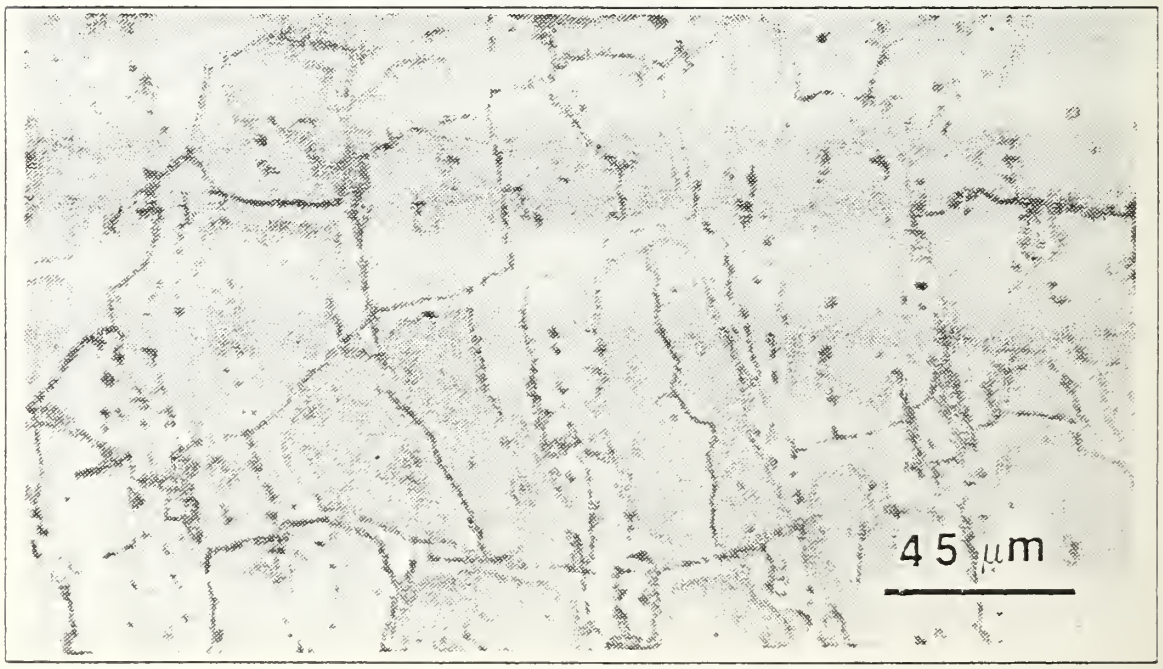

Figure 4.40 Optical Micrograph of 16-Hour Aged INCRAMUTE in the Stressed to about 51 KSI Under Polarized Light.

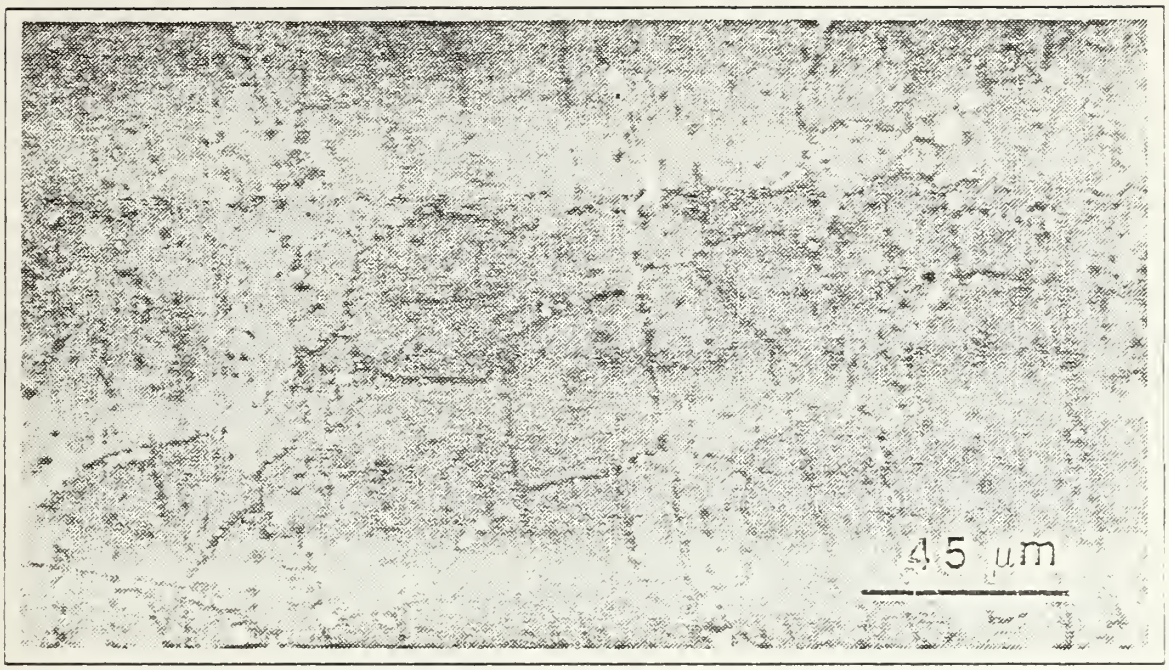

Figure 4.41 Optical Micrograph of 16-Hour Aged INCRAMUTE in the Stressed to about 64 KSI Under Polarized Light.

From the above, a reasonable doubt exists with respect to the stress-induced formation of martensitic twins in aged INCRAMUTE. To further verify this non-occurrence in aged INCRAMUTE, a specimen in the 8-hour aged condition was cold rolled 2.26% and an X-ray diffraction pattern obtained. As with the unworked and aged specimens, no peak splitting of (200) nor (220) reflections occurred. The calculated lattice parameter for the cold rolled specimen was 3.733479 Å and for the unworked specimen was 3.734718 Å (from Table III).

V. CONCLUSIONS AND RECOMMENDATIONS

A. CONCLUSIONS

It has been demonstrated that INCRAMUTE has a very high damping capacity under forced flexural vibration after it has been aged at 400°C for 16 hours. Development of reasonably high damping in INCRAMUTE requires a minimum aging treatment of no less than 4 hours at 400°C, and this corresponds microstructurally to the development of a directional tweed structure.

Unlike Cu-Mn alloys of Mn content greater than 50 w/o, which form matensitic twins for high damping, the high damping of INCRAMUTE is associated with a tweed structure alone. Since an FCT structure did not form in either aged or aged-and-stressed INCRAMUTE, Hedley's conclusions on the importance of a twinned tetragonal structure to high damping in Cu-Mn alloys and on the sufficiency of stress alone to form the tetragonal structure [Ref. 24:p. 137] apparently need not apply to INCRAMUTE. Twin boundary motion is apparently not the microstructural mechanism responsible for high damping in INCRAMUTE.

B. RECOMMENDATIONS

The following recommendations are proposed for further research and study on INCRAMUTE:

a. determination of strain-dependent damping characteristics at other aging conditions,
b. relationship of grain size to damping capacity by varying the solutionizing treatment prior to aging,
c. determination of damping characteristics by utilizing other damping techniques (i.e., Dew's forced torsion pendulum [Ref. 17]),
d. variation of Mn content below 45 w/o to determine extent of mottled and tweed structures in producing high damping characteristics,
e. utilization of cooling and heating stages in the TEM to observe possible thermoelastic effects in the morphological growth of the tweed structure in INCRAMUTE,

f. effects of room temperature aging on INCRAMUTE's damping properties correlated with a microstructural evaluation,

g. based on the aging effects above, determine optimal retransformation heat treatment to recover pre-aged damping properties,

h. damping and microstructural evaluation of furnace-cooled INCRAMUTE,

i. stability of step-aged INCRAMUTE to extend component service life to counter possible room temperature aging effects,

j. prolonged and continuous vibratory effects on damping properties (i.e., strain-aging),

k. characterizing strain-dependent damping of INCRAMUTE under forced vibration in various temperature-controlled environments.

APPENDIX A

FRACTURE SURFACE MICROGRAPHS FOR INCRAMUTE AT VARIOUS AGING TIMES

This appendix contains scanning electron microscopic (SEM) photographs of the fracture surfaces of tensile specimens corresponding to the as-quenched condition and the 1-, 4-, 16- and 64-hour aging conditions.

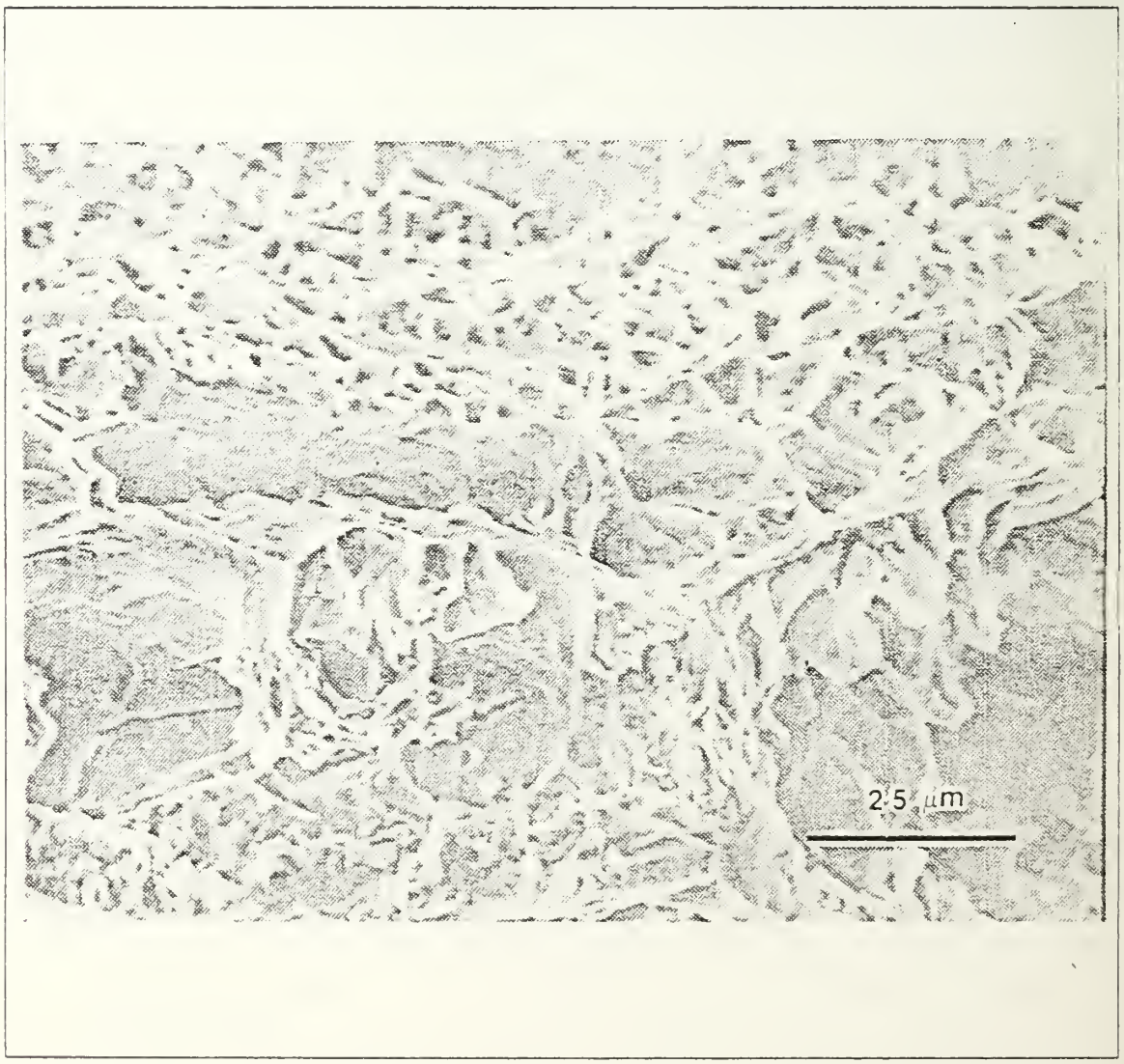

Figure A.1 Fracture Surface for Tensile Specimen of As-Quenched INCRAMUTE (at 200X and 823X).

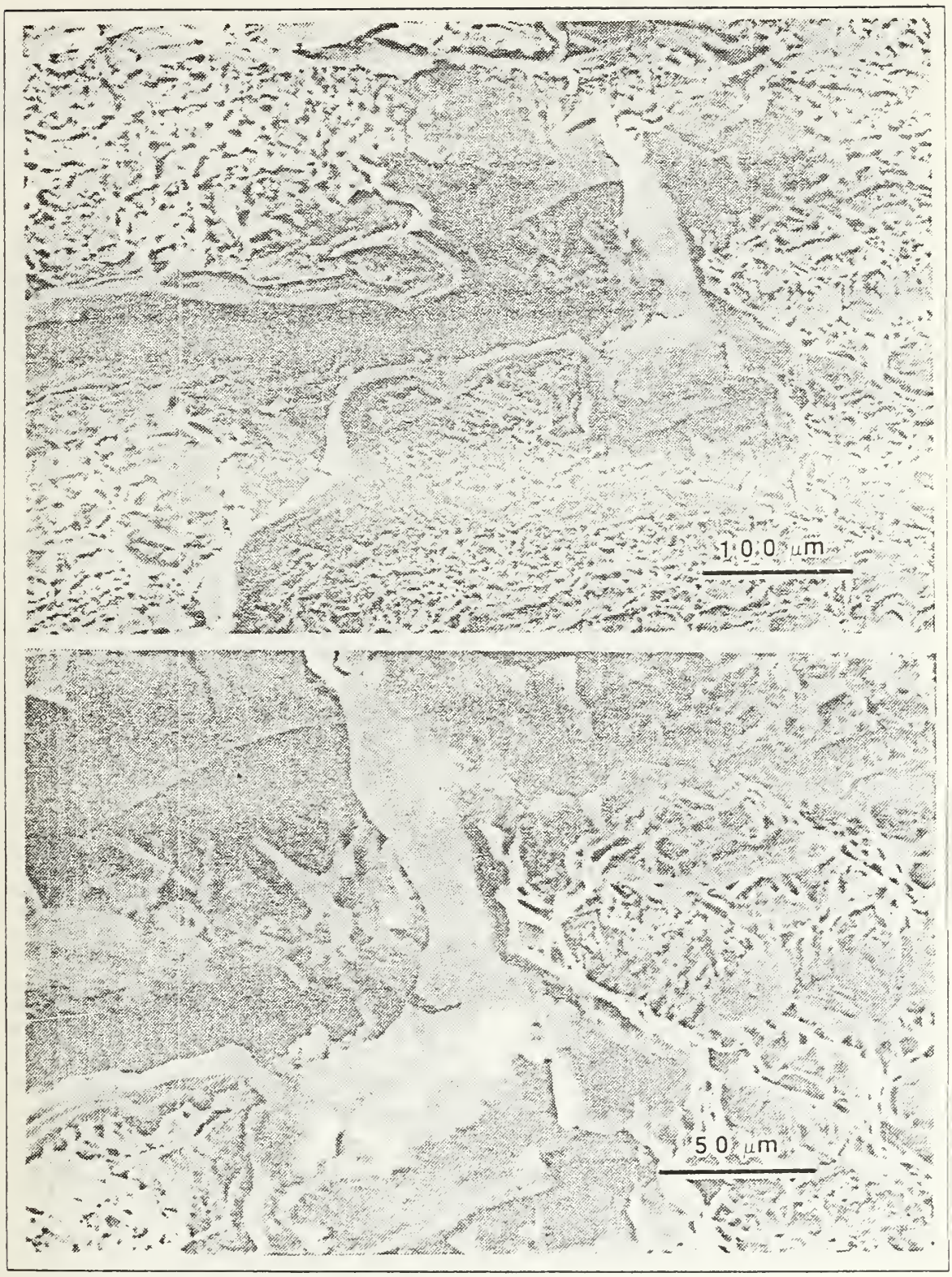

Figure A.2 Fracture Surface for Tensile Specimen of INCRAMUTE Aged at 400°C for 1 Hour (at 187X and 386X).

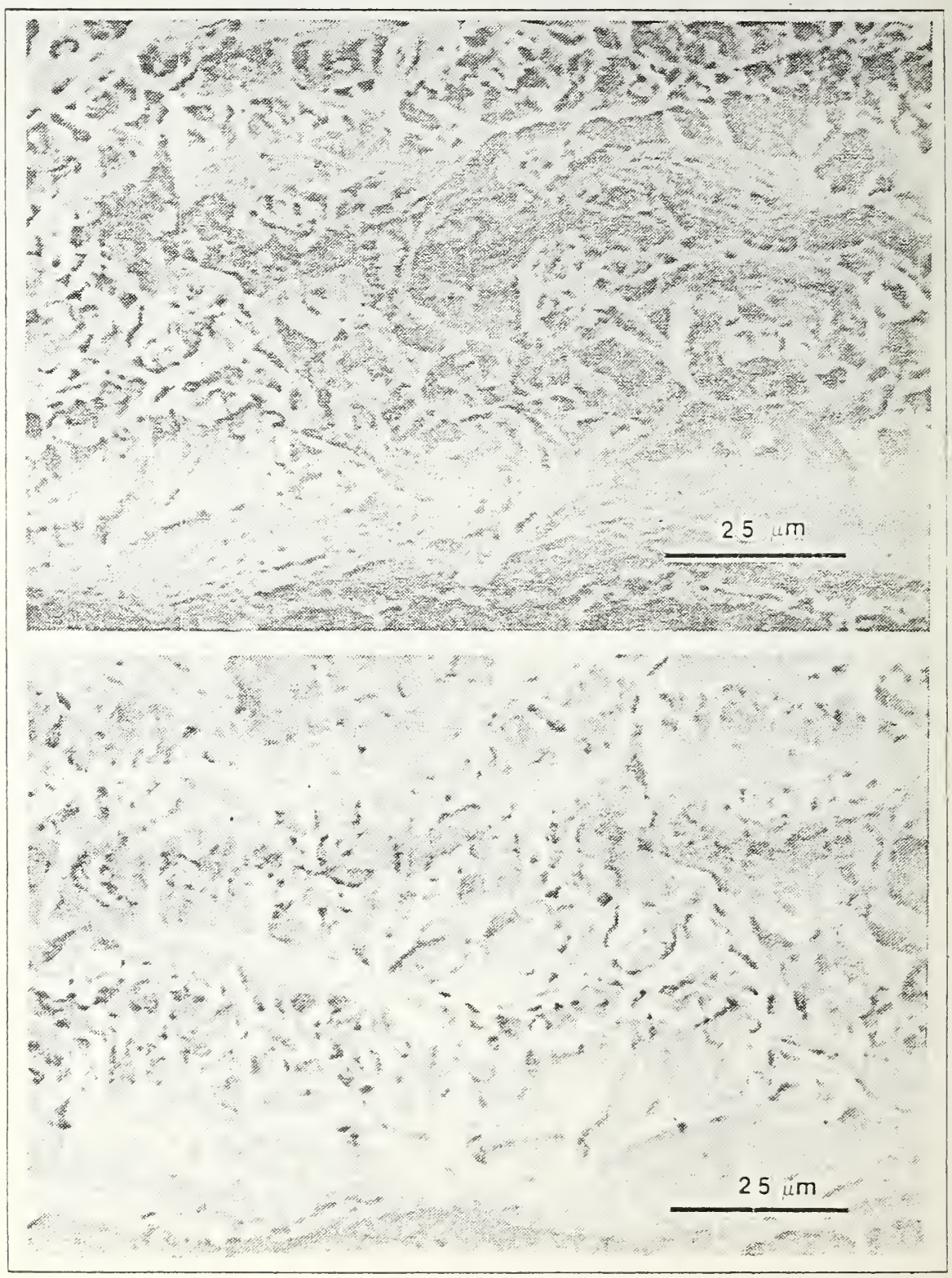

Figure A.3 Fracture Surface for Tensile Specimen of INCRAMUTE Aged at 400°C for 4 Hour (at 868X).

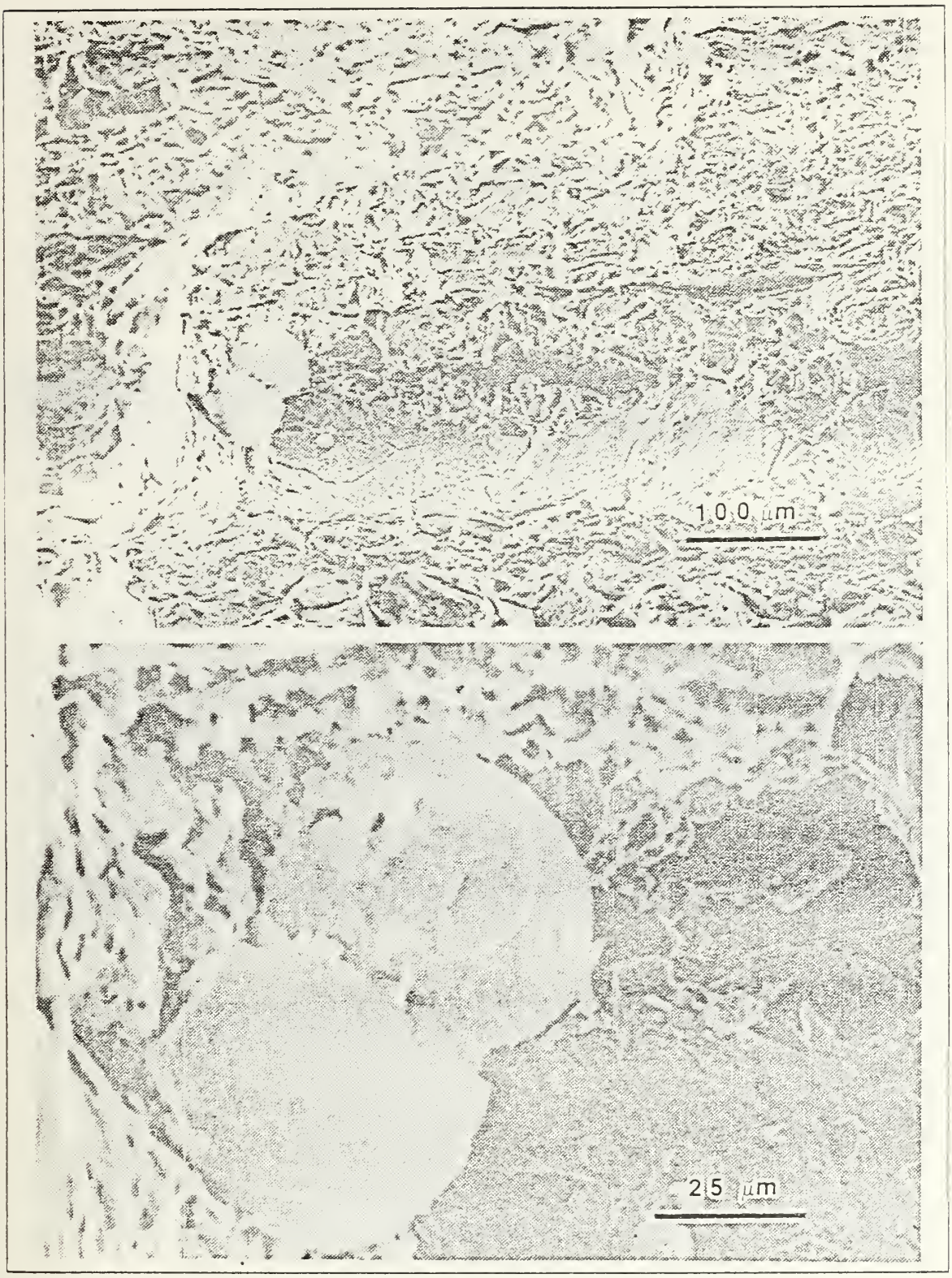

Figure A.4 Fracture Surface for Tensile Specimen of INCRAMUTE Aged at 400°C for 16 Hour (at 158X and 660X).

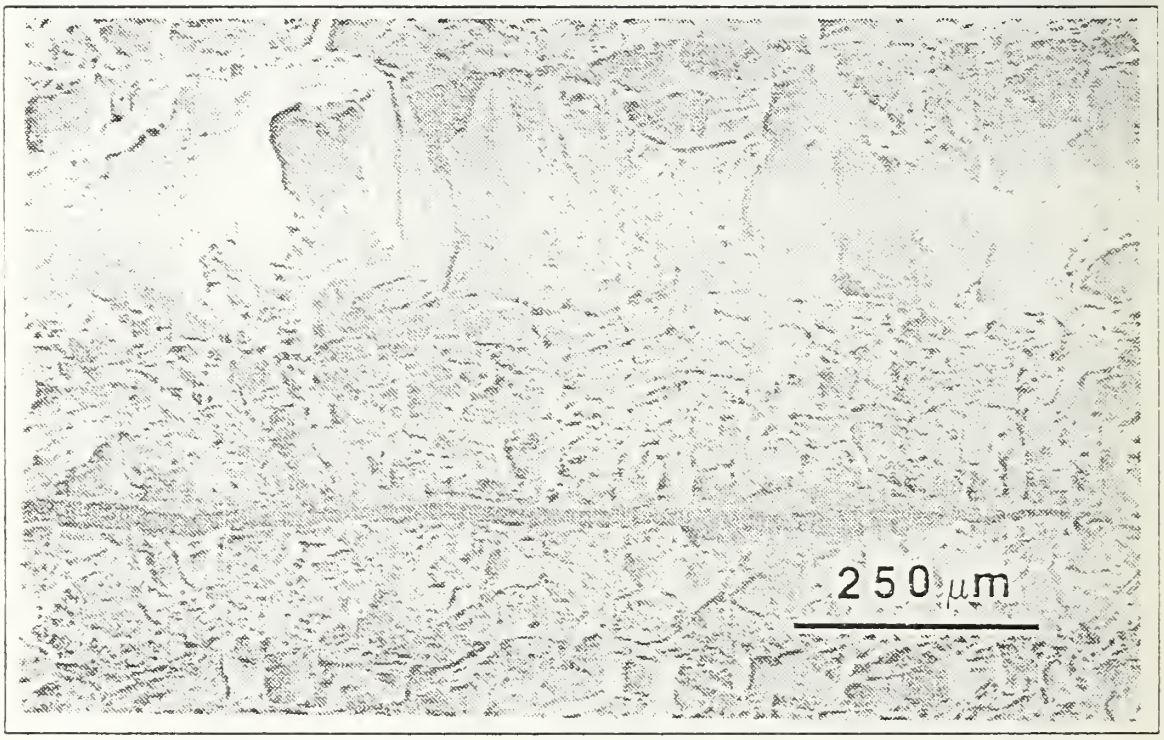

Figure A.5 Fracture Surface for Tensile Specimen of INCRAMUTE Aged at 400°C for 64 Hour (at 99X).

APPENDIX B

DAMPING DATA ON UNTREATED 1020 STEEL

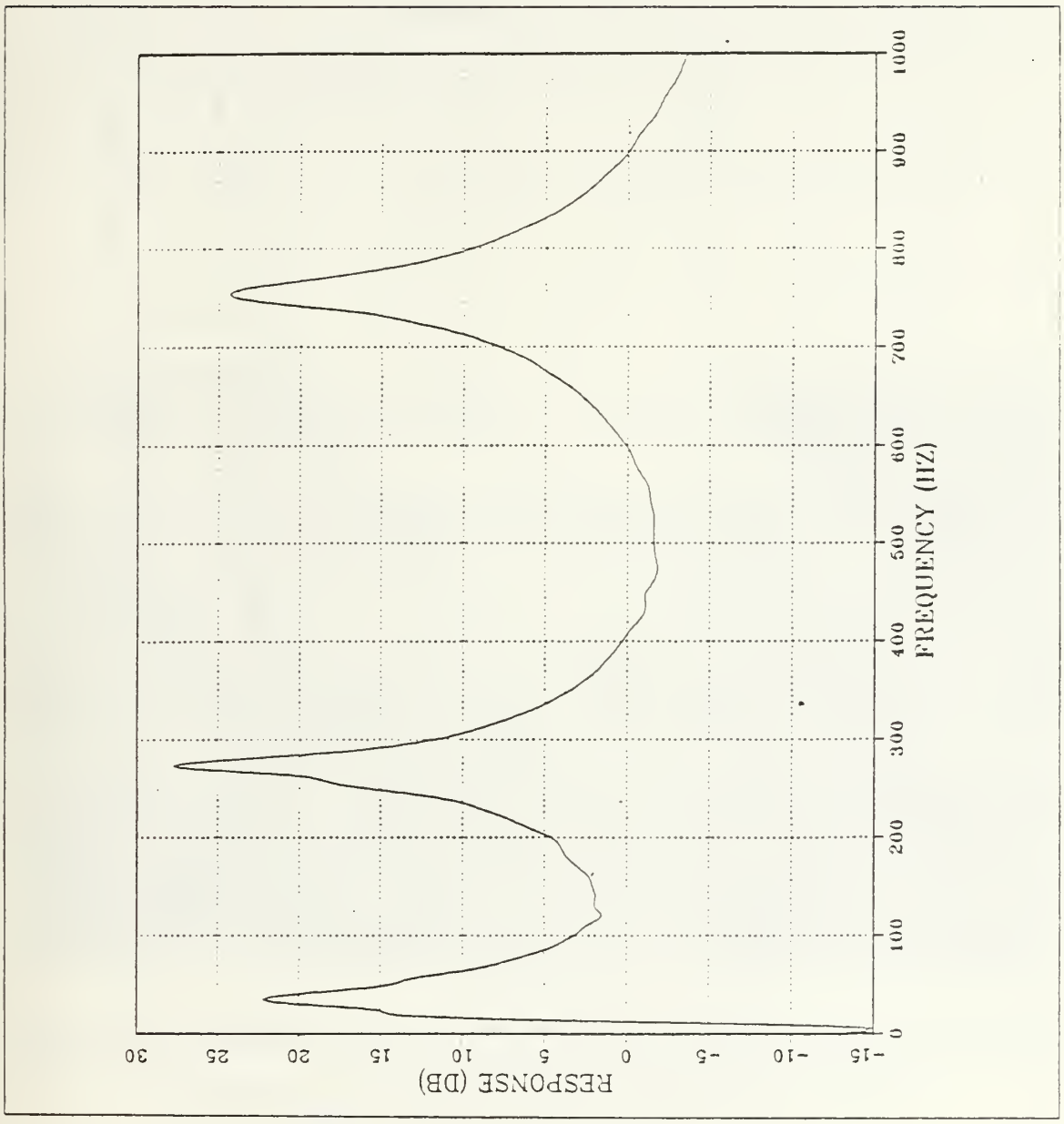

Figure B.1 Broadband Frequency Response of Untreated 1020 Steel.

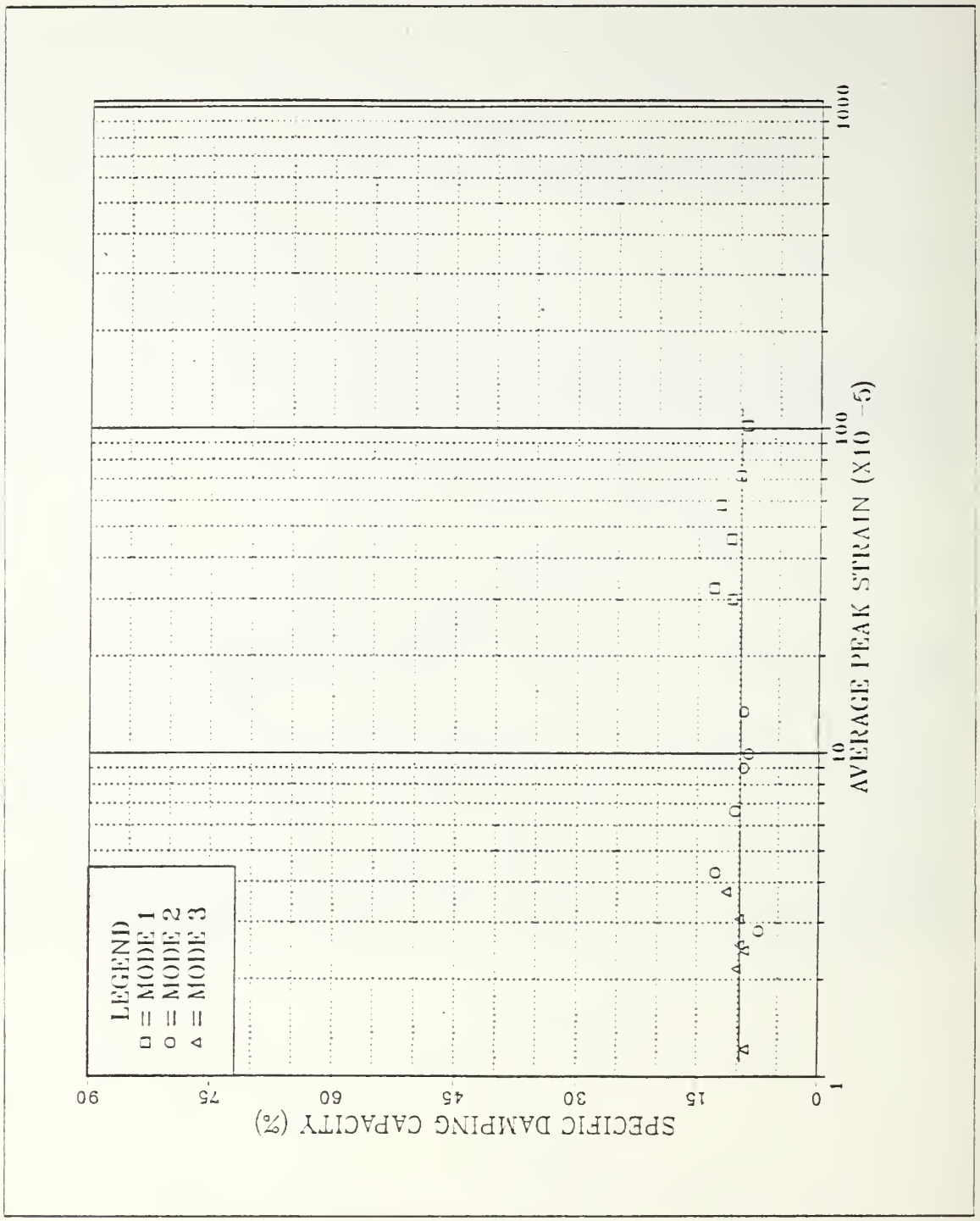

Figure B.2 SDC-Strain Relationship for Untreated 1020 Steel Under the First Three Harmonic Modes.

APPENDIX C

TRANSMISSION ELECTRON MICROGRAPHS OF INCRAMUTE FOR VARIOUS HEAT TREATMENTS

The following are additional transmission electron micrographs (TEM) of INCRAMUTE in the as-quenched condition and aged for 2, 8, and 16 hours. Similar features to those already mentioned in the text can be seen.

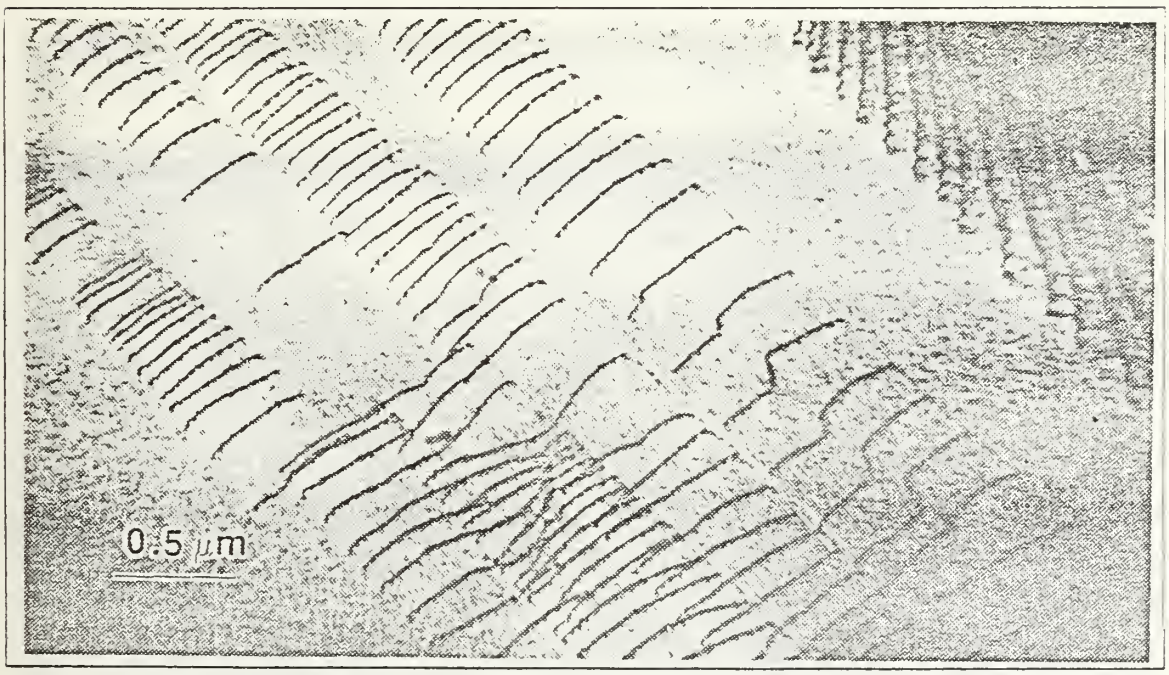

Figure C.1 Transmission Electron Micrograph of As-Quenched INCRAMUTE Foil.

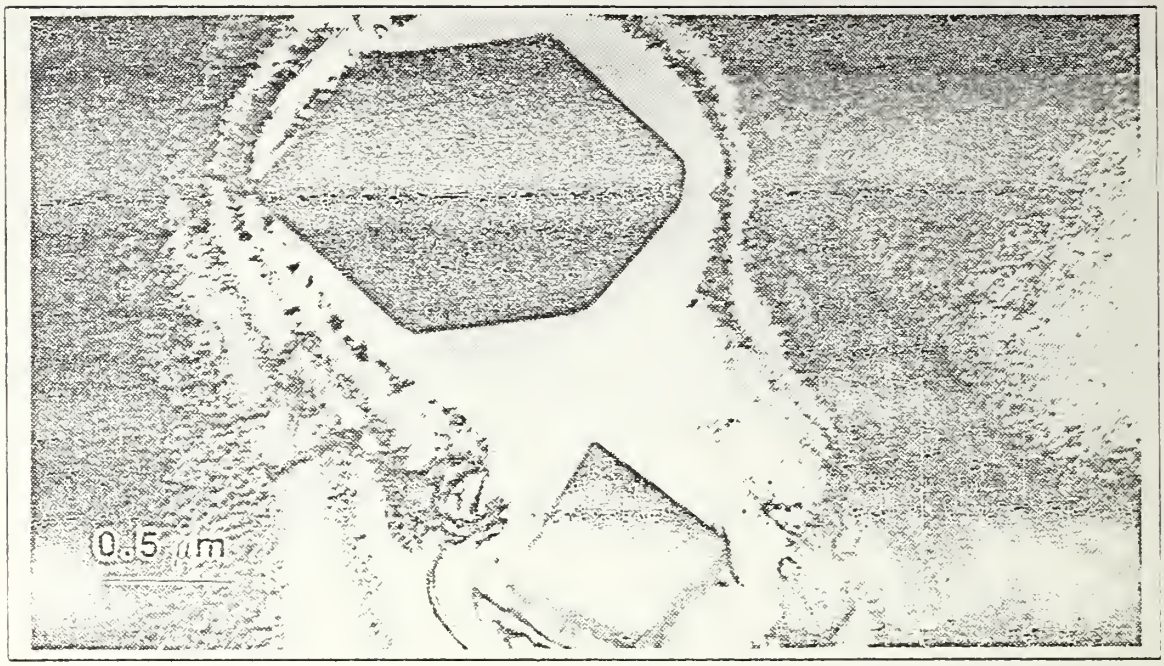

Figure C.2 Transmission Electron Micrograph of As-Quenched INCRAMUTE Foil.

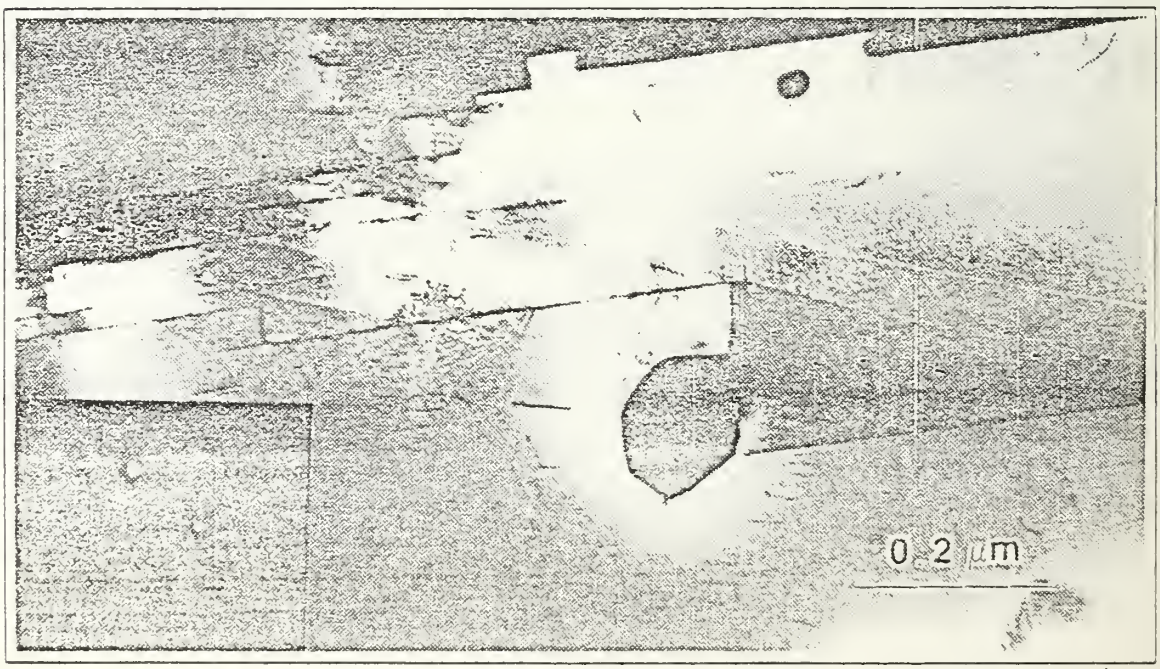

Figure C.3 Transmission Electron Micrograph of As-Quenched INCRAMUTE Foil.

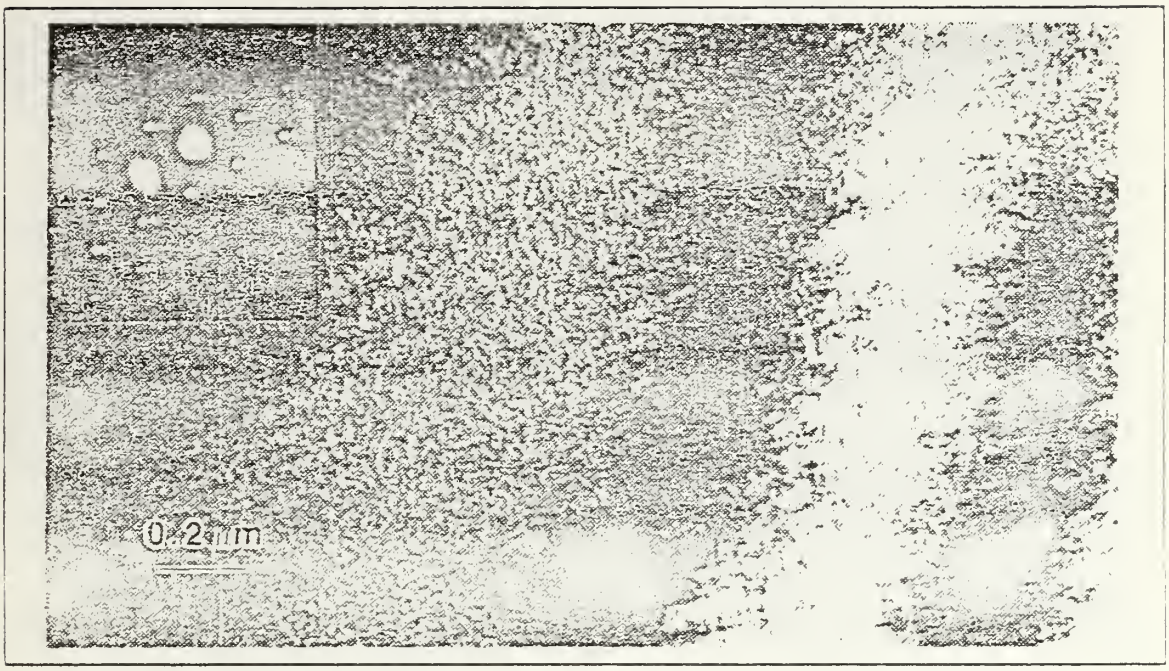

Figure C.4 Transmission Electron Micrograph of As-Quenched INCRAMUTE Foil.

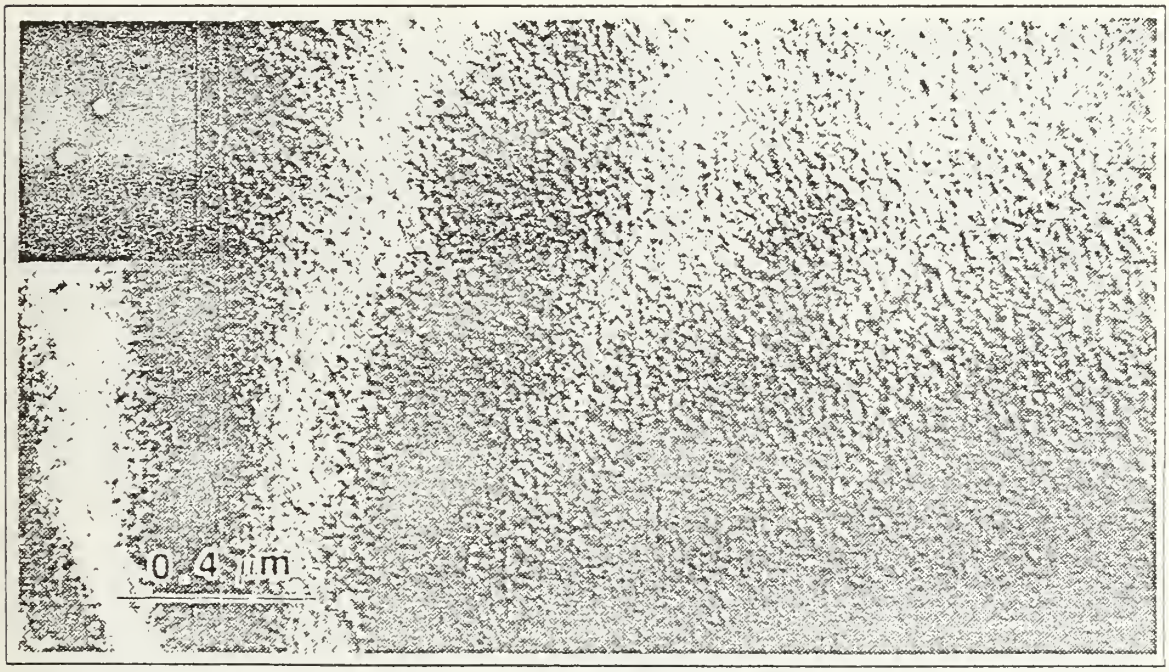

Figure C.5 Transmission Electron Micrograph of INCRAMUTE Foil Aged at 400°C for 2 Hours.

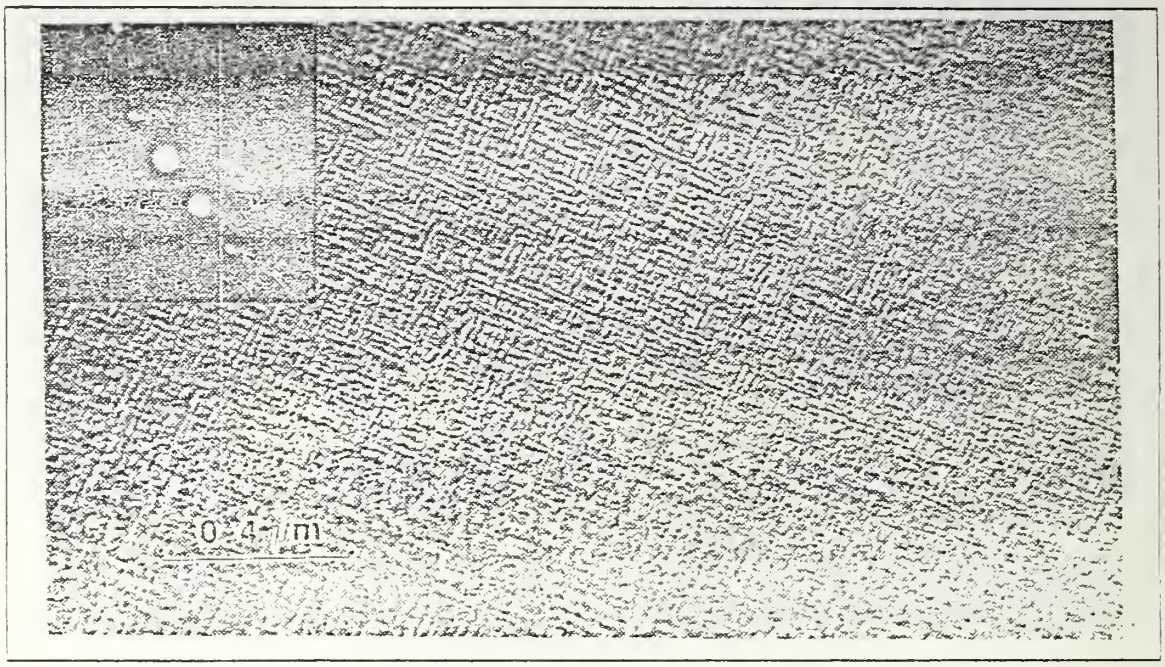

Figure C.6 Transmission Electron Micrograph of INCRAMUTE Foil Aged at 400°C for 8 Hours.

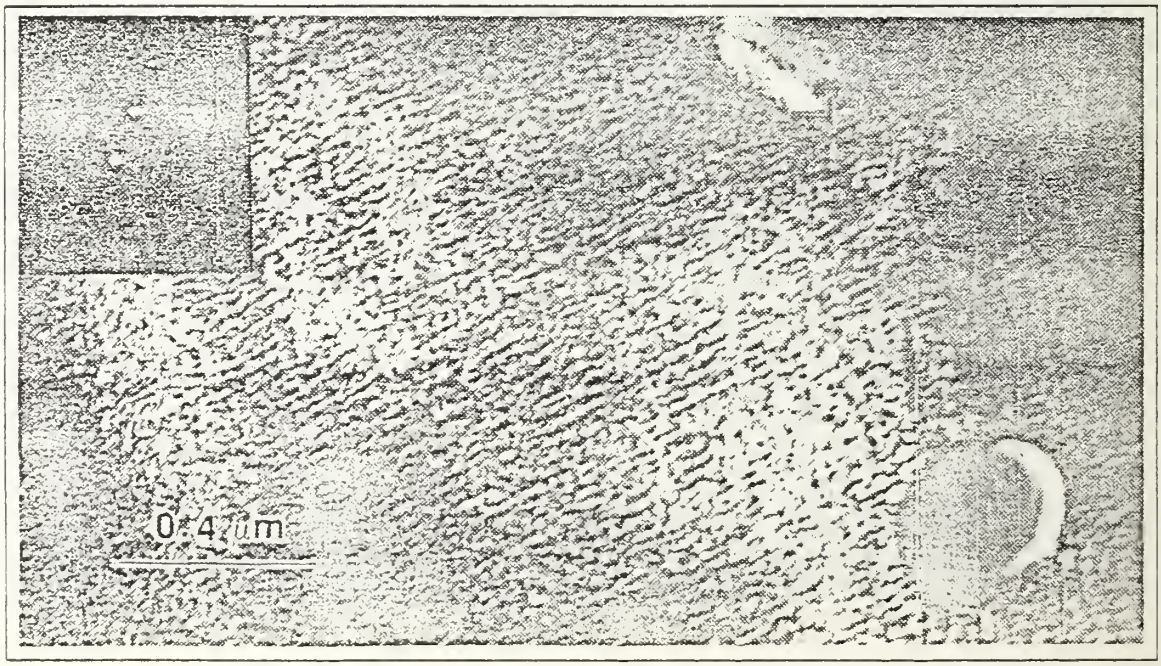

Figure C.7 Transmission Electron Micrograph of INCRAMUTE Foil Aged at 400°C for 8 Hours.

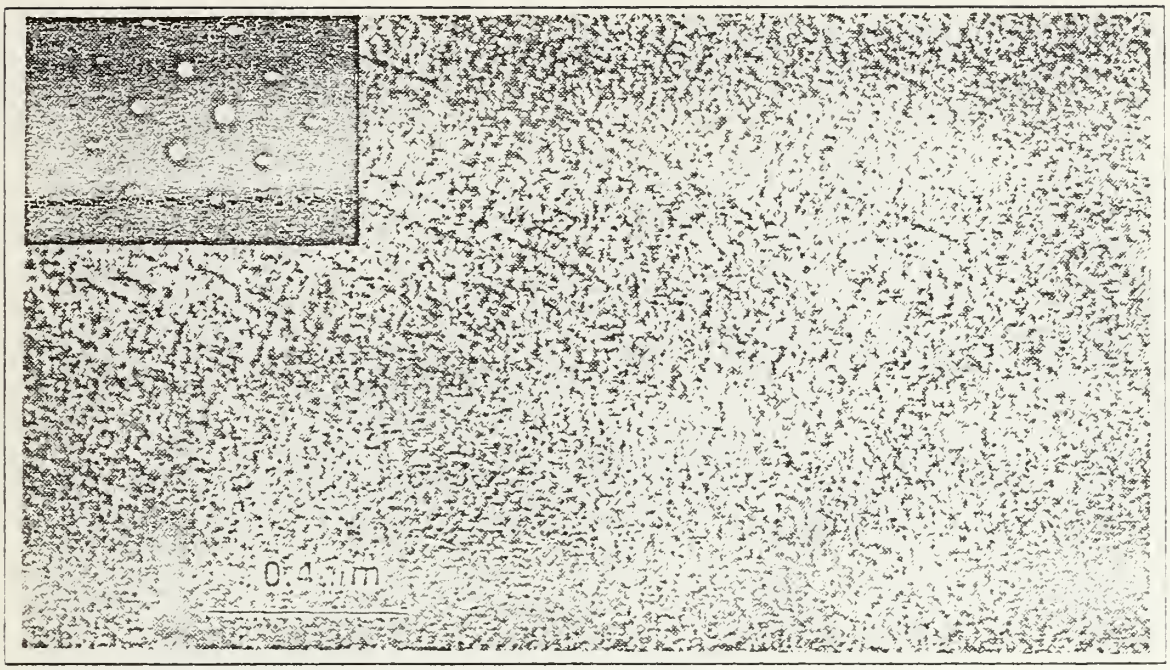

Figure C.8 Transmission Electron Micrograph of INCRAMUTE Foil Aged at 400°C for 8 Hours.

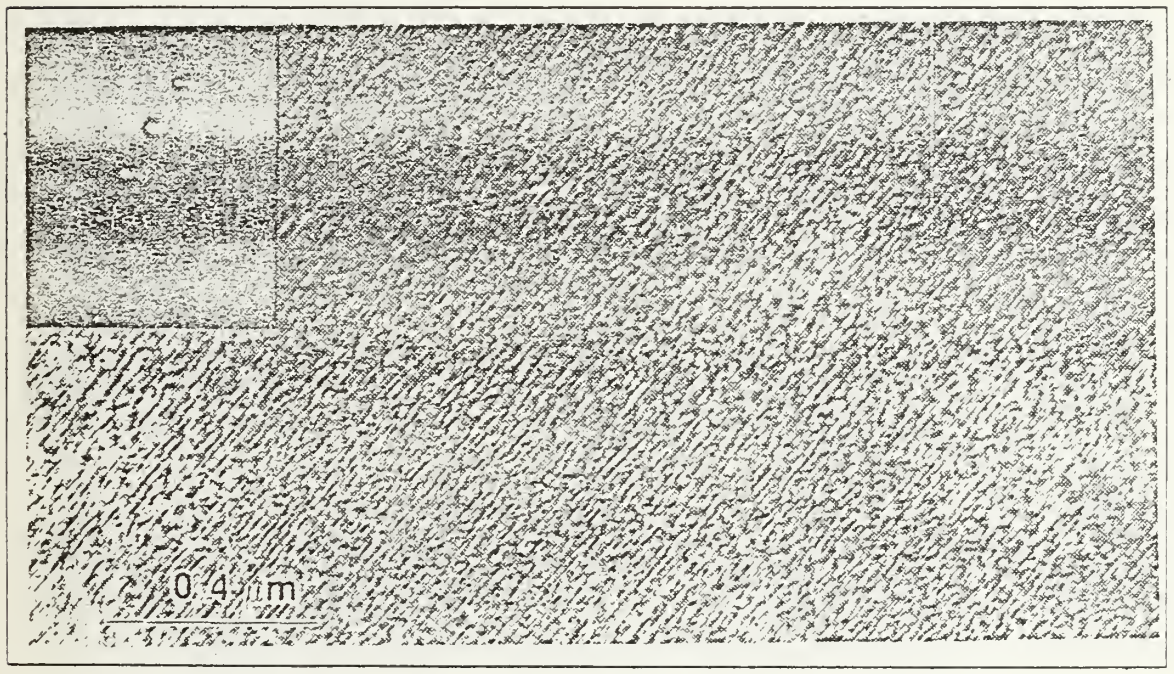

Figure C.9 Transmission Electron Micrograph of INCRAMUTE Foil Aged at 400°C for 8 Hours.

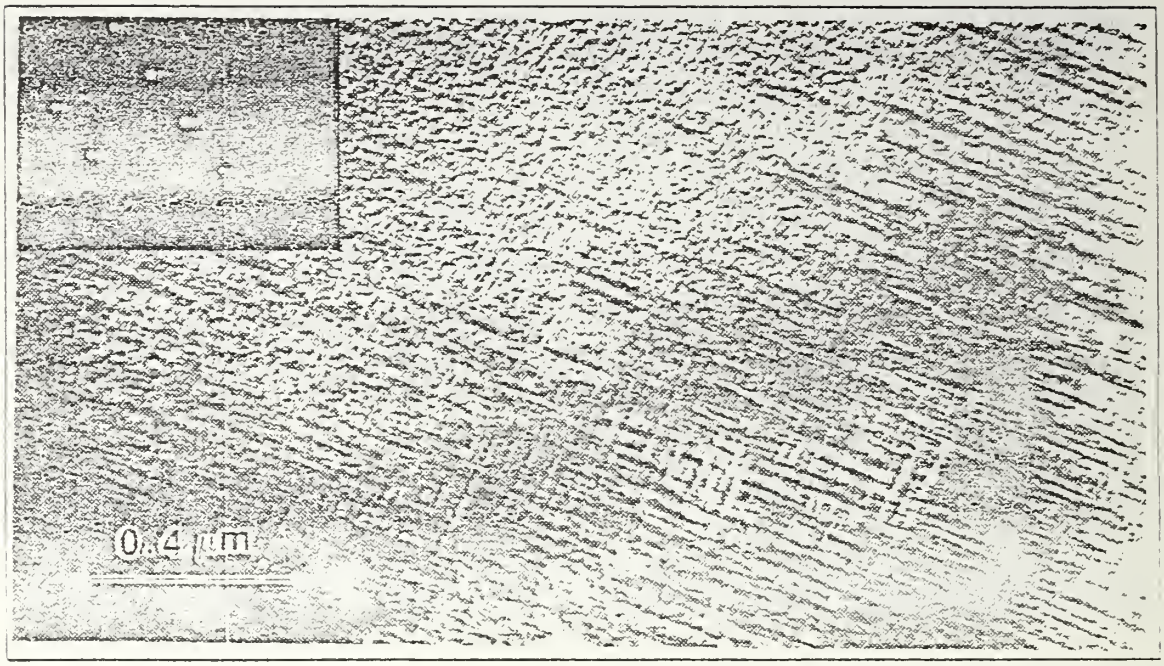

Figure C.10 Transmission Electron Micrograph of INCRAMUTE Foil Aged at 400°C for 8 Hours.

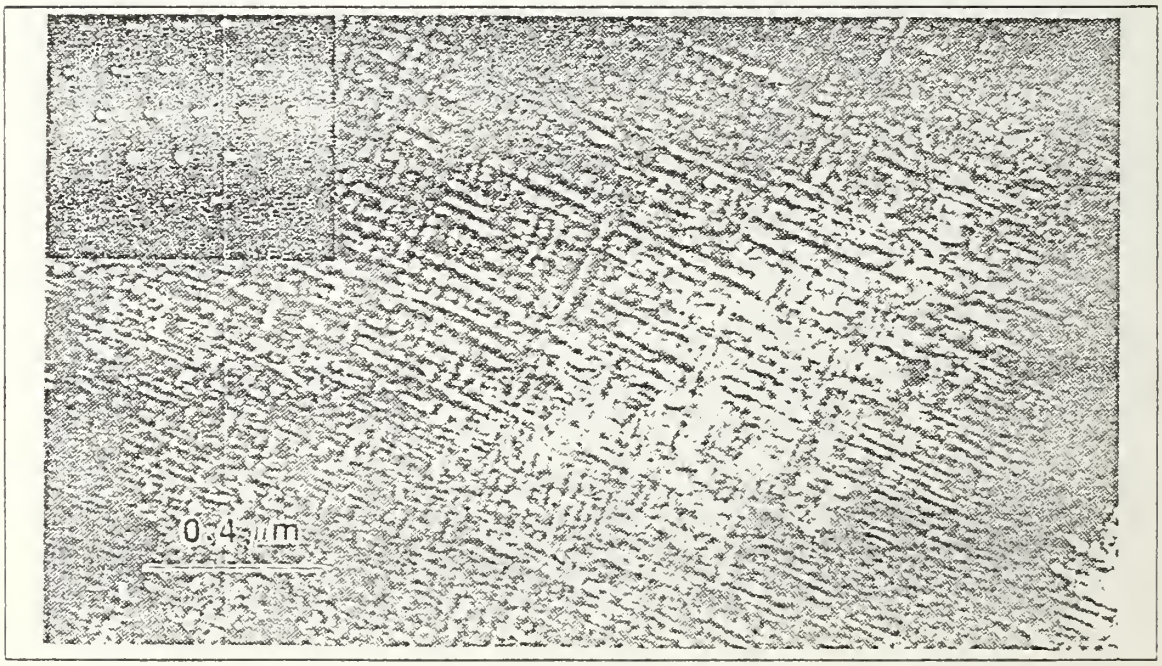

Figure C.11 Transmission Electron Micrograph of INCRAMUTE Foil Aged at 400°C for 8 Hours.

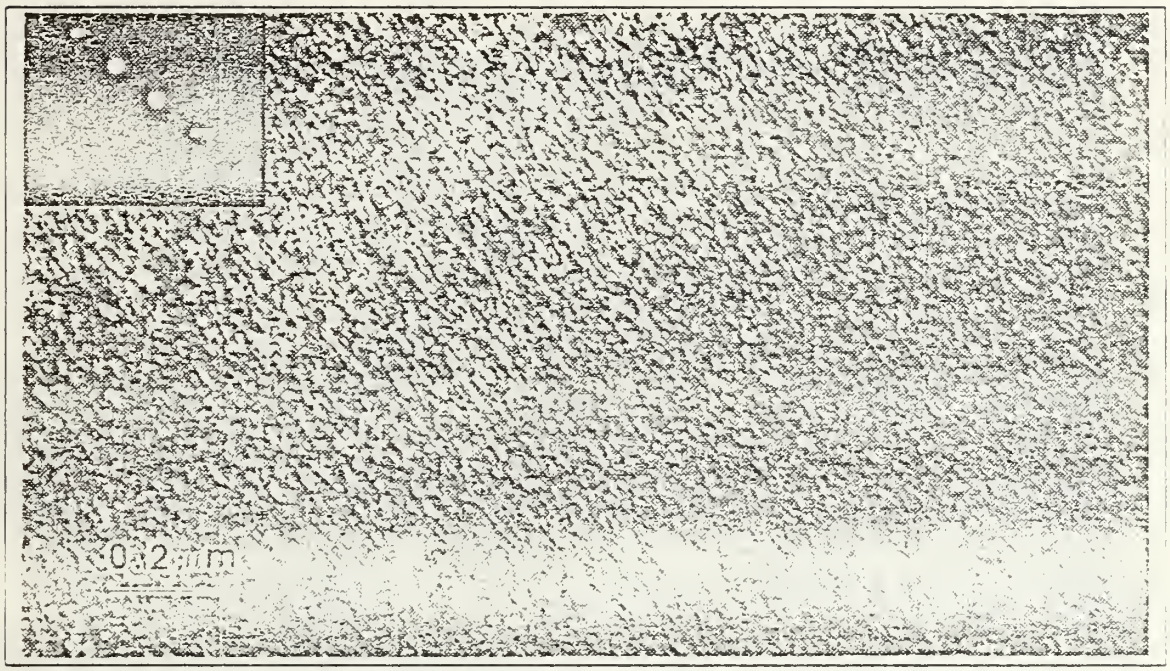

Figure C.12 Transmission Electron Micrograph of INCRAMUTE Foil Aged at 400°C for 16 Hours.

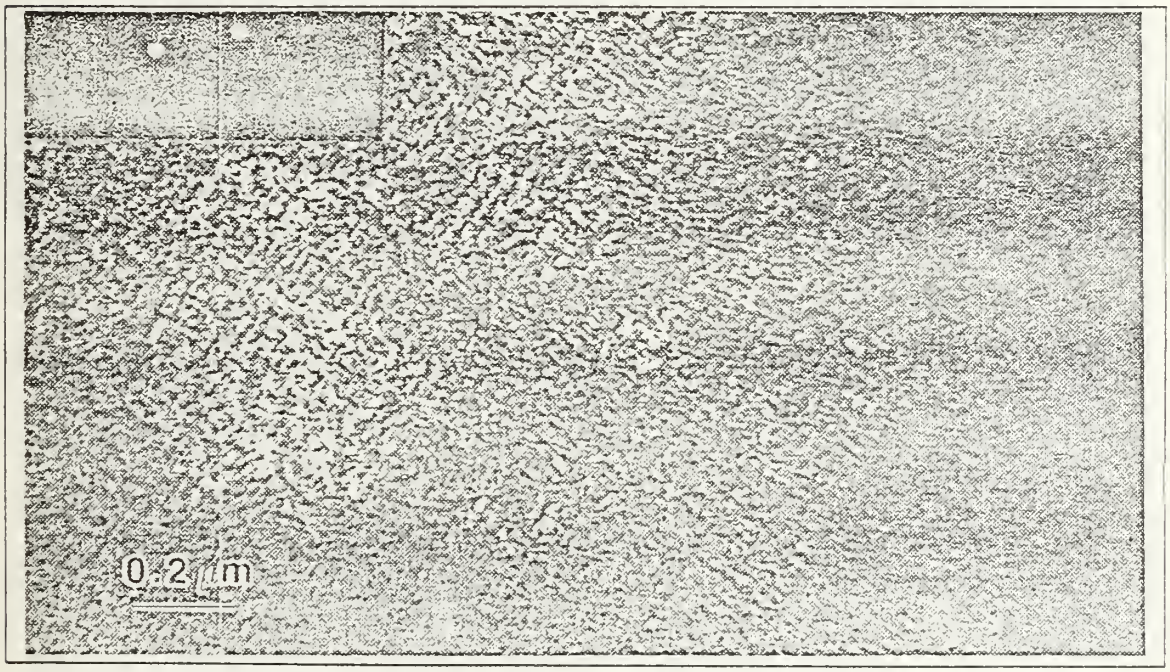

Figure C.13 Transmission Electron Micrograph of INCRAMUTE Foil Aged at 400°C for 16 Hours.

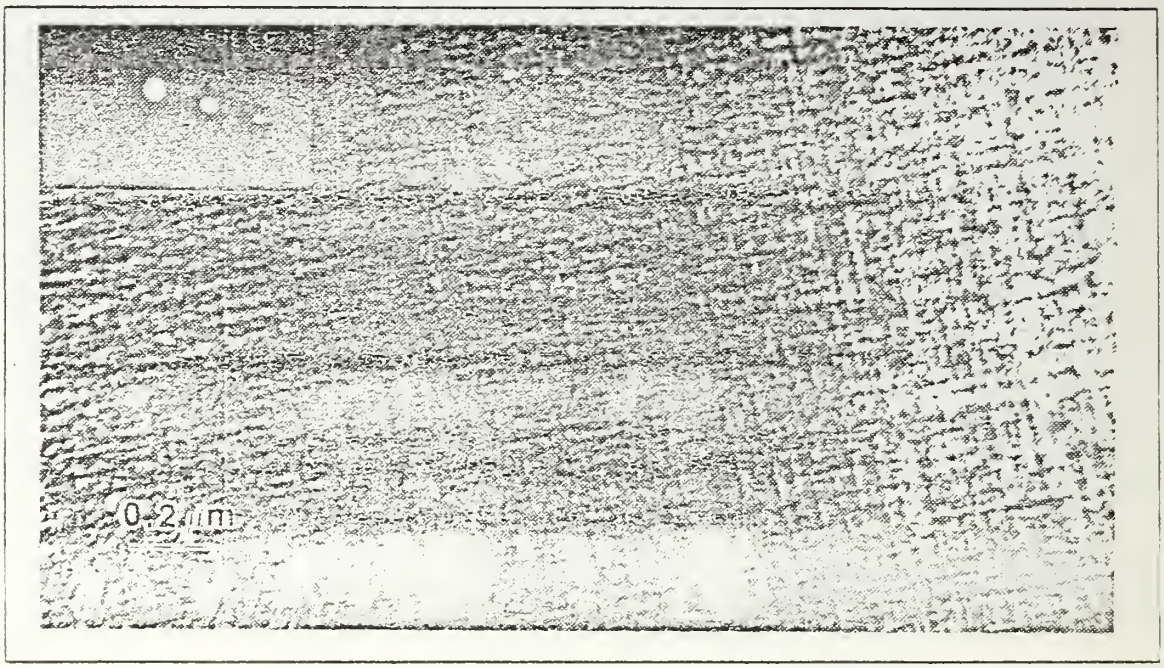

Figure C.14 Transmission Electron Micrograph of INCRAMUTE Foil Aged at 400°C for 16 Hours.

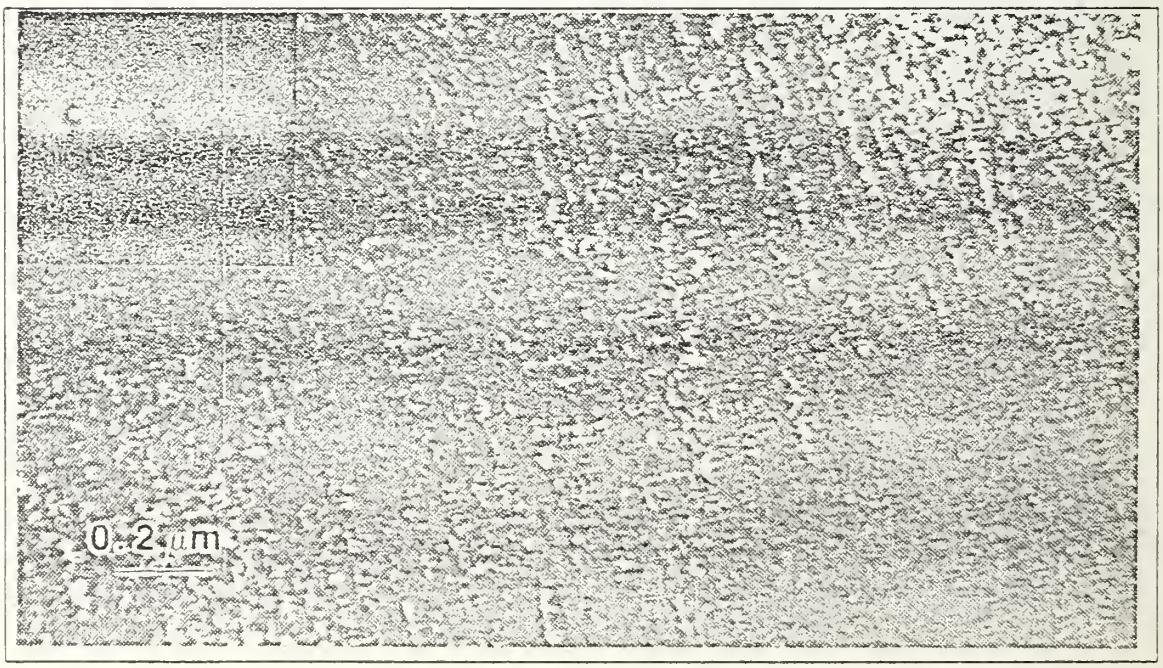

Figure C.15 Transmission Electron Micrograph of INCRAMUTE Foil Aged at 400°C for 16 Hours.

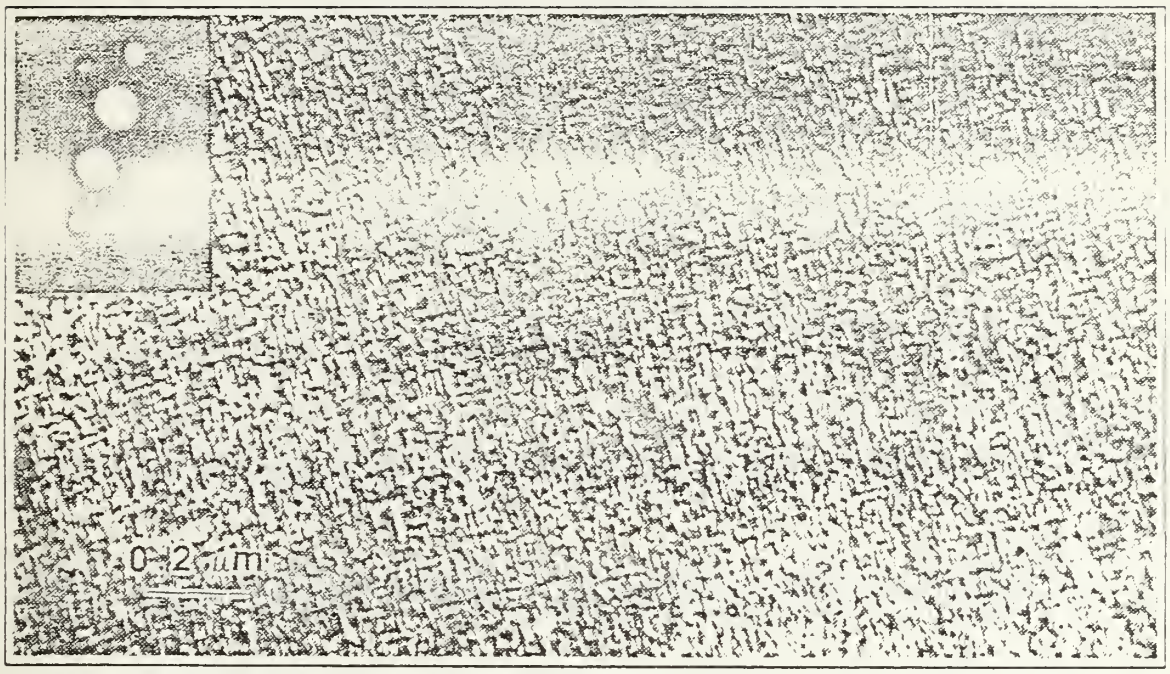

Figure C.16 Transmission Electron Micrograph of INCRAMUTE Foil Aged at 400°C for 16 Hours.

LIST OF REFERENCES

1. Bert, C.W., "Material Damping: An Introductory Review of Mathematical Models, Measures and Experimental Techniques," *Journal of Sound and Vibration* , Vol. 29, No. 2, pp. 129-153, 1973.

2. de Batist, R., *Internal Friction of Structural Defects in Crystalline Solids*, North-Holland Publishing Co., Amsterdam, 1972.

3. Sogabe, Y., Kishida, K., and Nakagawa, K., "Wave Propagation Analysis for Determining the Dynamic Properties of High Damping Alloys," *Bulletin of the JSME*, Vol. 25, No. 201, pp. 321-327, March 1982.

4. Reed-Hill, R.E., *Physical Metallurgical Principles*, Brooks Cole Engineering Div., 1973.

5. Thomson, W.T., *Theory of Vibration with Applications*, Prentice-Hall, Inc., 1981.

6. Ito, K. and Tsukishima, M., "Damping Capacity of $(Mn_{1-x}Co_x)_{0.95}Cu_{0.05}$ Metastable γ-Phase Alloys," *Transactions of the Japan Institute of Metals*, Vol. 26, No. 5, pp. 319-324, 1985.

7. Aoyagi, T. and Sumino, K., "Mechanical Behaviour of Crystals with Twinned Structure," *Physica Status Solidi*, Vol. 33, pp. 317-326, 1969.

8. Birchon, D., Bromley, D.E., and Healey, D., "Mechanism of Energy Dissipation in High-Damping-Capacity Manganese-Copper Alloys," *Metal Science Journal*, Vol. 2, pp. 41-46, 1968.

9. Butler, E.P., and Kelly, P.M., "High Damping Capacity - Copper Alloys. Part II - The Effect of Storage and of Deformation on the Damping Capacity of 70/30 Mn-Cu Alloy," *Transactions of the Metallurgical Society of AIME*, Vol. 242, pp. 2107-2109, October 1968.

10. Goodwin, R.J., "Manganese-Copper Alloys of High Damping Capacity," *Metal Science Journal*, Vol. 2, pp. 121-128, 1968.

11. Hills, N.A., *A Study of the Influence of Stress and Temperature on the Damping Capacity of Mn-Cu Alloys for Ship Silencing Applications*, M.S. Thesis, Naval Postgraduate School, Monterey, California, September 1974.

12. Sugimoto, K., Mori, T., and Shiode, S., "Effect of Composition on the Internal Friction and Young's Modulus in γ-Phase Mn-Cu Alloys," *Metal Science Journal*, Vol. 7, pp. 103-108, 1973.

13. Sugimoto, K. and Mizutani, K., "Changes of Internal Friction and Young's Modulus Associated with 400°C - Aging in High-Damping Mn-Cu and Mn-Cu-Ni Alloys," *Journal of Japan Institute of Metal* (in Japanese, *Nippon Kinzoku Gakkai-shi*), Vol. 39, No. 5, pp. 503-511, May 1975.

14. Bolt, Beranek, and Newman, Inc., Cambridge, Massachusetts, "Operations Manual for the Bolt, Beranek, and Newman, Inc., Resonant Dwell Apparatus," January 1973.

15. Heine, J.C., *The Stress and Frequency Dependence of Material Damping in Some Engineering Alloys*, Ph.D. Thesis, Massachusetts Institute of Technology, Cambridge, Massachusetts, June 1966

16. Kaufman, L., Kulin, S.A., and Neshe, P., "Internal Vibration Absorption in Potential Structural Materials," *Shape Memory Effects in Alloys*, Jeff Perkins, ed., Plenum Press, pp. 547-561, 1975.

17. Dew, D.D., *Strain Dependent Damping Characteristics of a High Damping* Manganese-Copper Alloy, M.S. and M.E. Thesis, Naval Postgraduate School, Monterey, California, September 1986.

18. de Batist, R., "High Damping Materials: Mechanisms and Applications," *Journal de Physique*, Vol. 44, pp. C9-39 - C9-50, December 1983.

19. Granato, A. and Lucke, K., "Theory of Mechanical Damping Due to Dislocations," *Journal of Applied Physics*, Vol. 17, No. 6, pp. 583-593, June 1956.

20. Birchon, D., "High Damping Alloys: Part 1," *Engineering Materials and Design*, pp. 606-608, September 1964.

21. Krishnan, R.V., Delaey, L., Tas, H., and Warlimont, H., "Thermoelasticity, Pseudoelasticity and the Memory Effects Associated with Martensitic Transformations: Part 2 The Macroscopic Mechanical Behaviour," *Journal of Materials Science*, Vol. 9, pp. 1536-1544, 1974.

22. Khachin, V.N. and Solovev, L.A., "Anelastic Behaviour of Materials During Martensitic Transformations," *Physica Status Solidi*, Vol. 30, pp. 671-682, 1975.

23. Sumino, K., "Experimental Determination of Intrinsic Resistive Stress for Twinning Surface Dislocations," *Physica Status Solidi*, Vol. 33, pp. 327-335, 1969.

24. Hedley, J.A., "The Mechanism of Damping in Manganese-Copper Alloys," *Metal Science Journal*, Vol. 2, pp. 129-137, July 1968.

25. "Discussion: The Physical Metallurgy of Alloys of High Damping Capacity," *Journal of the Institute of Metals*, Vol. 93, pp. 546-549, 1964-1965.

26. Butler, E.P. and Kelly, P.M., "High Damping Capacity Manganese-Copper Alloys. Part I - Metallography," *Transactions of the Metallurgical Society of AIME*, Vol. 242, pp. 2099-2106, October 1968.

27. Basinski, Z.S. and Christian, M.A., "The Cubic-Tetragonal Transformation in Manganese-Copper Alloys," *Journal of the Institute of Metals*, Vol. 80, pp. 659-666, 1951-1952.

28. Butler, E.P. and Kelly, P.M., "High Damping Capacity Manganese-Copper Alloys," *Proceedings of Sixth International Congress for Electron Microscopy*, Kyoto, Maruzen Co., Ltd., Nihonbashi, Tokyo, pp. 451-452, 1966.

29. Dean, R.S., Long, J.R., Graham, T.R., Roberson, A.H., and Armantrout, C.E., "The Alpha Solid Solution of the Copper-Manganese-Aluminum System," *Transactions of the AIME*, Vol. 171, pp. 70-88, 1947.

30. Smith, J.H. and Vance, E.R., "Decomposition of Gamma-Phase Manganese Copper Alloys," *Journal of Applied Physics*, Vol. 40, No. 12, pp. 4855-4858, November 1969.

31. Worrell, F.T., "Twinning in Tetragonal Alloys of Copper and Manganese," *Journal of Applied Physics*, Vol. 19, pp. 929-933, October 1948.

32. Bacon, G.E., Dunmur, I.W., Smith, J.H., and Street, R., "The Antiferromagnetism of Manganese Copper Alloys," *Proceedings of the Royal Society of London, Series A*, Vol. 241, pp. 223-238, 1957.

33. Meneghetti, D. and Sidhu, S.S., "Magnetic Structures in Copper-Manganese Alloys," *Physical Review*, Vol. 105, No. 1, pp. 130-135, 1 January 1957.

34. Street, R., "Magnetic Properties of Manganese Copper Alloys," *Journal of Applied Physics*, Supplement to Vol. 31, No. 5, pp. 310S-317S, May 1960.

35. Schwaneke, A.F. and Jensen, J.W., "Magnetic Susceptibility and Internal Friction of Tetragonal Manganese-Copper Alloys Containing 70 Percent Manganese," *Journal of Applied Physics*, Supplement to Vol. 33, No. 3, pp. 1350-1351, March 1962.

36. Vitek, J.M. and Warlimont, H., "On a Metastable Miscibility Gap in γ-Mn-Cu Alloys and the Origin of Their High Damping Capacity," *Metal Science*, Vol. 10, No. 1, pp. 7-13, January 1976.

37. Men'shikov, A.Z., Faystov, Yu. K., Kochetkova, L.P., Konoplev, L.M., and Dorofeyev, Yu. A., "Structural Transformations During the Tempering of High-Damping Manganese-Copper Alloys," *Physics of Metals and Metallography* (in Russian, *Fiz. metal. metalloved.*), Vol. 39, No. 4, pp. 793-800, 1975.

38. Vintaykin, Ye. Z., Litvin, D.F., and Udovenko, V.A., "Fine Crystalline Structure in Highly Shock-Absorbing Alloys of Manganese and Copper," *Physics of Metals and Metallography* (in Russian, *Fiz. metal. metalloved.*), Vol. 37, No. 6, pp. 1228-1237, 1974.

39. Venkateswarao, P. and Chatterjee, D.K., "Structural Studies on the Alloying Behaviour of γ-Mn and the Development of a High Damping Capacity in Mn-Cu Alloys," *Journal of Material Science*, Vol. 15, pp. 139-148, 1980.

40. Guseva, L.N., Dolinskaya, L.K., and Skurikhin, M.N., "Aging of Alloy Cu + 72% Mn Alloyed with Nickel, Iron and Aluminum," *Izvestiya Akademii Nauk SSSR. Metally*, No. 6, pp. 138-142, 1984.

41. Hermann, C., Lohrmann, O., and Philipp, H., *Strukturbericht Band II 1928-1932*, Edwards Brothers, Inc., 1943.

42. Villars, P. and Calvert, L.D., *Pearson's Handbook of Crystallographic Data for Intermetallic Phases*, Vol. 1, American Society for Metals, 1985.

43. Sugimoto, K., "Internal Friction Phenomena Associated with Diffusionless Phase Transformations in Alloys," *Journal de Physique*, Vol. 42, pp. C5-971 - C5-982, October 1981.

44. Rakhshtadt, A.G., Favstov, Yu. K., and Kochetkova, L.P., "Structural Transformations in Mn-Cu Alloys with High Damping Capacity," *Metal Science and Heat Treatment* (in Russian, *Metallovedenie i Termichskaya Obrabotka Metallov*), Vol. 15, No. 1-2, pp. 108-112, January February 1973.

45. Bichinashvili, A.J., Vintaykin, Ye. Z., Litvin, D.F., and Udovenko, V.A., "X-Ray Investigation of the FCC——>FCT Transformation in Manganese-Copper Alloy," *Physics of Metals and Metallography* (in Russian, *Fiz. metal. metalloved.*), Vol. 41, No. 1, pp. 112-117, 1976.

46. Vintaykin, Ye. Z., Dmitriyev, V.B., and Udovenko, V.A., "Antiferromagnetism in Heterogeneous Manganese-Copper Alloys," *Physics of Metals and Metallography* (in Russian, *Fiz. metal. metalloved.*), Vol. 44, No. 5, pp. 107-113, 1979.

47. Wolfenden, A., "Mechanical Damping at 40 kHz in Mn-Cu Alloys," *Physica Status Solidi (A)*, Vol. 44, pp. K171-K175, 1977.

48. Zolotukhin, I.V., Tkachenko, T.V., Skorobogatov, V.S., and Shvetsov, N.F., "Effect of Heat Treatment on Damping Mechanical Oscillations in a 70% Mn-30% Cu Alloy," *Soviet Journal of Non-Ferrous Metals* (in Russian, *Tsvetnye Metally*), pp. 63-64, 1974.

49. Sugimoto, K. and Mori, T., "Internal Friction Peak Associated with Phase Transformation in Mn-Cu Alloys," *Proceedings of the International Conference on Internal Friction and Ultrasonic Attenuation in Crystalline Solids*, Vol. 1, pp. 418-425, 1975.

50. Tanner, L.E., "Diffraction Contrast from Elastic Shear Strains Due to Coherent Phases," *The Philosophical Magazine*, Vol. 14, No. 127, pp. 111-130, July 1966.

51. Tanner, L.E., "The Ordering Transformation in Ni_2V," *Acta Metallurgica*, Vol. 20, pp. 1197-1227, October 1972.

52. Delaey, L, Perkins, A.J., and Massalski, T.B., "Review: On the Structure and Microstructure of Quenched Beta-Brass Type Alloys," *Journal of Material Science*, Vol. 7, pp. 1197-1215, 1972.

53. Robertson, I.M. and Wayman, C.M., "Modulated Microstructures in Copper-Zinc and Copper-Aluminum-Nickel," *Metallurgical Transactions A*, Vol. 15A, pp. 269-276, February 1984.

54. Laughlin, D.E., Sinclair, R., and Tanner, L.E., "Comments on 'The Early Stages of the Transformation in Dilute Alloys of Titanium in Nickel'," *Scripta Metallurgica*, Vol. 14, pp. 373-376, 1980.

55. Moine, P., Michal, G.M., and Sinclair, R., "A Morphological Study of 'Premartensitic' Effects in TiNi," *Acta Metallurgica*, Vol. 30, pp. 109-123, 1982.

56. Onozuka, T., Yamamoto, T., and Hirabayashi, M., "High Resolution Images and Martensitic Transition of V_3Si by 1 MV Electron Microscopy," *Science Reports of the Research Institutes, Tohoku University*, Sendai, Japan, pp. 21-31, March 1984.

57. Onozuka, T., Ohnishi, N., and Hirabayashi, M., "Low Temperature Electron Microscopy on the Cubic-Tetragonal Transformation of V_3Si," (unpublished) presented at the 115th Annual Meeting of The Metallurgical Society of AIME at New Orleans, Louisiana, 2-6 March 1986.

58. Oshima, R., Sugiyama, M., and Fujita, F.E., "Tweed Structure Associated with FCC-FCT Transformations in Fe-Pd Alloys," (unpublished) presented at the 115th Annual Meeting of The Metallurgical Society of AIME at New Orleans, Louisiana, 2-6 March 1986.

59. Strychor, R., Williams, J.C., and Soffa, W.A., "Phase Transformations and Modulated Microstructures in Ti-Al-Nb Alloys," (unpublished) presented at the 115th Annual Meeting of The Metallurgical Society of AIME at New Orleans, Louisiana, 2-6 March 1986.

60. Kalman, Z.H., Lee, L.H., He, X.C., and Weissmann, S., "Premartensitic Strain Tensor Analysis of $Ni_{58}Al_{42}$ by the X-Ray Divergent Beam Method," TMS Technical Paper No. A86-49, The Metallurgical Society of AIME, 1986, pp. 1-26.

61. Wen, S.H., Khatchaturyan, A.G., and Morris, Jr., J.W., "Computer Simulation of a 'Tweed-Transformation' in an Idealized Elastic Crystal," *Metallurgical Transactions A*, Vol. 12A, pp. 581-587, April 1981.

62. "Standard Methods of Tension Testing of Metallic Materials," ASTM E8-83, American Society for Testing and Materials, Vol. 03.01, pp. 130-150, 1983.

63. "Standard Hardness Conversion Tables for Metals", ASTM E140-84, American Society for Testing and Materials, Vol. 03.01, pp. 325-341, 1984.

64. Khachaturyan, A.G., *Theory of Structural Transformations in Solids*, John Wiley and Sons, 1983.

BIBLIOGRAPHY

Aravin, B.P., Kuz'min, S.L., and Likhachev, V.A., "Shape Memory Effect in MnCu Alloys," *Physics of Metals* (in Russian, *Metallofizika*), Vol. 3, No. 4, pp. 739-753, 1981.

Dean, R.S., Long, J.R., and Graham, T.R., "Copper-Manganese-Aluminum Alloys - Properties of Wrought Alpha Solid Solution Alloys," *Transactions of the AIME*, Vol. 171, pp. 89-104, 1947.

Delaey, L., Krishnan, R.V., Tas, H., and Warlimont, H., "Thermoelasticity, Pseudoelasticity and the Shape Memory Effects Associated with Martensitic Transformations: Part 1 Structural and Microstructural Changes Associated with the Transformations," *Journal of Materials Science*, Vol. 9, pp. 1521-1535, 1974.

Demin, S.A., Ustinov, A.I., and Chuistov, K.V., "The Nature of the Volume Effect in Mn-Cu Alloys," *Soviet Physics Dokladi* (in Russian, *Dokladi Akademii Nauk SSSR*), Vol. 24, No. 5, pp. 387-389, May 1979.

Ito, K., Tsukishima, M., and Kobayashi, M., "Temperature Dependence of Lattice Parameters and FCC FCT FCO Transformations in Some Mn-Base Metastable γ-Phase Alloys," *Transactions of the Japan Institute of Metals*, Vol. 24, No. 7, pp. 487-490, 1983.

Jensen, J.W. and Walsh, D.F., "Manganese-Copper Damping Alloys," Bureau of Mines Bulletin 624, U.S. Department of Interior, 1965.

Kuporev, A.L. and Khandros, L.G., "Elastic Twinning in the Martensitic γ' Phase of Cu-Al-Mn and Cu-Al-Ni Alloys," *Physical Metallurgy and Metallography* (in Russian, *Fiz. metal. metalloved.*), Vol. 32, No. 6, pp. 214-217, 1971.

Kuteliya, E.R.,Kerashvili, V.N., and Sanadze, V.V., "Electron Microscope Investigation of the Processes of High Copper Cu-Mn Alloys," *Physical Metallurgy and Metallography* (in Russian, *Fiz. metal. metalloved.*), Vol. 44, No. 5, pp. 190-194, 1977.

Michal, G.M., Moine, P., and Sinclair, R., "Characterization of the Lattice Displacement Waves in Premartensitic TiNi," *Acta Metallurgica*, Vol. 30, pp. 125-138, 1982.

Nittono, O., Satoh, T., and Koyama, Y, "Cubic-Tetragonal Transformation and Reversible Shape Memory Effect in Manganese-Copper Alloys," *Transactions of the Japan Institute of Metals*, Vol. 22, No. 4, pp. 225-236, 1981.

Otsuka, K., Kubo, H., and Wayman, C.M., "Diffuse Electron Scattering and 'Streaming' Effects," *Metallurgical Transactions A*, Vol. 12A, pp. 595-605, April 1981.

Perkins, J., Edwards, G.R., and Hills, N., "Materials Approaches to Ship Silencing," Naval Postgraduate School Fiscal Year 1974 Annual Report, June 1974.

Schaller, R. and Benoit, W., "Internal Friction Associated with Precipitation and Recrystallization," *Journal de Physique*, Vol. 44, pp. C9-17 - C9-27, December 1983.

Schetky, L.M. and Perkins, J., "The 'Quiet' Alloys," *Machine Design*, pp. 202-206, 6 April 1978.

Shimizu, K., Okumura, Y., and Kubo, H., "Crystallographic and Morphological Studies on the FCC to FCT Transformation in Mn-Cu Alloys," *Transactions of the Japan Institute of Metals*, Vol. 23, No. 2, pp. 53-59, 1982.

Stokes, H.J. and Hewin, I.D., "The Effect of Ageing on Young's Modulus, Electrical Resistivity, and Hardness of 80:20 Manganese-Copper Alloy," *Journal of the Institute of Metals*, Vol. 89, pp. 77-79, 1960-1961.

Tanner, L.E., Pelton, A.R., and Gronsky, R., "The Characterization of Pretransformation Morphologies: Periodic Strain Modulations," *Journal de Physique*, Colloquium C4, Vol. 43, Supplement to No. 12, pp. C4-169 - C4-172, December 1982.

Titman, J.M., "The Heat Capacities of Some Copper-Manganese Alloys," *Proceedings of the Physical Society of London*, Vol. 77, pp. 807-810, 1961.

Vintaikin, E.Z., Litvin, D.F., and Makushev, S. Yu., "Critical Shear Stresses of Twinning and Glide in Manganese-Copper Alloys with Tetragonal Structure," *Soviet Physics Dokladi* (in Russian, *Dokladi Akademii Nauk SSSR*), Vol. 23, No. 6, pp. 425-427, June 1978.

Vintaikin, E.Z., Sakhno, V.M., and Udovenko, V.A., "Local Premartensitic Instability in FCC Manganese-Copper Alloys," *Soviet Physics Dokladi* (in Russian, *Dokladi Akademii Nauk SSSR*), Vol. 24, No. 5, May 1979, pp. 393-395, May 1979.

Vintaykin, Ye. Z. and Udovenko, V.A., "Premartensitic Instability in Manganese-Copper Alloys," *Physical Metallurgy and Metallography* (in Russian, *Fiz. metal. metalloved.*), Vol. 51, No. 5, pp. 160-162, 1981.

Vintaykin, Ye. Z., Udovenko, V.A., Litvin, D.F., and Serebryakov, V.G., "Elastic Constants of Manganese-Copper Alloys," *Physical Metallurgy and Metallography* (in Russian, *Fiz. metal. metalloved.*), Vol. 49, No. 4, pp. 182-185, 1980.

Vintaykin, Ye. Z., Udovenko, V.A., Makushev, S. Yu., and Litvin, D.F., "The Shape Memory Effect and Mechanism of Plastic Deformation in Manganese-Copper Alloys," *Physical Metallurgy and Metallography* (in Russian, *Fiz. metal. metalloved.*), Vol. 45, No. 4, pp. 139-144, 1978.

V'yunenko, Yu.N. and Likhachev, V.A., "Internal Friction in Alloys Based on CuMn," *Problemy prochnosti* (translated into English by Plenum Publishing Corp., 1986), No. 5, pp. 59-62, May 1985.

Warlimont, H., "Zur Bedeutung des Gefuges hochdampfender Legierungen," *Radex-Rundshau* (in German), Vol. 1/2, pp.108-114, 1980.

Warlimont, H., Delaey, L., Krishnan, R.V., and Tas, H., "Thermoelasticity, Pseudoelasticity and the Shape Memory Effects Associated with Martensitic Transformations: Part 3 Thermodynamics and Kinetics," *Journal of Materials Science*, Vol. 9, pp. 1545-1555, 1974.

Wayman, C.M., "Some Applications of Shape-Memory Alloys," *Journal of Metals*, Vol. 32, No. 6, pp. 129-137, January 1980.

Yamada, Y., " 'Modulated Lattice Relaxation' in β-based Premartensitic Phase" (unpublished), presented at the 115th Annual Meeting of The Metallurgical Society of AIME at New Orleans, Louisiana, 2-6 March 1986.

Youngblood, F.L., *Characterizing and Controlling the Metallurgical Properties of a Cu-Mn Alloy for Ship Silencing Applications*, M.S. Thesis, Naval Postgraduate School, Monterey, California, June 1975.

Zimmerman, J.E., Arrott, A., Sato, H., and Shinozaki, S., "Antiferromagnetic Transition in γ-Phase Mn Alloys," *Journal of Applied Physics*, Vol. 35, No. 3, Part 2, pp. 942-943, March 1964.

INITIAL DISTRIBUTION LIST

		No. Copies
1.	Defense Technical Information Center Cameron Station Alexandria, Virginia 22304-6145	2
2.	Library, Code 0142 Naval Postgraduate School Monterey, California 93943-5002	2
3.	Department Chairman, Code 69Hy Department of Mechanical Engineering Naval Postgraduate School Monterey, California 93943-5000	1
4.	Professor A.J. Perkins, Code 69Ps Department of Mechanical Engineering Naval Postgraduate School Monterey, California 93943-5000	10
5.	Professor Y.S. Shin, Code 69Sg Department of Mechanical Engineering Naval Postgraduate School Monterey, California 93943-5000	2
6.	LCDR John Reskusich, USN Puget Sound Naval Shipyard Bremerton, Washington 98314-5000	5
6.	Dr. Ming-Hsiung Wu Memory Metals, Inc. 84 West Park Place Stamford, Connecticutt 06901	1
7.	Mr. Robert Hardy, Code 2803 David W. Taylor Naval Ship Research and Development Center Annapolis, Maryland 21402	5
8.	Ms. Cathy Wong, Code 2812 David W. Taylor Naval Ship Research and Development Center Annapolis, Maryland 21402	5
9.	Dr. I.M. Imam Naval Research Laboratory Washington, D.C. 20375-5000	1
10.	Mr. Dale T. Peters Technical Director, Metallurgy INCRA 708 Third Avenue New York, New York 10017	1
11.	Dr. John Breedis Supervisor Metals Research Laboratories 91 Shelton Avenue P.O. Box 30-9643 New Haven, Connecticut 06511	1